Christof Holzer, BSc.

Palladium Complexes with Mercaptoaryl-oxazoline Ligands: Synthesis and Activity in Suzuki-Miyaura Couplings

MASTER'S THESIS

to achieve the university degree of

Master of Science

Master's degree programme: Chemistry

submitted to

Graz University of Technology

Supervisor

Univ.-Prof. Dipl.-Chem. Dr.rer.nat. Nadia Carmen Mösch-Zanetti

Institut für Chemie
Karl-Franzens Universität Graz

Graz, 05. February 2015

AFFIDAVIT

I declare that I have authored this thesis independently, that I have not used other than the declared sources/resources, and that I have explicitly indicated all material which has been quoted either literally or by content from the sources used. The text document uploaded to TUGRAZonline is identical to the present master‘s thesis dissertation.

24.02.2015

Date

Signature

Inhaltsverzeichnis

Abstract

The synthesis of a variety of palladium(II) complexes with the monoanionic, bidentate ligand 2-(2-thiophenyl)-4,4-dimethyloxazoline, S-Phoz, was carried out. The complexes of type [Pd(S-Phoz)$_2$], [{PdX(S-Phoz)}$_2$] (X=Cl,Br,I **K3-K5**) and [PdX(S-Phoz)(IMes)] (X=Cl,Br,I **K6-K8**) have been synthesized and described. All complexes have been characterized by NMR, IR and UV/Vis measurements. The catalytic activity of the described complexes in Suzuki-Miyaura coupling in an aqueous environment has been determined. The [Pd(S-Phoz)$_2$] complex showed no catalytic activity while all other complexes are catalytically active. For catalytic activity in Suzuki-Miyaura coupling the halogenide substituent had significant impact on the catalytic activity. While Cl (**K3,K6**) and Br (**K4,K7**)-substituted complexes showed an overall very similar behavior complexes with I (**K5,K8**) were substantially different. Iodine increased the catalytic activity in Suzuki-Miyaura for the complex of type [PdX(S-Phoz)(IMes)] while it decreased the catalytic activity in those reactions in the dimeric complex type [{PdX(S-Phoz)}$_2$]. For comparison to the N-heterocyclic carbene ligand IMes also the corresponding chloride-complexes of type [PdCl(S-Phoz)(EPh$_3$), E=P (**K10**), As (**K11**), Sb (**K12**), were synthesized and tested as catalysts. PPh$_3$ showed to be the better ligand compared to the N-heterocyclic carbene IMes for Suzuki-Miyaura reactions in water. The heavier group-15 donor ligands showed an expected decrease in catalytic activity. In general the ligands can be ordered in the following fashion by their catalytic activity (within [PdCl(S-Phoz)L]: L = PPh$_3$ > IMes ≈ AsPh$_3$ > SbPh$_3$.

The obtained UV/Vis and DFT data for the electronic excitation spectra of the synthesized complexes was used to rationalize the catalytic activity of the synthesized complexes. It was shown that complexes with S → Pd LM-CT transition energies between 460 – 495 nm also showed the highest catalytic activity. Complexes that deviate from this range show a significant decrease in catalytic activity in Suzuki-Miyaura couplings in water. The crystal field splitting in complexes [PdX(S-Phoz)(IMes)] (X=Cl,Br,I **K6-K8**) showed the expected trend. The first electronic excitation energy is lowered as the atomic number of the halogenide increases, i.e. $I^- < Br^- < Cl^-$. The increase of the first electronic excitation energy in these complexes is nearly linear increasing from I^- to Br^- and Br^- to Cl^- by 800 cm^{-1} for each step.

Danksagung

Als Erstes möchte ich Fr. Prof. Dr. Mösch-Zanetti danke die mir diese Arbeit in ihrer Gruppe ermöglicht hat. Auch möchte ich meinen Kollegen danken, an erster Stelle Dr. Jörg Schachner und Lydia Peschel für ihre Hilfe bei meinen Aufgaben und auch für ihre unermüdliche Korrekturarbeit im Zuge dieser Masterarbeit. Ebenso großen Dank schulde ich Hr. Prof. Dr. Belaj, der auch aus dem kleinsten, verwachsenen Kristall immer eine Kristallstruktur entlocken konnte. Hr. Prof. Dr. Gatterer möchte ich für die Bereitstellung der Messgeräte und die Unterstützung für den spektroskopischen Teil dieser Arbeit danken. Fr. Dr. Kelterer möchte ich für die Rechenzeit am bCluster und hilfreiche Gespräche bezüglich aller möglichen Themen der Quantenchemie, auch weit über diese Arbeit hinaus, herzlichst danken.

Auch bei unserer immer freundlichen Doris stehe ich wahrscheinlich tiefer in der Kreide als das ich es jemals wieder gut machen kann. Vielen Dank, ohne dich hätte ich doppelt so lange gebraucht – unzählige Chemikalienlieferungen, Messungen und etwaige Laborprobleme wurden immer schnellstmöglich erledigt.

Bei meinen Arbeitskollegen Stefan, Alexander, Kathi L.(1), Kathi F.(2), Niklas, Mike und Nathalie möchte ich mich für die netten Gespräche und die gute Unterhaltung während meiner Zeit als Masterstudent bedanken. Dear Antoine, I also enjoyed the conversations with you. They gave me lots of helpful ideas.

Auch ein großes Dankeschön gebührt Fr. Isabel Fuchs und Fr. Dr. Steinschifter die mir sehr beim Erledigen des „Papierkrams“ geholfen haben – so manches Formular wäre sonst wahrscheinlich nicht rechtzeitig angekommen.

1. Introduction

1.1 The Suzuki-Miyaura coupling

The first palladium catalyzed cross-coupling reaction that has been established is shown in Scheme 1 and was discovered and published in 1981 by Miyaura, Yanagi and Suzuki.[1] This reaction may seem simple but led to the Nobel Prize for A. Suzuki in 2010, together with R. Heck and E. Negishi. All three were active researchers in the early years of palladium catalyzed cross couplings in organic synthesis.

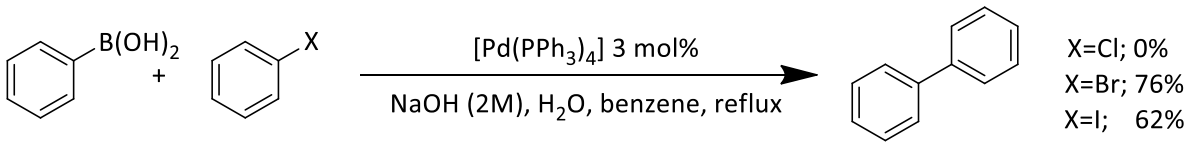

Scheme 1: First published Suzuki-Miyaura type reaction

In the prototype Suzuki-Miyaura reaction shown in Scheme 1 an arylboronic acid is reacted with an aryl halide to yield the corresponding biphenyl. This reaction was the first example of a cross-coupling of sp^2-hybridized aromatic carbon atoms under mild conditions, being highly tolerable towards functional groups at the aromatic system. Palladium cross-coupling are nowadays used in industrial syntheses of a wide variety of products, including pharmaceutical products. Maybe the best known pharmaceutical application is the synthesis of discodermolide, a natural toxin from a marine microorganism that has been identified as a potent anti-cancer drug. There it was used to couple two large subunits at the end of the synthesis in a Suzuki-type coupling to produce 60 g of discodermolide for clinical studies.[2]

1.2 Palladium catalysts used in Suzuki-Miyaura couplings

In the last three decades a variety of palladium catalysts used in cross-coupling reactions has been developed. In this thesis only a short overview of the developed catalysts and ligands will be given. The palladium catalysts used for Suzuki-Miyaura cross-coupling reactions discussed in this thesis can roughly be grouped into three categories: phosphine complexes, N-heterocyclic carbene complexes and palladacycles. These groups will be discussed in the following chapter.

1.2.1 Pd-phosphine catalysts for Suzuki-Miyaura couplings

Pd-phosphine complexes are among the first used catalysts in cross-coupling reactions. They mainly occur as Pd^0 and Pd^{II} complexes, but also some Pd^{I} complexes found application as active catalysts. Also the first catalysts used by Suzuki and Miyaura was the zero-valent phosphine complex ($[Pd(PPh_3)_4]$).[1]

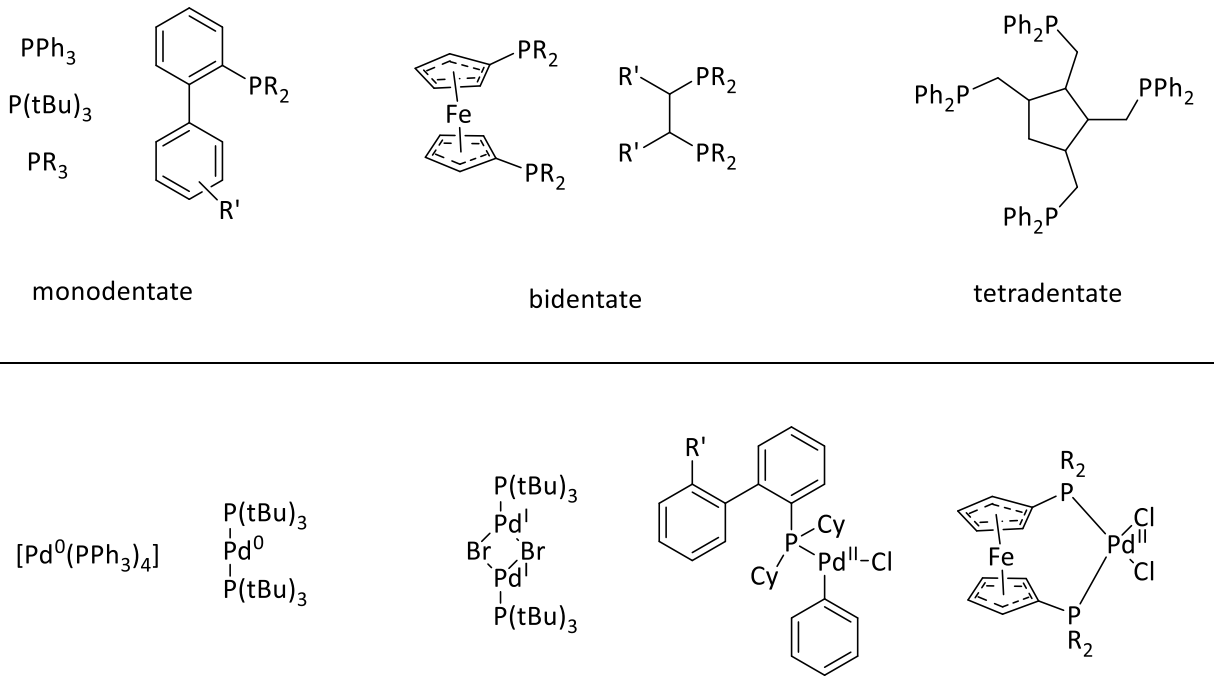

Figure 1: Common phosphines (upper) and well-defined Pd catalysts (lower) used in Suzuki-Miyaura cross coupling reactions

Figure 1 gives an overview of monodentate, bidentate and tetradentate ligands. The first two classes are commonly used in Suzuki-Miyaura cross-coupling reactions. A defined complex is not always necessary, and often the Pd catalyst is generated in-situ by adding palladium precursor and ligand 1:2 (monodentate) or 1:1 (bidentate) to the reaction mixture. Pd^0 (e.g. $[Pd_2(dba)_3]$) or Pd^{II} (e.g. $PdCl_2$, $Pd(OAc)_2$) compounds are popular Pd sources of Pd and ligand are supplied separately. Newer catalyst systems make use of the wide variability of tertiary phosphines, allowing for stereoelectronic fine-tuning at the active site.[3] Also some well-defined palladium complexes are used in catalytic reactions with $[PdCl_2(dppf)]$ being probably the most prominent example.[4] These well-defined catalysts occur in oxidation state 0, +1 and +2. The coordination geometry depends on oxidation state and steric demand of the phosphine ligand. While Pd^{II} complexes prefer square-planar coordination (e.g. $[PdCl_2(dppf)_2]$, d^8) the Pd^0 complexes often prefer tetrahedral coordination (e.g. $[Pd(PPh_3)_4]$, d^{10}). Bulky phosphines can stabilize the oxidation state +1 and also the uncommon coordination number three as in the complex $[\{Pd^{I}Br(P(tBu)_3)\}_2]$.[5] NMR and computational studies however conclude that the cross-coupling reactivity of this Pd(I) complex is consistent with Pd(0)L complexes and therefore the active species is generated by reduction to Pd^0 during catalysis.[5]

Monodentate biarylphosphine ligands were a popular research topic in the last decade. Due to the variability of the organic residues their electronic and steric demand is fine-tunable, and there have been extensive studies on the dependence of catalytic activity to the choice of this residues.[6,7] Biarylphosphines are considered as state-of-art ligand type in cross-coupling reactions nowadays and are widely used not only in laboratories but also in industrial applications. Also the bidentate phosphine ligands emerging from the ferrocene backbone are well explored, and the famous "Josiphos" ligands are indeed modified versions of this ligand system, and they are particularly active for coupling mesylates.[8]

The tetradentate phosphine ligand shown in Figure 1 is one of very few examples of its class. Together with the Pd precursor [{PdCl(C_3H_5)}$_2$] it forms a highly active catalysts system that is active in Suzuki-Miyaura couplings as well as other types of palladium catalyzed cross-coupling reactions.[9]

The catalytic activity of Pd-phosphine complexes is well explored in many publications and although they were the first used in Suzuki-Miyaura reactions they remain the most active type of complexes until now. The monodentate biarylphosphines and bidentate diphosphinoferrocene derivatives are the most recently developed generation of Pd-phosphine complexes which show the highest overall activity of all catalysts (vide infra, chapter 4).[3,10]

1.2.2 Pd-NHC catalysts for Suzuki-Miyaura couplings

N-heterocyclic carbenes (NHC, "Arduengo-carbenes") marked the advent of a second generation of catalysts with improved catalytic activites.[11] By replacing tertiary phosphines with these N-heterocyclic carbenes promising new candidates for homogenous catalysts with increased activity were developed.[12] An overview of N-heterocyclic carbene palladium complexes with Pd in catalysis was written by Fortman and Nolan.[13] NHCs can generally be regarded as stronger σ-donors than typical phosphine ligands. The Pd-C bond is very stable (usually not moisture or air-sensitive) and standard orbital models predicts that Pd-NHC complexes carry more electron density at the Pd core when compared to similar Pd-phosphine complexes. The overall π-acceptor capability of NHCs is still subject to research and more work is needed to conclude on this property.[14,15]

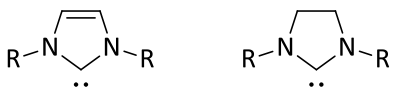

"I" "SI"

Figure 2: Left Unsaturated NHC; Right: Saturated NHC

Basically two variants of NHC are used in Pd chemistry, based on a unsaturated (Figure 2, left) and saturated (Figure 2, right) imidazole-2-ylidine backbone. The nomenclature of NHCs follows a simple scheme, the first one or two letters are determined by the saturation of the backbone followed by the trivial abbreviation of the organic residue –R. For example if R=mesityl and the NHC has an unsaturated backbone it is called "IMes". With –R=adamantyl and a saturated NHC backbone the NHC is called "SIAd".

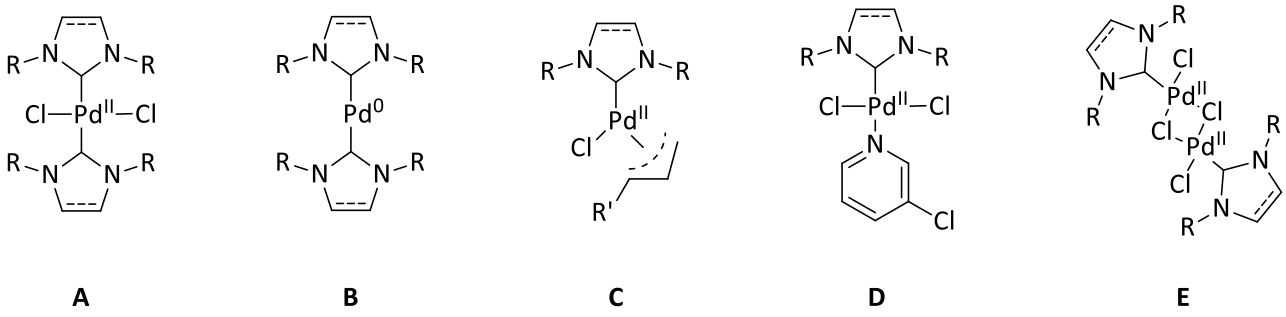

Figure 3: Common Pd-NHC structural motives

Mainly NHC ligands with small substituents like methyl or ethyl groups and their corresponding complexes of type $[PdCl_2(NHC)_2]$ (**A**) have proven successful in Suzuki-Miyaura couplings.[12] Also palladium(0) complexes with very bulky NHCs (**B**) (e.g. adamantyl) have proven to yield very active Suzuki-Miyaura cross-coupling catalysts.[16]

Bulky ligands –R also stabilize complexes of type **C** (R = diisopropylphenyl, adamantyl) with a coordination number of three in the oxidation state +2 similar to their bulky phosphine counterparts. Suzuki-Miyaura couplings with catalyst loadings as low as 0.001 mol% **C** have been performed with these η^3-allyl coordinated complexes. The main drawback of type C in laboratory is the sensitivity to air, which decomposes the complex slowly.[17,18] Complexes of type **D** are directly prepared from the NHC (as imidazolium salt) and $PdCl_2$ in the corresponding pyridine in the presence of a base, e.g. K_2CO_3. This type is air- and moisture stable but nevertheless shows high activity in cross-coupling reactions.[19] The bridged dimers (**E** in Figure 3) are also excellent cross-coupling catalysts, enabling cross-coupling reactions between sterical hindered substrates with three or four substituents at the aromatic ring system of the coupling partner. Also these dimeric complexes show a remarkable functional group tolerance against nitrogen- and sulfur based heterocycles.[20]

1.2.2.1 Pd-IMes complexes

As IMes was the main NHC used in this thesis a deeper analysis of its known palladium chemistry is given. The complex $[PdCl_2(IMes)_2]$, in contrast to many other $[PdCl_2(NHC)_2]$ complexes, was initially found to be inactive in either Suzuki-Miyaura or Heck-couplings. The IMes ligand and especially its saturated version SIMes however became famous in the highly improved, second generation Grubbs-II Ru olefin metathesis catalyst.[21]

Lebel et al. could give an explanation for this unexpected inactivity. Reacting the precursors $PdCl_2$ or $Pd(OAc)_2$ with the IMes carbene ligand changed the binding mode of the NHC ligand.[22] When using $Pd(OAc)_2$ as precursor the IMes ligand does not bind via the C2 carbon as expected, but via the C4 carbon of the NHC backbone (Scheme 2). In contrast the $PdCl_2$ precursor lead to the expected product where both IMes ligands are bound with the C2 atom to the palladium(II) center.

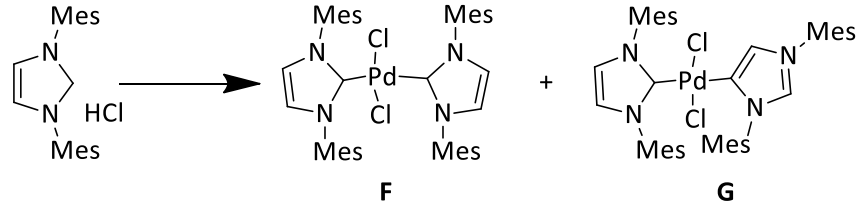

F **G**

$Pd(OAc)_2$ Dioxane, 80 °C	< 1%	74 %
$PdCl_2$, Cs_2CO_3 Dioxane 80 °C	68 %	< 1%

Scheme 2: Different outcome of reaction with IMes·HCl and $PdCl_2$ or $Pd(OAc)_2$ [22]

Furthermore it was found that complex **F** is inactive in Suzuki-Miyaura and Heck-coupling while catalyst **G** is active for both reactions. Interestingly it was proven that the in-situ generated catalyst **G** (from $Pd(OAc)_2$ and IMes·HCl) is even more active than the defined, isolated catalyst **G**. One possible explanation is that beside catalyst **G** other species, probably with only one carbene coordinated, are formed. These species are more active than the corresponding palladium complexes with two coordinated carbenes.[23]

1.2.3 Palladacycle catalysts for Suzuki-Miyaura couplings

Palladacycles are five- or six-membered rings were the palladium atom is often (but not necessarily) attached to a carbon atom and a second donor atom further coordinates the central Pd atom. Palladacycles are limited to the formal +2 oxidation state at the Pd center due to the Pd-C bond and where initially thought to release Pd^0 upon heating in reaction mixture. Due to the high thermal stability of

palladacycles this assumption is however no longer retained, and the reduction to Pd^0 is assumed to take place by reaction with other components during the Suzuki-Miyaura reaction.[24] Figure 4 shows three groups of palladacycles.

Among the palladacycles with bidentate ligands (upper part in Figure 4) a variety of neutral donor atoms has been employed, mainly sulfur (**H**), phosphor (**I**) and nitrogen (**J**). The nature of donor atoms affects the binding to the Pd center and therefore enables tuning of the catalyst. Also dimerization is observed for these complexes to saturate the valence shell of the central Pd atom. These dimers can be split into monomeric units by the addition of donor molecules (e.g. phosphines (**N**), NHCs (**M**), lower right in Figure 4).[25] These monomeric and dimeric units show similar activity (per palladium atom) in catalysis and only differ at very low catalyst loadings (10^{-3} mol% and lower) were the additional donor is assumed to stabilize the reactive Pd^0 species.[24] Complex **M** was shown to be an efficient catalyst for coupling ortho substituted aryl chlorides with ortho substituted arylboronic acids therefore accepting bulky substrates and deactivated aryl chlorides.[26]

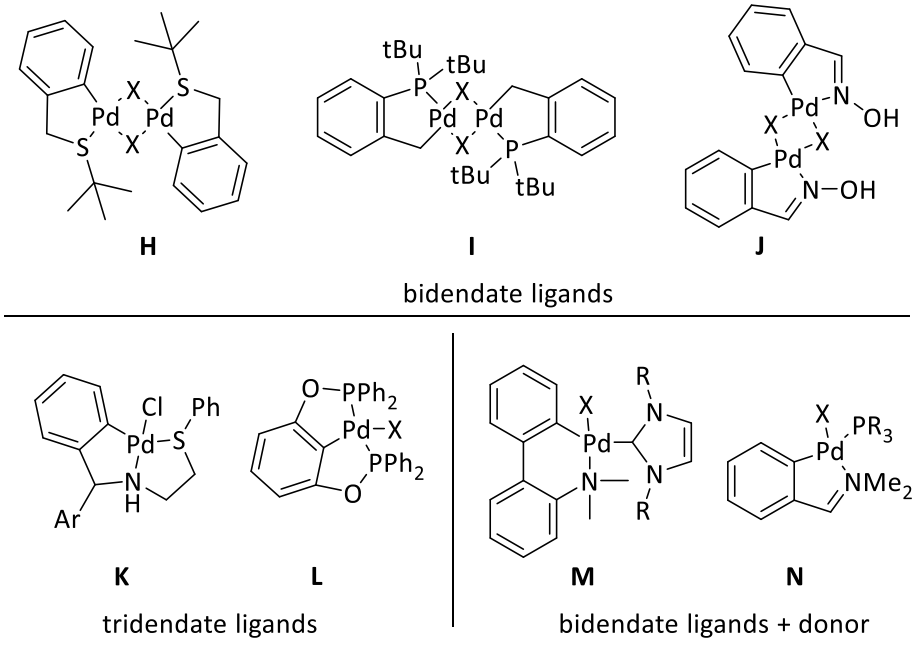

Figure 4: Palladacycle catalysts for cross-coupling reactions, X=halogenide, (trifluoro)acetate

Among the tridentate ligands forming palladacycles the most recognized class are the so called “pincer” ligands (**L**). These compounds are exceptionally stable and are discussed to not decompose during catalysis but largely retain their structure, which could give rise to a possible Pd^{IV} species.[27] For a pincer type ligand with two NHC moieties replacing the phosphines the active species was confirmed to be homogenous and

not reduced metallic Pd^0 from decomposition.[28] There has been some effort to replace the phosphines in the pincer-type ligand **L** by sulfur or nitrogen donor atoms which however led to catalysts which lost near all of their catalytic activity.[29]

The sulfur and nitrogen containing palladacyclus **K** and other sulfur containing palladacycles are in contrast to **L** are assumed to form active palladium nanoparticles instead of a homogenous active species.[29,30]

The turn-over numbers of palladacycle catalysts are generally among the highest known for any Pd catalyzed cross-coupling reactions, yielding turn-over numbers as high as 10^8 turnovers per Pd center. Although announced as highly active catalysts palladacycles only rarely find their way in preparative laboratory chemistry or even industrial applications. Only a handful (less than ten) are commercially available at the moment, with most of these available catalysts being modified biarylphosphines discussed in chapter 1.2.1.[24] Nevertheless the class of palladacycle catalysts gave rise to the usage of sulfur containing moieties in active Suzuki-Miyaura catalysts

1.3 Suzuki-Miyaura couplings in water

A main goal of current cross-coupling catalyst research is the usage of water as solvent in these couplings, mainly in the presence of air. Therefore the number of publications developing Suzuki-Miyaura couplings in aqueous solution steadily increased in the last few years and the presence of convenient, cheap bases and low loadings of catalyst is a common target in newer publications on Suzuki-Miyaura couplings.[31-36] Carrying out Suzuki-Miyaura reactions in water puts high demands on the catalyst. It has to be water-stable while remaining reactive towards cross-coupling reactions. Also the solubility of palladium catalyst and especially the aryl halides in water is low for typical substrates. For the palladium catalyst the introduction of water-soluble groups often helps to overcome solubility problems and often the ligand is sulfonated to make the catalyst more water-soluble.[37-41] Aryl bromides and aryl iodides are commonly better soluble in hot water when compared to their aryl chloride homologues. Therefore for the latter (aryl chlorides) a phase-transfer agent has to be employed in Suzuki-Miyaura couplings with homogenous palladium catalysts which are carried out in neat water. Alternatively the palladium loading was increased by typically the ten-fold when compared to catalyst loadings with phase transfer agents.[37,42,43] Water soluble aryl chlorides (e.g. chlorobenzoic acid) do not need phase-transfer agents. As the usage of water as solvent is nowadays referred to as “green” chemistry the usage of mostly toxic phase-transfer agents (often in stoichiometric amounts) is a step backwards from being environmental friendly.

1.3.1 Sulfur containing Pd catalysts in water

Sulfur compounds, especially anionic sulfur compounds such as thiolates, are known as potent catalyst poisons for precious metal catalysts, but this is mainly true for heterogenic catalysts and does not necessarily apply for homogenous catalysts. Due to the soft character of Pd and S the Pd-S bond is thermodynamic stable and unlikely to be broken under all but the harshest conditions. This thermodynamic robust Pd-S bond could therefore prove useful under aqueous conditions at elevated temperatures by protecting the active palladium species from aggregating and other catalyst-inactivating side reactions. Since the anionic sulfur moiety is strongly bound to the Pd center detachment during the catalytic cycle becomes unlikely.

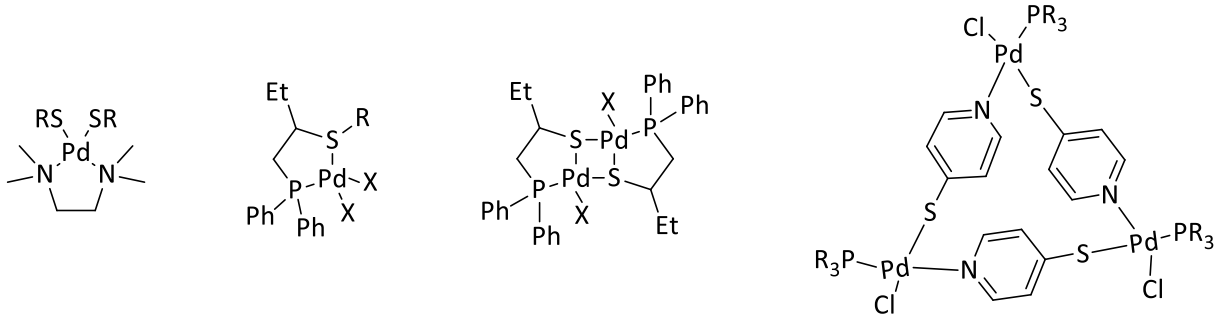

Figure 5: Palladium-sulfur complexes that are active catalysts in Suzuki-Miyaura couplings in water

The first few catalysts featuring Pd-thiolate bonds were already synthesized.[36,44,45,46] All Pd-thiolate complexes up to now show their highest activity at elevated temperatures (100 °C and above) and are active at low concentrations (typically under 1 mol%).[36,44,45,46] One may note that among four active catalysts in water shown in Figure 5 three contain anionic sulfur and only one a neutral sulfur donor.

Recently a set of complexes with modified NHC ligands equipped featuring an anionic thiol side-arm, have been synthesized.[35,36,47]

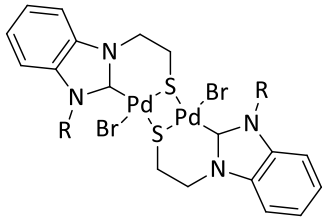

R=benzyl, mesityl

Figure 6: Sulfur-bridged dimeric Pd-NHC complexes [35]

The palladium complexes of this modified NHC ligand (Figure 6) exhibits catalytic activity for Suzuki-Miyaura couplings in an aqueous environment and dioxane employing the cheap base K_2CO_3. The activity of palladium complexes with sulfur ligands is therefore not inhibited by the presence of anionic sulfur. The catalyst is indeed very active even at low loadings which is another hint that sulfur poisons heterogeneous noble metal catalysts, but not necessarily homogeneous catalysts. The sulfur ligands instead allow a high activity in water due to the formation of a thermodynamic stable Pd-S bond that is thermally resistant in aqueous solutions.

The promising stability of the Pd-thiophenolate bond under basic conditions at elevated temperatures is a good starting point for the search of new, highly active cross-coupling catalysts that are active in aqueous environments.

1.4 The mercaptoaryl-oxazoline ligand and corresponding metal complexes

Sulfur plays an important role in bioinorganic chemistry being involved in many enzymes that coordinate towards metal centers. Especially representative examples are molybdenum and tungsten centers, which often occur in sulfur rich environment in natural binding pockets.[48,49] Both elements (molybdenum and tungsten) strongly bind to sulfur moieties. One focus of the Mösch-Zanetti group is to mimic the catalytic activity of oxygen-atom transfer processes occurring at Mo and W centers in biological system. Also active center of acetylene hydratases are a current research topic in the Mösch-Zanetti group. Both enzyme classes feature a molybdopterin cofactor providing sulfur and nitrogen moieties to bind to the metal center.

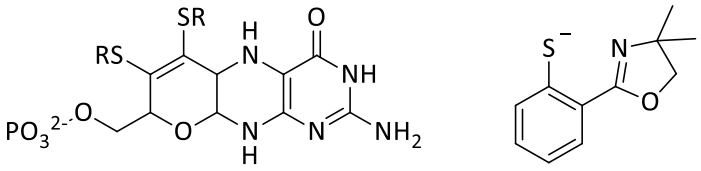

molybdopterin S-Phoz

Figure 7: Left: Molybdopterin cofactor, Right: 2-(2-Thiophenyl)-4,4-dimethyloxazoline, S-Phoz

As a biological mimic to molybdopterin the monoanionic 2-(2-thiophenyl)-4,4-dimethyloxazoline (S-Phoz) ligand was synthesized to be used in conjunction with molybdenum and tungsten metal centers in lower oxidation states.[50]

The S-Phoz ligand belongs to the class of mercaptoaryl-oxazolines which has first been reported in 1994- Qi-Lin and Pfaltz published the enantioselective copper-catalyzed 1,4-addition of a Grignard reagent to enones.[51] Over the last 20 years research efforts have increased employing chiral or non-chiral

mercaptoaryl-oxazolines. Complexes with mercaptoaryl-oxazolines are known for various metals, namely (in chronological order of the synthesis of their mercaptoaryl-oxazoline complexes) Zn[52], Cd[52], Hg[52], Ir[53], Fe[54] and Ru[55]. We noticed a complete lack of investigation of group-10 metals Ni, Pd and Pt although especially Pd and Pt are soft metal centers binding strongly towards sulfur moieties.[56] Part of this thesis, namely basic coordination chemistry of the S-Phoz ligand towards group-10 metals (Ni, Pd, Pt), we published recently in 2015.[57]

We further recognized the growing interest of anionic sulfur ligands for Suzuki-Miyaura couplings in water and therefore investigated the behavior of the S-Phoz ligand in the corresponding complexes. The [Pd(S-Phoz)]-type complexes were further modified according to the principal structural features of active cross-coupling catalysts introduced in chapter 1.2 and 1.3 to optimize Suzuki-Miyaura coupling in water with the S-Phoz ligand.

1.5 Mechanism of palladium catalyzed cross coupling reactions

The generally accepted mechanism is discussed in the following section. Scheme 3 shows the two most likely catalytic cycles that occur in palladium catalyzed cross couplings in a simplified way.

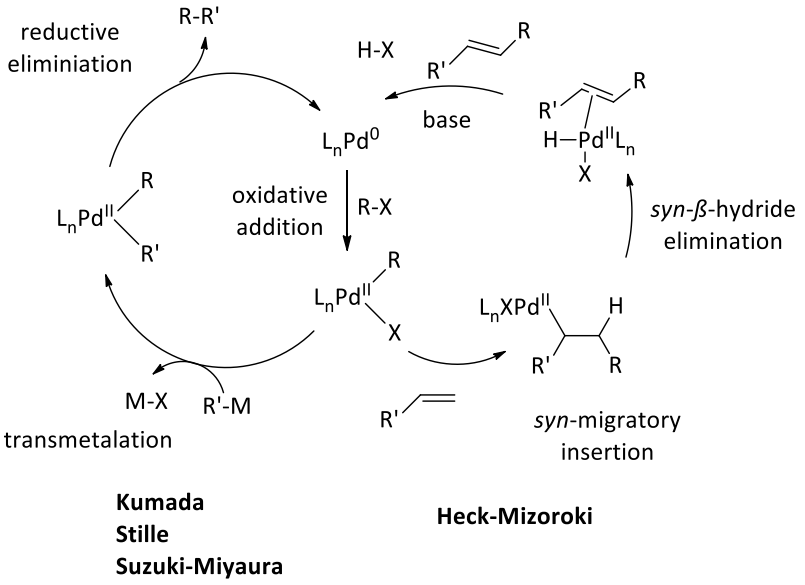

Scheme 3: Schematic Pd-catalyzed coupling cycles [58]

For the Suzuki-Miyaura and related coupling reactions (Kumada, Stille, left cycle in Scheme 3) it is assumed that a catalytically active Pd^0 species first undergoes oxidative addition of the corresponding aryl halide.[59,60] Then the coupling partner (boronic acid in Suzuki-couplings, organozinc compound for the Negishi-coupling, Grignard reagent for the Kumada-coupling) undergoes transmetalation. Both groups R

and R' have to be coordinated in *cis*-position on the palladium(II) center to allow for the product forming reductive elimination step. At this step the initial catalyst is regenerated and ready for the next turnover in the cycle. The Heck-type reaction definitely follows another mechanistic pathway.[58,61] The active palladium(0) species undergoes oxidative addition of the aryl halide R-X, identical to the Suzuki-reaction pathway. However the alkene inserts into the Pd-R bond, and the inserted product is eliminated via β-hydrogen abstraction. Protodehalogenation is then promoted by a base, regenerating the active species.

A more recent mechanism was proposed by Amatore and Jutand (from now on called "Amatore-Jutand mechanism"). In 1991 they investigated the reaction rates of the reversible oxidative addition to low-coordinated zero-valent palladium centers.[62] A second investigation pointed out that the rate of reaction does not solely depend on the palladium(0)-ligand species that is formed by reduction of the palladium(II) precursor , but rather the cations and especially anions in solution (from precursor, or added externally) play a vital role in the overall observed kinetics.[63]

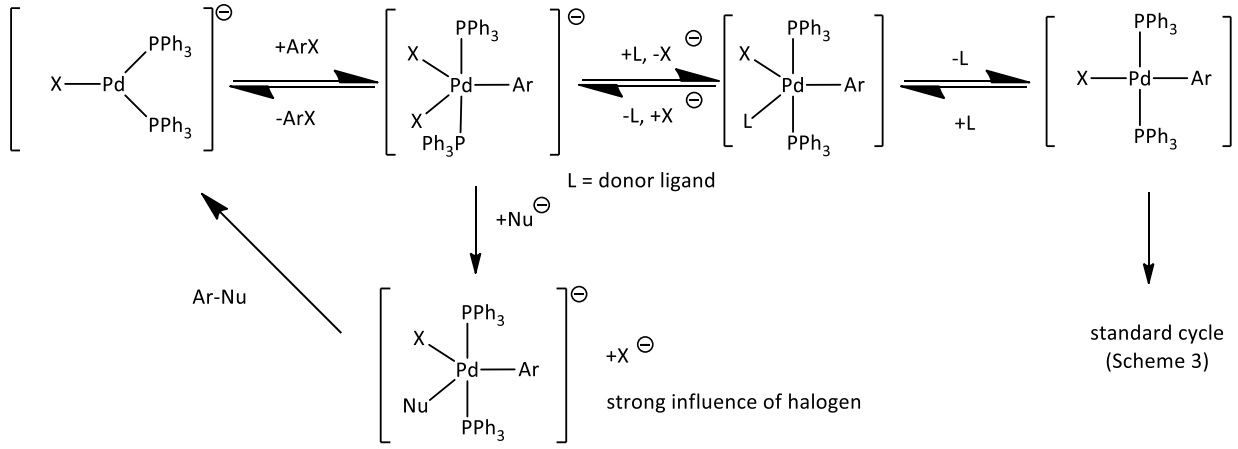

Scheme 4: Amatore-Jutand mechanism for Pd catalyzed cross-coupling, L=donor ligand

As shown in Scheme 4 the Amatore-Jutand mechanism involves a penta-coordinated anionic zero-valent palladium species which is likely to occur during the catalytic cycle. The equilibrium between the three-coordinated active species before and the penta-coordinated compound after oxidative insertion depends on a whole set of reaction conditions. The equilibria in Scheme 4 can be strongly influenced by the nature of the donor ligand (phosphines or other donor ligands).

A penta-coordinated palladium(0) seems as it represents a 20 electron species of a late 4d metal. However, its concentration is described to be very low and its formation to be a fairly endergonic step but still it can be observed via cyclic voltammetry. The nature of the anions and cations also strongly influences the equilibria in Scheme 4. Ion-pairing is suggested to affect reactivity of the anionic complexes proposed in

the cycle. Addition of $LiClO_4$ to a solution of electrochemically generated $[PdL_2Cl]^-$ increased the reaction rate of the oxidative addition of iodobenzene by a factor of two. Compared to that the addition of $NaBF_4$ led to an increase of the formation of the *trans*-$[PdI(Ph)(PPh_3)_2]$-species by a factor of over 10.000.[62-65]

To conclude the "standard cycle" (Scheme 3) found in popular textbooks can also take place but is often overcome by other catalytic mechanisms (e.g. Amatore-Jutand mechanism) in palladium catalyzed cross couplings, e.g. Suzuki-Miyaura or Negishi couplings.[62-66] Which mechanism takes place can often not be concluded for a whole reaction type, but depends, as discussed above, on the ligand (e.g. PR_3), the presence of halides and other anions ions (Cl^-, acetate…) and on the nature of the substrate and even the products.

1.5 Ligand field in palladium(II) complexes

The preferred oxidation state of palladium is +2 with a d^8 electron configuration and complexes are usually square planar.[67] The square planar ligand field can be derived from an octahedral ligand field by "pulling" away the axial ligands. For complexes with an inversion center (e.g. square planar $[PdCl_4]^{2-}$) d-d transitions are forbidden by symmetry ("Laporte rule"). Nevertheless such d-d transitions are observable due to vibronic effects lowering the symmetry of the system. The observation of d-d bands in an inversion symmetric ligand field cannot be assigned to spin-orbit coupling. Spin-orbit coupling cannot remove inversion symmetry constraints but can lead to a non-vanishing intensity of spin-forbidden transitions.[68] The effects of ligands on the ligand field splitting of palladium complexes have only been studied for a small number of palladium(II) complexes so far. Most studied complexes are homoleptic, e.g. $[PdCl_4]^{2-}$. The ligand field of $[PdCl_4]^{2-}$ was studied by VanQuickenborne and Ceulemas using UV/Vis spectroscopy on translucent crystals.[69] They concluded that palladium is already sufficiently heavy that spin-orbit coupling constants can give rise to singlet-triplet excitations. Also they found that the d_{z^2} orbital of the square-planar palladium complex is anomalously low-lying. This low-lying d_{z^2} orbital arises from the fact that in the square-planar (D_{4h}) geometry the (n-1) d_{z^2} orbital is allowed to mix with the ns-orbital. Due to the complicated structure of the electronic spectra of palladium(II) the overall number of papers dedicated to the ligand field splitting of palladium(II) complexes is limited.[68]

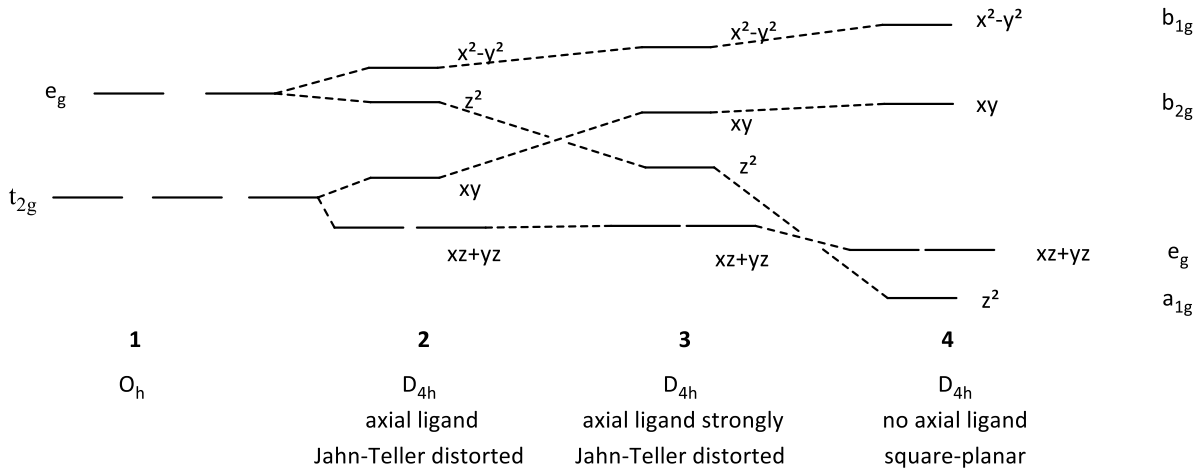

Figure 8: Ligand field splitting from octahedron to square planar ligand field[70]

1.6 Scope of this thesis

The intention of this thesis project was to shed light on the synthesis, isolation, catalytic abilities and in-depth characterization of new mercaptoaryl-palladium complexes. The focus was set on palladium complexes of the general formula [PdX(S-Phoz)(L)], with L being different neutral donor ligands (L = EPh_3 (E =P, As, Sb or IMes) and X being an anionic halide ligand (X = Cl, Br, I, CF_3CO_2). The new complexes were tested in Suzuki-Miyaura type cross-coupling reactions under aqueous conditions. In a systematic study the influence of the neutral ligand L as well as the anionic ligand X was investigated with respect to chemical properties (solid state structure, nuclearity, color, thermal stability) as well as catalytic activity. In-depth spectroscopic studies (NMR, solid state UV-Vis, IR) were performed and DFT calculations (geometry optimization, calculation of excitation spectra) were used to explain and discuss the observed spectroscopic properties. To the best of my knowledge there is no similar study on the ligand field effects in NHC-palladium(II) complexes. These ligands are generally referred to as σ-donor ligands with nearly no π-acceptor capability and as such they have a predictable influence on the electronic spectrum of corresponding complexes. Knowledge of the electronic and spectroscopic behavior of this type of NHC-complexes as well as their phosphine derivatives could be helpful in predicting and understanding mechanistic details of palladium catalysis in general.

Results & discussion

2. Synthesis of mercaptoaryl-oxazolines

Within this thesis an attempt to synthesize substituted mercaptoaryl-oxazolines with mainly electron-withdrawing substituents was made.

2.1 Directed ortho-metalation (DOM)

A conventional method to prepare such compounds is the directed ortho-metalation (DOM) of thiophenols and subsequent reaction with sulfur (Scheme 5). The lithiated species are reacted with 1.0 equiv. of sulfur (1/8 S_8) to obtain the corresponding mercaptoaryl-oxazolines **2, 6, 7** and **8.** Substrate 2-(phenyl)-4,4-dimethyloxazoline **1** can be converted by this procedure to compound **2** as shown in Scheme 5.[50] The off-white product 2-(2-thiophenyl)-4,4-dimethyloxazoline **2** (referred to as S-Phoz in this thesis) precipitates from the ethereal solution as lithium salt. The lithium salt is soluble in acetonitrile and solutions of **2** show an intense yellow color.

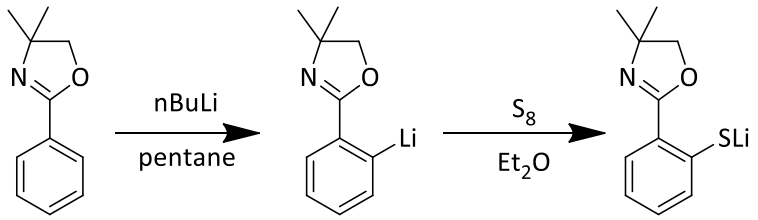

1 **1-Li** **2**

Scheme 5: Synthesis of 2-(2-thiophenyl)-4,4-dimethyloxazoline

For any other substrate featuring electron withdrawing substituents (-CF_3, -F) on the aromatic ring system shown in Scheme 6 the reaction was not successful as no sulfur could be found in the product. When quenching the reaction with diluted aqueous HCl the starting compounds **3, 4** and **5** were obtained nearly quantitatively. Therefore the question arose if the lithiation or the sulfuration failed during the reaction of compounds **3**, **4** and **5**. Thus lithiated **3** and **4** repetitively were quenched with deuterated water, D_2O. The mono-deuterated products d-**3** and d-**4** could clearly be identified via GC-MS, showing a fragment at the same retention time as the starting material with a +1 higher mass. For compound **5** the lithiated species was described in literature, therefore it is assumed that the lithiation step is working.[71,72]

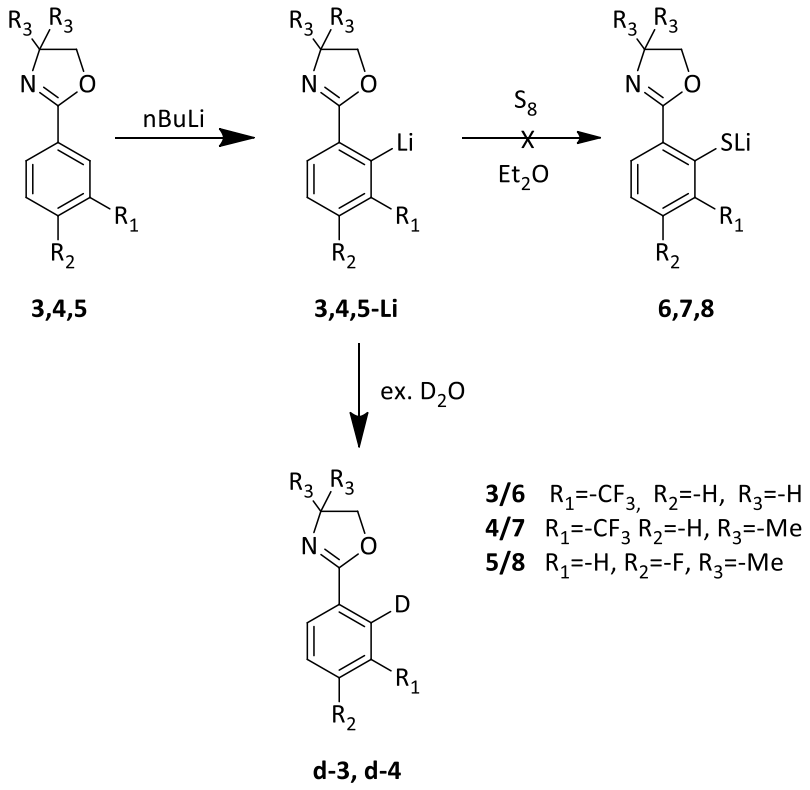

Scheme 6: Lithiation and follow-up reactions of compounds **3, 4** and **5**

Since it was determined that **3**, **4** and **5** can be lithiated the reaction conditions for the sulfuration forming **6** and **7** were systematically tested employing different solvent/temperature combinations. Heptane, toluene, diethyl ether and tetrahydrofuran were used at different temperatures (-78 °C, 20 °C and reflux). In the given solvent 1.0 equiv. **3** or **4** were lithiated with 1.05 equiv. n-BuLi at 0 °C. After 4 hours 0.95 equiv. 1/8 S_8 were added and reaction heated to the given temperature. For diethyl ether no separate reflux reaction was carried out due to its low boiling point. All reactions were quenched with 2 M aqueous HCl, the pH adjusted to 4-5 and the aqueous layer extracted with dichloromethane, dried with $MgSO_4$ and solvent removed in vacuo. Samples were analyzed via GC-MS and NMR spectroscopy. None of the combinations led to the desired mercaptoaryl-oxazoline target compounds **6** or **7**. Except for THF at 20 °C and reflux conditions the mainly obtained products were the starting compounds **3** and **4**. Reactions in THF at higher temperatures lead to a black, unidentifiable product mixture with significant amounts of starting material detectable.

2.2.2 Newman-Kwart rearrangement

The Newman-Kwart rearrangement is one of the oldest reactions to rearrange phenols to thiophenols via a thiocarbamate intermediate. The original version was carried out at 250 °C (or higher), therefore being prohibitive for many substrates. A newly developed catalyzed Newman-Kwart rearrangement can be carried out at 100 °C in toluene with 2-8 mol% of catalyst.[73] The fluorine substituted phenol precursor **9** could be readily synthesized in 3 steps from commercially available 3-fluorosalicylic acid (see experimental section). This compound was used to test the scope of the Pd-catalyzed NKR.

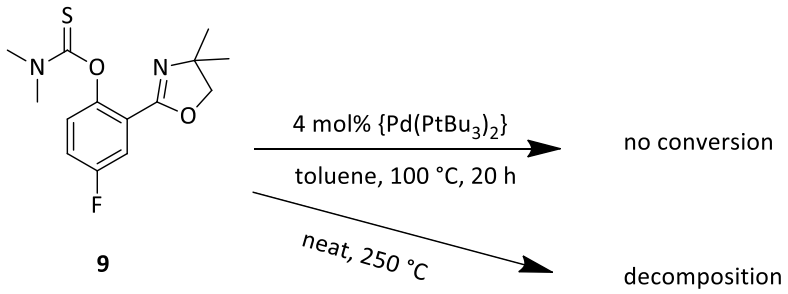

Scheme 7: Catalyzed and uncatalyzed Newman-Kwart rearrangement of **9**

A similar compound to **9** but without the oxazolines moiety, namely 4-fluorophenole was found to react slowly to the rearranged product in 98 % yield (21 h, 100 °C in toluene).[73] The oxazoline further reduces the reactivity of 2-(5-fluoro-2-hydroxyphenyl)oxazoline compared to p-fluorophenol. No conversion occurred after 20 h as determined by GC-MS and ^{1}H NMR spectroscopy. Also the neat reaction at high temperatures only yielded a black slurry, probably because of decomposition of the starting material **9**.

2.3 Synthesis of mercaptoaryl-oxazolines: discussion

The introduction of the sulfur atom to form the desired mercaptoaryl-oxazolines failed for all substituted oxazolines and only worked for the unsubstituted 2-phenyl-4,4-dimethyloxazoline **1**. It has to be noted that until now no mercaptoaryl-oxazolines with electron withdrawing substituents were reported besides nitro-substituted derivatives.[55] It is assumed that the unsubstituted 2-phenyl-4,4-dimethyloxazoline meets the right balance between reactivity and low sterical hindrance, therefore the lithiated species reacts with elemental sulfur. As none of the other substrates showed any conversion to the desired product when lithiated species were employed, further research at this pathway has to be discouraged at the moment. Nevertheless it is not clear why the method fails completely for substrates **3**, **4** and **5**. One possible explanation might be that sulfur is a weak electrophile when compared to other electrophiles like ketones or especially halides like Br_2. As the lithiation was shown to be successful (Scheme 6) the limiting step in

the synthesis of mercaptoaryl-oxazolines with electron withdrawing substituents seems to be the insertion of sulfur into the Li-aryl bond. The slow insertion of sulfur into the Li-aryl bind combination with the stabilizing effect of the electron withdrawing group (stabilizing the intermediate anion as it pulls out electron density from the system, making it less reactive) may explain why no reaction to the corresponding mercaptoaryl-oxazoline was observed for **3**, **4** and **5**.

The Newman-Kwart rearrangement was also not successful for arenes with electron withdrawing substituents, neither catalyzed nor uncatalyzed. For the catalyzed reaction it may be possible that the oxazoline moiety to some extend inhibits the catalyst by coordinating to Pd, blocking the free coordination sites. Up to now the method of choice seems to be aromatic nucleophilic substitution. This method should be preferred as long as there are no other halides or similar (-OTs, -OMs etc.) groups present that could be substituted first leading to polysubstituted species.[55] The main drawback of nucleophilic substitution is found in the substitution pattern of the starting compounds. It does not tolerate any fluorine/chlorine nor bromine atoms that are sterically less hindered than the substituent in ortho-position to the oxazoline. A fluoride substituent in meta position to the oxazoline would preferably be substituted by thiolate yielding the 2-(3-thiophenyl)-oxazoline instead of the wanted (2-thiophenyl)-oxazoline.

3. Palladium complexes of mercaptoaryl-oxazolines

3.1 Palladium(II) complexes with two S-Phoz ligands

3.1.1 Complex synthesis with $PdCl_2$ and related precursors

The first synthetic target molecule was the parent [Pd(S-Phoz)$_2$] complex (**K1**). In this complex palladium(II) is sterically and electronically (16 e^-) saturated, enabling a straightforward synthesis.

The syntheses were performed in toluene at RT under ambient conditions. 1.0 equiv. of starting material were reacted with 2.0 equiv. LiS-Phoz. After 4 h the suspension was filtered through a pad of celite. The solvent was removed vacuo and reprecipitation from CH_2Cl_2 with heptane yielded the pure, dark red crystalline product [Pd(S-Phoz)$_2$] (**K1**) in 60 % yield. The obtained red solid is air-stable for at least months and soluble in common polar aprotic solvent ($CHCl_3$, toluene, acetonitrile) but only moderately soluble in aliphatic or protic solvents.[57]

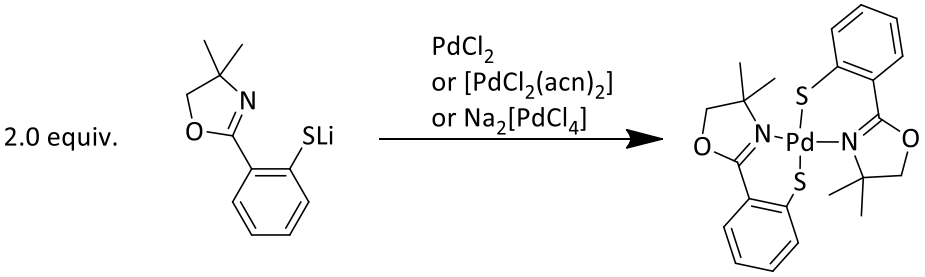

Scheme 8: Synthesis of [Pd(S-Phoz)$_2$] (**K1**)

K1 was characterized using ^{1}H and ^{13}C NMR spectroscopy. In the ^{1}H NMR spectrum the singlet –CH_2 and singlet –CH_3 peak are particularly indicative. The ^{1}H and ^{13}C NMR spectra of **K1** point out that two isomers exists in solution. Due to the similarity to *trans*-[Pt(S-Phoz)$_2$] recently published by our group the major isomer was assigned to the (S,S)-*trans* isomer of **K1**.[57] The minor isomer exhibits two broad duplets for the –CH_2- moiety and two broader singlet for the –CH_3 moiety. Therefore the minor isomer is assumed to be the less symmetric (S,S)-*cis* isomer. Indeed **K1** could be obtained starting from three different palladium(II) precursors (Scheme 8).Neither the palladium precursor nor silica-gel column chromatography are able to change the *trans*:*cis* ratio of complex **K1** as determined by ^{1}H NMR spectroscopy.[57] The equilibrium between the (S,S)-*trans* and the (S,S)-*cis* varies with the solvent and temperature used for ^{1}H NMR spectroscopy. IR resonances confirm that the S-Phoz ligand is coordinated. The C=N resonance is shifted

from 1627 cm^{-1} to 1615 cm^{-1} in **K1**.Single crystal X-ray diffraction analysis confirms the structure of *trans*-**K1** (vide infra).

3.1.2 Temperature and solvent dependency of K1[57]

Variable temperature (VT) ^{1}H NMR spectra of **K1** were recorded in CD_2Cl_2 from +23 °C (rt) to -50 °C and in acetonitrile-d_3 from +23 °C (rt) to +58 °C (Figure 9). No coalescence of the resonances for the cis- and trans-isomer occurred throughout the observed temperature range as the *cis*/*trans* ratio remained constant. This suggests a high energy of *cis/trans* conversion. Only the flipping of the puckered oxazoline rings in *cis*-**K1** is decreased evidenced by the sharpening of the CH_2 doublets (red boxes) while the resonances for *trans*-**K1** remained uninfluenced (blue boxes).[57]

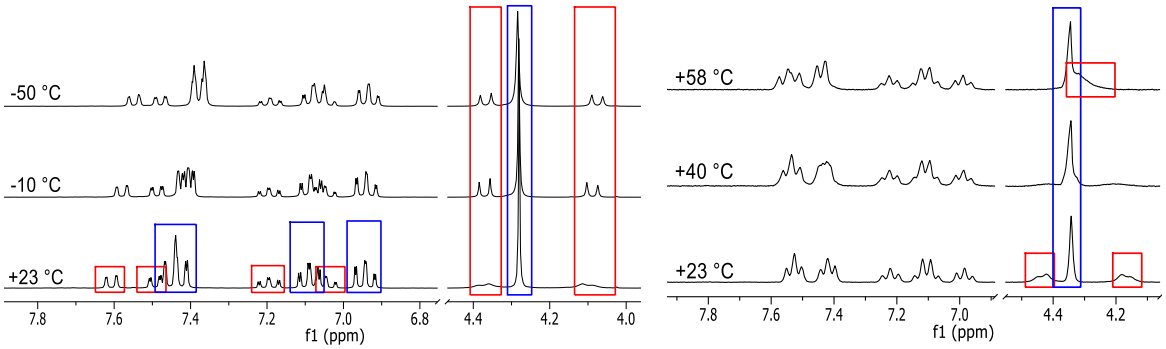

Figure 9: VT ^{1}H NMR spectra of [Pd(S-Phoz)$_2$] (**K1**), signals of *trans*-**K1** are highlighted with blue, dotted boxes and signals of *cis*-**K1** with red, dashed boxes. Left: Behavior upon cooling (CD_2Cl_2) Right: Behavior upon heating (acetonitrile-d_3)[57]

Dissolving **K1** in various solvents showed the *cis/trans* ratio to be significantly influenced. This points to an equilibrium which is due to the altered stabilization of the two isomers in solvents with different dielectric constants (see Figure 10). The less polar *trans*-complex is better stabilized in benzene, while in the more polar acetonitrile the amount of *cis*-complex is increased. This suggests that the equilibrium is indeed occurring but is dominated by the influence of the solvent.[57]

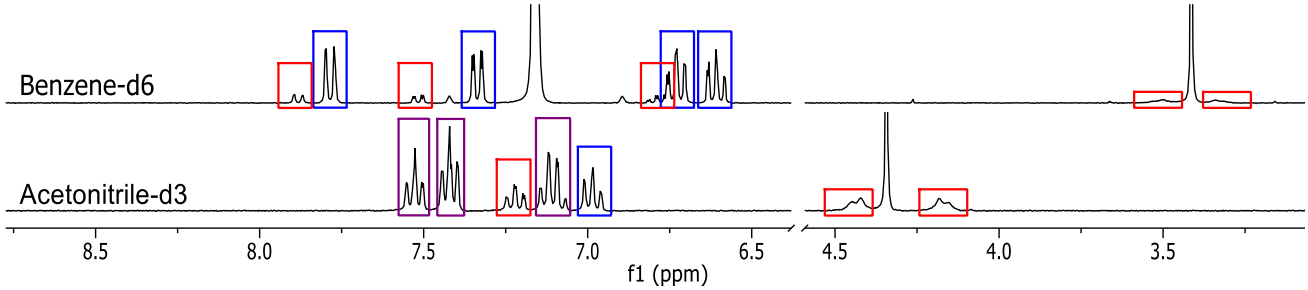

Figure 10: In benzene-d6 cis/trans ratios of 0.18:1, in acetonitrile-d3 of 0.70:1 in CD_2Cl_2 of 0.36:1 were observed

3.1.3 Complex synthesis with the $[PdCl_2(PPh_3)_2]$-precursor

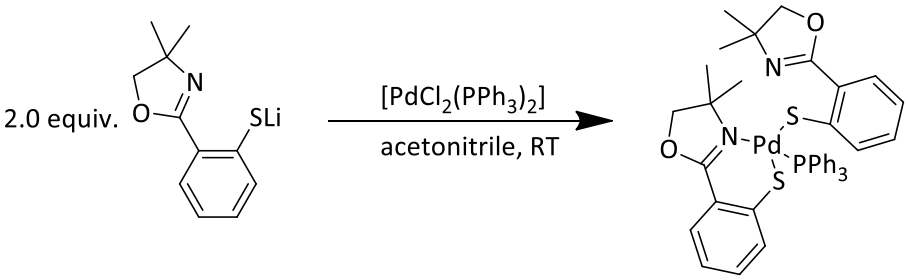

LiS-Phoz **K2**; 74 %

Scheme 9: Synthesis of $[Pd(S\text{-}Phoz)_2(PPh_3)]$ (**K2**)

The reaction 1.0 equiv. of precursors $[PdCl_2(PPh_3)_2]$ with 2.0 equiv. of LiS-Phoz in toluene yielded $[Pd(S\text{-}Phoz)_2(PPh_3)]$ (**K2**) after workup in good yield. Complex **K2** is soluble in chlorinated and polar solvents but insoluble in diethyl ether. Solution behavior of **K2** was investigated by ^{1}H, ^{31}P and ^{13}C NMR spectroscopy. The ^{31}P NMR spectrum in CD_2Cl_2 features signals for both, coordinated PPh_3 (+35.2 ppm) and free PPh_3 (-5.6 ppm).[57] The ^{1}H NMR spectrum shows three sets of coordinated S-Phoz protons in a ratio of approx. 1:0.4:0.2. With the known ^{1}H-NMR data of *cis*- and *trans*-**K1** these could be assigned to *cis*- and *trans*-$[Pd(S\text{-}Phoz)_2]$ (**K1**) and to **K2** indicating an equilibrium between these three species as given in Scheme 10. Thus, by adding excess PPh_3 to **K1** the equilibrium could be shifted towards **K2**; with 2.5 equiv. of PPh_3 75% and with 5 equiv. 90% of **K2** were observed while both *cis*-**K1** and *trans*-**K1** were successively depleted.[57] According to the temperature/solvent dependency of ^{1}H NMR spectra of **K1** also the ^{1}H NMR spectra of **K2** show the corresponding dependencies. These solvent/temperature dependencies were discussed by Peschel et al.[57] (The author of this thesis is co-author of this paper and was a main contributor to synthesis and characterization of equilibrium of **K1** and **K2**)

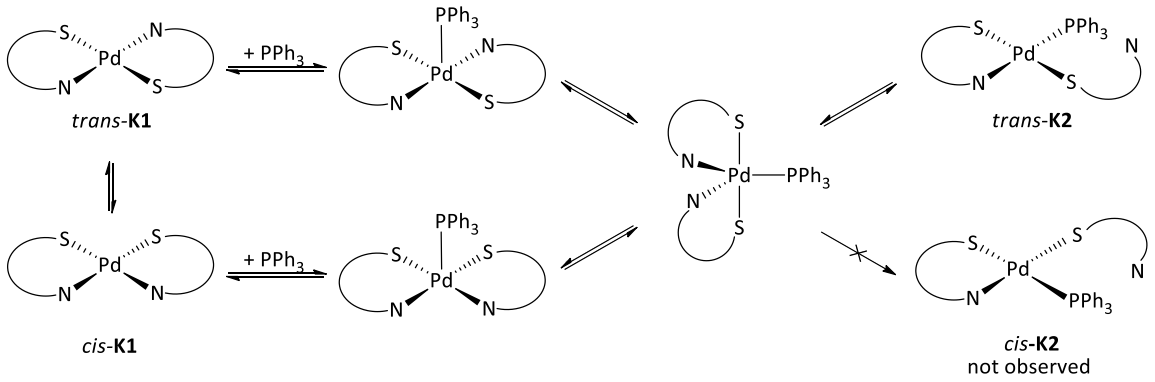

Scheme 10: Observed behavior of **K2** in solution. Equilibrium with cis- and trans-[Pd(S-Phoz)$_2$] (**K1**) and PPh$_3$[57]

As a logical consequence of the equilibria depicted in Scheme 10 any attempts to remove free triphenylphosphine found in ^{1}H and ^{31}P NMR by solvent extraction/washing ended in a dark red, oily product. The IR spectrum of **K2** shows two different C=N resonances at 1660 cm^{-1} and 1633 cm^{-1} in agreement with the assumption of one κ^1 and one κ^2-coordinated S-Phoz ligand. Single crystal X-ray diffraction analysis confirms the structure of **K2** (vide infra).

3.1.4 Molecular structures of complexes with two S-Phoz ligands per palladium atom

Crystals of **K1** suitable for single crystal X-ray diffraction analysis were obtained by slowly evaporating of a saturated solution in benzene. Crystals suitable for single crystal X-ray diffraction analysis of **K2** were obtained by slow evaporation of a saturated solution of **K2** in acetonitrile.

A molecular view of the structure of both complexes is given in Figure 11. Selected bond parameters can be found in Table 1. Crystallographic details can be found in Appendix A. In **K1** the methyl groups were disordered over three orientations. Only the conformer with highest density probability [0.4066(3)] is discussed. For **K2** two conformers with near equal distribution were found were the oxazoline moiety is rotated by about 90° conforming the high flexibility of the S-Phoz ligand. Both palladium(II) atoms are coordinated in a slightly distorted square-planar fashion, with **K2** being slightly more distorted (S2-Pd1-S4 175.21(17)° for **K1** and 167.092(16)° for **K2**. In **K2** the Pd-S bond of the κ^2-S-Phoz ligand is slightly shorter (2.3228(4)) Å than the Pd1-S2 bond length of the κ^1-coordinated S-Phoz ligand (2.3497(4)) Å. All bond distances and bond angles are within the expected range.[57]

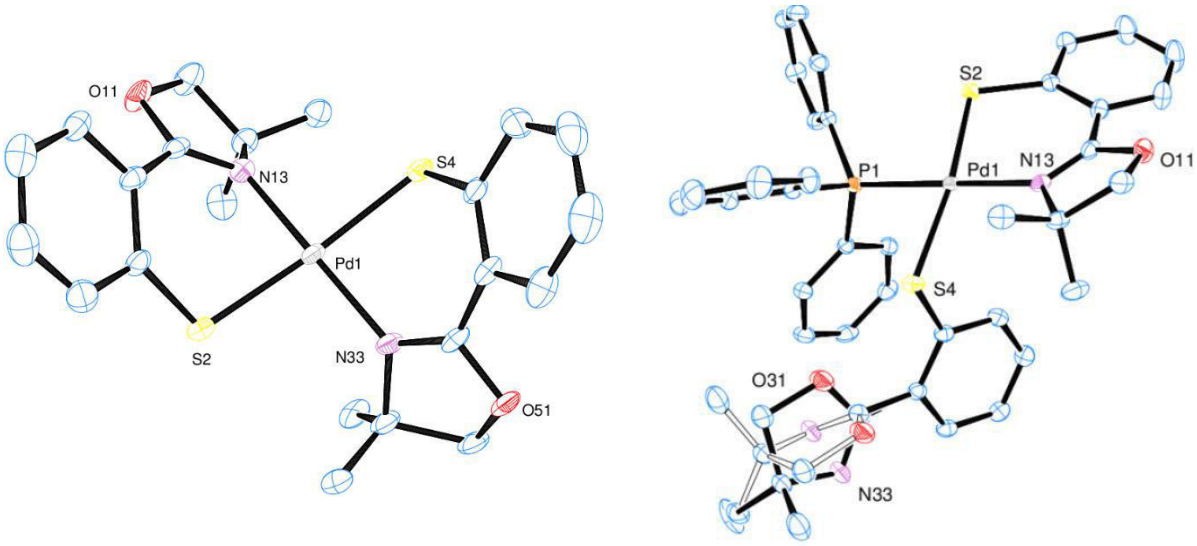

Figure 11: Molecular view of **K1** and **K2.** Both Pd atoms are coordinated in square-planar fashion typical for palladium(II) complexes

Table 1: Selected bond lengths [Å] and angles [°] of complexes **K1** and **K2**

Selected bond length		**Selected bond angles**	
	K1 [Å]		**K1 [°]**
Pd1-N13	2.012(4)	**S4-Pd1-S2**	169.28(6)
Pd1-N33	2.046(4)	**N13-Pd1-N33**	175.21(17)
Pd1-S2	2.3243(14)	**N13-Pd1-S2**	87.32(13)
Pd1-S4	2.3426(14)	**N33-Pd1-S2**	94.05(13)
		N13-Pd1-S4	91.67(13)
		N33-Pd1-S4	87.83(13)
	K2 [Å]		**K2 [°]**
Pd1-N13	2.1168(13)	**N13-Pd1-P1**	170.46(4)
Pd1-P1	2.2343(4)	**S2-Pd1-S4**	167.092(16)
Pd1-S2	2.3228(4)	**N13-Pd1-S2**	87.36(4)
Pd1-S4	2.3497(4)	**P1-Pd1-S2**	86.274(15)
Pd1-O31	5.619	**N13-Pd1-S4**	97.83(4)
Pd1-N33	5.792	**P1-Pd1-S4**	89.876(15)

3.2 Dimeric palladium(II) complexes with a $[Pd_2S_2]$-core

3.2.1 Dimeric palladium (II) complexes: chlorido- and bromido-complexes

The synthesis of **K1** and **K2** underlines the importance of reaction conditions and choice of precursor for the outcome of the reaction.

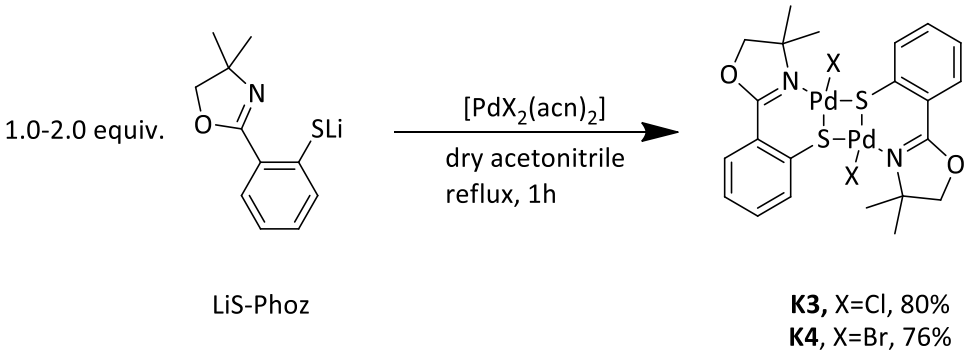

LiS-Phoz

K3, X=Cl, 80%
K4, X=Br, 76%

Scheme 11: Synthesis of dimer $[\{PdCl(S\text{-}Phoz)\}_2]$ (**K3**) and $[\{PdBr(S\text{-}Phoz)\}_2]$ (**K4**)

1.0 equiv. of $[PdCl_2(S\text{-}Phoz)_2]$ or $[PdBr_2(S\text{-}Phoz)_2]$ where reacted in dry acetonitrile under reflux conditions with 1.0 equiv. of LiS-Phoz ligand. A yellow-orange precipitate starts forming within minutes after the addition of LiS-Phoz. After filtration and washing with hot acetonitrile the products $[\{PdCl(S\text{-}Phoz)\}_2]$ (**K3**) and $[\{PdBr(S\text{-}Phoz)\}_2]$ (**K4**) where obtained as orange crystalline powders. **K3** is only slightly soluble in the chlorinated solvents CH_2Cl_2, $CHCl_3$ and $EtCl_2$ and insoluble in most other organic solvents such as benzene, toluene, acetonitrile. **K4** is even less soluble than **K3** with a solubility of 1.68 g/L $CHCl_3$ and also insoluble in other non-chlorinated common laboratory solvents. **K3** and **K4** show similar ^1H NMR spectra in solution which are indicative for the supposed structure. The methyl groups show on sharp singlet in the aliphatic region. The singlet $–CH_2-$ band is significantly broadened in both complexes indicating some dynamic in the complex in solution. One aromatic proton is significantly shifted to lower field (8.86 ppm in $CDCl_3$) when compared to the free ligand (7.92 ppm) due to its proximity to a halide atom.[50] The ^{13}C NMR spectrum is also indicative for the supposed structure of complex **K3**. Due the low solubility of **K4** no ^{13}C NMR spectrum could be recorded. The IR spectra of **K3** and **K4** show C=N resonances at 1607 cm^{-1} (**K3**) and 1611 cm^{-1} (**K4**) very similar to the single C=N resonance of **K1** at 1615 cm^{-1}. EI-MS indicates that the composition of complex **K4** is described as $[\{PdBr(S\text{-}Phoz)\}_2]$ showing the corresponding M^+-peak. Also the occurrence of this peak with the hard ionization EI method refers to a high thermal stability of **K4**. Single crystal X-ray diffraction analysis confirms the dimeric nature of **K3** (vide infra).

The stability of **K3** is shown by the fact that when 2.0 equiv. of LiS-Phoz are used during synthesis still the dimer **K3** was obtained in about 75 % yield, and **K1** was only formed as a by-product in low yields. The preferred formation of the dimer may therefore be caused by its insolubility in the reaction solvent causing precipitation during the reaction. The coordination of the second equivalent of LiS-Phoz to dimer **K3** is therefore hindered.

3.2.2 Dimeric palladium (II) complexes: iodido-complex

The corresponding iodide-complex [{PdI(S-Phoz)}$_2$] (**K5**) could not be synthesized in the same way as **K3** and **K4** since the precursor [PdI$_2$(acn)$_2$] is neither commercially available nor described in literature. Instead the dimeric complex **K3** was reacted with potassium iodide in refluxing acetone for four hours. This lead to the conversion of the orange-yellow [Pd(S-Phoz)Cl]$_2$ **K3** to a red precipitate. After workup the complex [{PdI(S-Phoz)}$_2$] (**K5**) was obtained in near quantitative yield as a red powder.

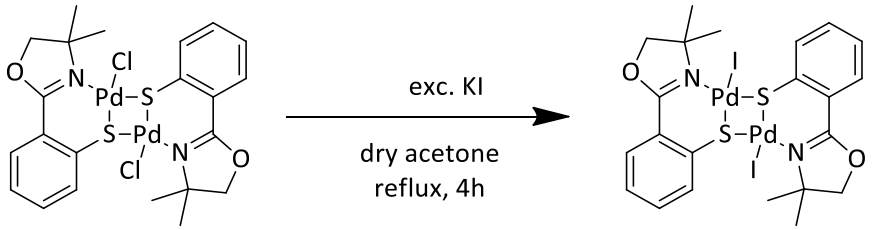

K3 **K5**, 99%

Scheme 12: Synthesis of dimeric complex [{PdI(S-Phoz)}$_2$] (**K5**)

K5 is barely soluble in most common organic solvents, e.g. acetone, benzene and also chlorinated solvents (289 mg/L $CHCl_3$). ^{1}H NMR spectroscopy was possible in $CDCl_3$ with an enhanced number of scans. The ^{1}H NMR spectrum indicates formation of the desired complex. The broad singlet –CH_2- peak was shifted from 4.34 (**K3**) to 3.96 (**K5**) ppm and the singlet –CH_3 was shifted from 1.73 ppm (**K3**) to 1.57 ppm (**K5**). The pattern of the ^{1}H NMR spectrum remained unchanged. No signs of remaining starting material **K3** where found in ^{1}H NMR spectra of **K5**. Recording of ^{13}C NMR spectra was not possible due to low solubility in all available deuterated solvents.

The IR spectrum of **K5** shows a significant C=N resonance at 1612 cm^{-1} being very similar to those from **K3** (1607 cm^{-1}) and **K4** (1611 cm^{-1}) indicating that the ligand is coordinated to the palladium(II) center. EI-MS indicates that the composition of complex **K5** is described as [PdI(S-Phoz)]$_2$ showing the corresponding M$^+$-peak.

3.2.3 Molecular structure of dimeric complexes K3-K5

For complex **K3** single crystals were obtained by dissolving **K3** in $CHCl_3$ and slow cooling. The molecular structure was determined by single crystal X-ray diffraction analysis from these crystals. A molecular view of [{PdCl(S-Phoz)}$_2$] (**K3**) is given in Figure 12. Selected bond parameters can be found in Table 2. All atoms lie on general positions and there are two molecules of **K3** in the unit cell. The binuclear complexes **K3** are arranged around centers of symmetry. The Pd atoms adopt a square-planar coordination mode.

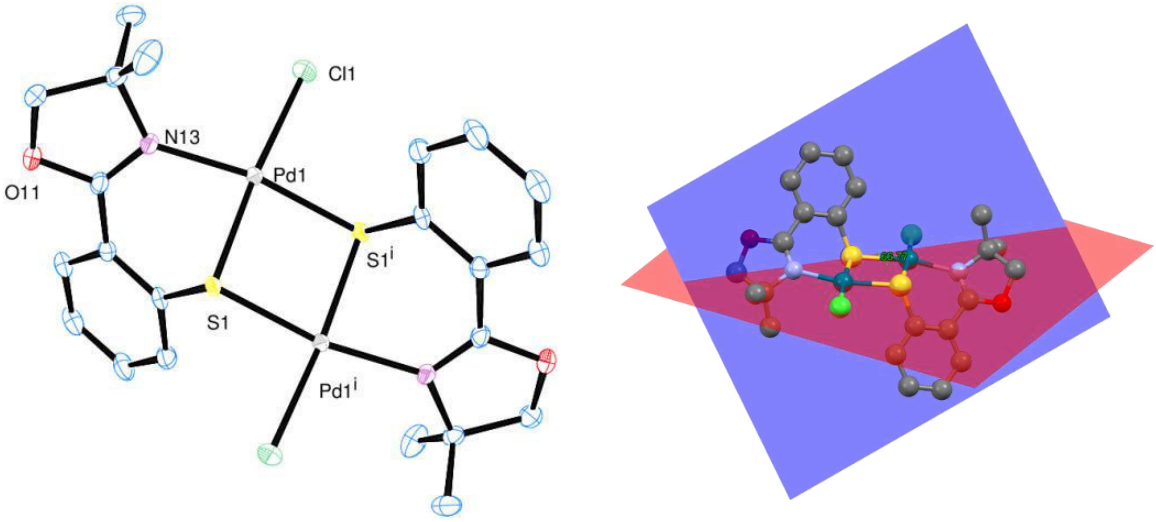

Figure 12 Left: Molecular view of dimeric complex [{PdCl(S-Phoz)}$_2$] (**K3**) Right: Intersection of planes containing the [Pd_2S_2] core and the phenyl moieties of the S-Phoz ligands

Table 2: Selected bond lengths [Å] and angles [°] of complex [{PdCl(S-Phoz)}$_2$] (**K3**)

Selected bond length		**Selected bond angles**	
	K3 [Å]		**K3 [°]**
Pd1-N13	2.065(4)	**S1-Pd1-Cl1**	174.48(5)
Pd1-S1	2.2697(11)	**N13-Pd1-S1**	86.20(11)
Pd1-S1i	2.2861(11)	**N13-Pd1-Cl1**	98.52(11)
Pd1-Cl1	2.3400(12)	**S1i -Pd1-Cl1**	90.90(4)
		N13-Pd1-S1i	168.08(11)
		S1-Pd1-S1i	84.06(4)
		Intersecting angle	65.02(4)

The two palladium centers in **K3** are bridged via the thiophenol sulfur atoms. The formation of soft sulfur bridges is preferred over the chlorine bridged mode even though some steric strain may be induced. All bond distances and bond angles are within the expected range.[74-77]

The exact molecular structure of **K4** and **K5** was not determined. Basically both are assumed to adopt similar structures. However with increasing atomic number of the halide it gets softer and larger allowing more flexibility in bonding angles. Owing to the VSEPR-principle the possibility of bridging two palladium centers gets higher when going from Cl < Br < I. However DFT calculations (PBE0/def2-TZVP+D3, see computational section in the experimental part for details on structure optimization) suggest that for the whole series **K3-K5** the μ-S bridged mode is stabilized by about 60 kJ/mol, when compared to the μ-Cl/ μ-Br/μ-I bridged mode. Therefore all complexes are referred to as μ-S bridged throughout this thesis although the structure of **K4** and **K5** was not validated by single crystal X-ray diffraction analysis. The corresponding energies, energy differences and dipole moments can be found in Appendix B1.

3.3 Synthesis of monomeric complexes of the form [PdX(S-Phoz)L] ,L=donor ligand

For the preparation of mononuclear complexes from **K3-K5**, cleavage of the binuclear complexes has to occur, which should be possible using a suitable donor molecule (see chapter 1.2.3). As N-heterocyclic carbenes (NHCs) are known to be excellent σ-donors they were tested for this task. In the synthesis of the monomeric NHC-complexes **K6-K8** shown in Scheme 13 it is advantageous to use a slight excess of the dimeric complexes **K3-K5** due to their insolubility in toluene. As the free N-heterocyclic carbene is sensitive to moisture and air these reactions had to be carried out under an inert atmosphere (Schlenk-conditions or glovebox).

3.3.1 Synthesis of monomeric complexes of the form [PdX(S-Phoz)(IMes)], X=Cl,Br,I

As N-heterocyclic carbene (NHC) ligands have been successfully applied in palladium catalysis in the last few years the synthesis of palladium complexes with the S-Phoz ligand and an N-heterocyclic carbene was attempted. The bulky 1,3-bis(2,4,6-trimethylphenyl)-imidazolium,1,3-bis(2,4,6-trimethylphenyl)imidazol-2-ylidene (“IMes”) carbene was chosen as ligand of choice due to its availability and high steric bulk.

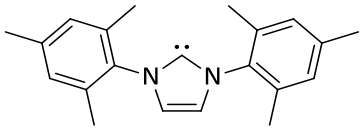

Figure 13: The “IMes” N-heterocyclic carbene ligand

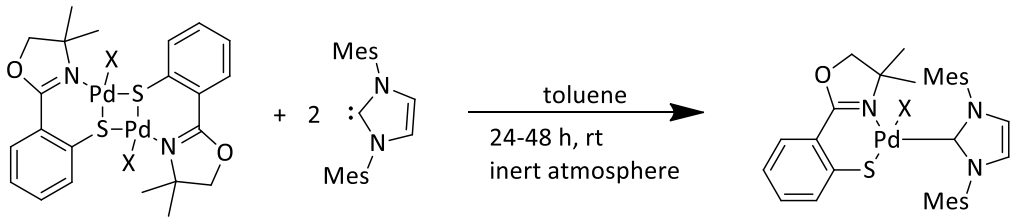

K3 X=Cl
K4 X=Br
K5 X=I

K6 X=Cl, 68%
K7 X=Br, 91%
K8 X=I, 88%

Scheme 13: Synthesis of complexes [PdX(S-Phoz)(IMes)] **K6** (X=Cl), **K7** (X=Br) and **K8** (X=I)

Dimers **K3-K5** (1.0 equiv.) were reacted with 1.0 equiv. IMes in toluene in a glovebox. The solutions were stirred for 24 h and then the solvent removed in vacuo. For purification the compounds **K6-K8** dissolved in benzene, filtered and crystallized. Complexes **K6-K8** were obtained in good to excellent yields as yellow (**K6**), yellow-orange (**K7**) and orange (**K8**) crystals.

The complexes [PdCl(S-Phoz)(IMes)] (**K6**), [PdBr(S-Phoz)(IMes)] (**K7**) and [PdI(S-Phoz)(IMes)] (**K8**) are soluble in aromatic solvents (toluene, benzene), polar solvents (acetonitrile), chlorinated solvents ($CHCl_3$, CH_2Cl_2) and only slightly soluble in apolar aprotic solvents (pentane, heptane). **K6-K8** were analyzed via ^1H NMR and ^{13}C NMR spectroscopy. ^1H NMR spectra of **K6-K8** showing the same pattern with slightly different shifts indicate that all complexes formed are of similar structure. The ^1H NMR spectrum shows four distinct, sharp $–CH_3$ singlets in the aliphatic region for all three compounds **K6-K8**. The $–CH_2$- resonances are located at 3.15 ppm (**K6**), 3.18 ppm (**K7**) and a broad band at 3.20 ppm (**K8**). The second distinct feature seen in all three complexes is the N-CH=CH-N proton shift, interestingly showing a singlet (not doublet) at 6.19 ppm (**K6**), 6.21 ppm (**K7**) and 6.20 ppm (**K8**). Also ^{13}C NMR spectra confirm the related structure of **K6-K8**. IR spectra show the typical C=N resonances at 1610 cm^{-1} (**K6**), 1612 cm^{-1} (**K7**) and 1614 cm^{-1} (**K8**). The solid state structure of complex **K6** was confirmed by single crystal X-ray diffraction analysis (vide infra). For the corresponding bromo- and iodo-complexes **K7** and **K8** no solid state structures were obtained.

3.3.2 Synthesis of monomeric complex [Pd(CF_3CO_2)(S-Phoz)(IMes)]·$AgCF_3CO_2$

In addition to the three different halide complexes **K6-K8** a complex with a weakly coordinating ligand was of interest in order to further test catalysis and spectroscopic properties of the palladium center coordinated by the S-Phoz ligand. Therefore the halide ligand was substituted with the weakly coordinating trifluoroacetate anion, which also is a good leaving group resulting in often very active pre-

catalysts. A simple salt metathesis reaction with $Ag(CF_3CO_2)$ and complex **K6** was envisioned to replace the chloro with the trifluoroacetate ligand.

K6 (1.0 equiv.) was reacted with 3.0 equiv. of $AgCF_3CO_2$ in acetonitrile at reflux conditions under exclusion of light. Excess silver trifluoroacetate was used to ensure complete conversion of complex **K6.** After 6 hours AgCl was filtered off and solvent removed. To remove excess $AgCF_3CO_2$ the residue was dissolved in benzene, filtered and the solvent again removed in vacuo. The product is obtained in good yield as shown in Scheme 14 as a pale yellow powder.

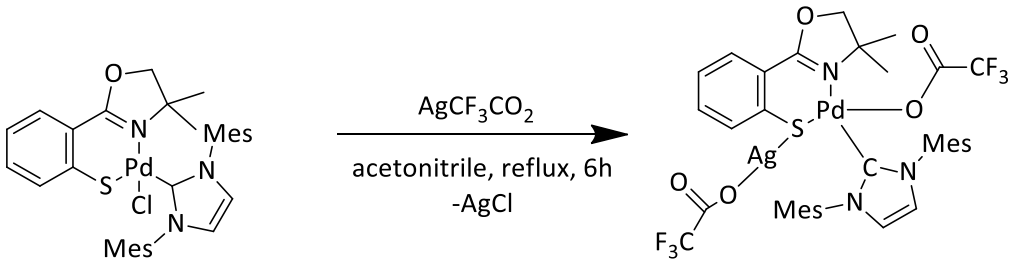

K6 **K9**, 86%

Scheme 14: Synthesis of complex **K9** from **K6**

Complex **K9** is soluble in chlorinated solvents (CH_2Cl_2, $CHCl_3$), aromatic solvents (toluene, benzene) and other polar solvents (acetonitrile, DMSO). It is only slightly soluble in apolar solvents like pentane or heptane. ^{1}H NMR, ^{13}C NMR and ^{19}F NMR spectroscopy were employed for characterization. The ^{19}F NMR spectrum shows two peaks at 72.94 ppm and 72.62 ppm, indicating that both $CF_3CO_2^-$ groups are very similar in solution. The ^{1}H NMR and ^{13}C NMR spectra show the same pattern as their related complexes **K6-K8** with significant broadening of the $-CH_3$ peaks. The $-CH_2-$ group is shifted to significant lower field at 3.61 ppm when compared to starting material **K6**. No residual peaks of **K6** could be found in the ^{1}H NMR spectrum. The IR spectrum of **K9** shows the resonance of the C=N bond at 1626 cm^{-1}. The solid state structure of **K9** was confirmed by single crystal X-ray diffraction analysis.

The synthesis of a silver-free adduct by employing 1.0 equiv. $Ag(CF_3CO_2)$ was not successful and lead to a product with an UV/Vis spectrum indicating that silver(I) still coordinates to the thiophenol sulfur atom. It is therefore assumed that the complex is also capable of coordinating quite insoluble silver salt, e.g. AgCl.

3.3.3 Synthesis of monomeric complexes of the form [PdCl(S-Phoz)(EPh_3)], E=P, As, Sb

In order to compare the strong σ-donor IMes to typical σ-donor/π-acceptor ligands dimeric **K3** was also reacted with triphenyl derivatives of group 15 elements (EPh_3, E=P, As, Sb).

Dimer **K3** (1.0 equiv.) was reacted with 0.95-1.00 equiv. of the corresponding donor (PPh_3, $AsPh_3$, $SbPh_3$) in chloroform at room temperature. After the given reaction time (indicated in Scheme 15) the suspension was filtered through celite and the solvent removed in vacuo. The residue was dissolved in benzene and filtrated to remove excess starting material **K3**. After removal of solvents the complexes **K10-K12** are obtained in good to excellent yields as orange-red (**K10**) and deep red (**K11, K12**) powders.

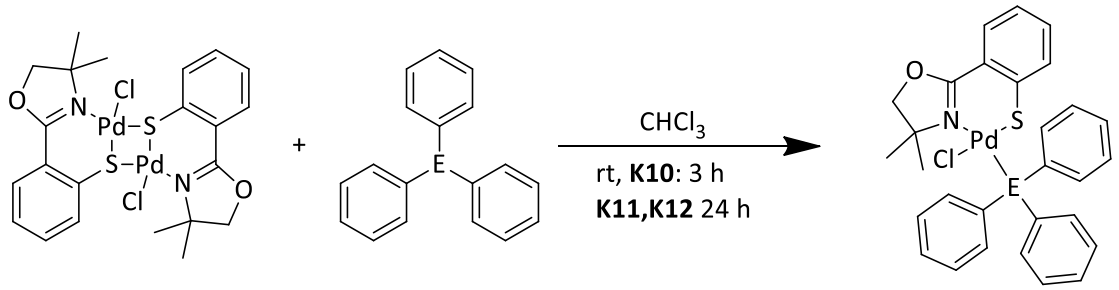

K3

K10 E=P, 95 %
K11 E=As, 78 %
K12 E=Sb, 83 %

Scheme 15: Synthesis of complexes **K10-K12**

A slight excess of the starting material **K3** was used in all reactions to ensure that the group-15 donor is coordinated during reaction. Excess **K3** can be removed by filtration after reaction, while removing excess PPh_3/$AsPh_3$/$SbPh_3$ was only possible by subsequent washing and resulted in overall lower yields. This method proved to yield product **K10** in nearly quantitative yield after 3 h and **K11** and **K12** in acceptable yields after 24 h. The obtained products were washed with pentane or precipitated from benzene with heptane if necessary.

Complexes **K10-K12** are soluble in halogenated solvents ($CHCl_3$, CH_2Cl_2), aromatic solvents (toluene, benzene) but are not soluble in apolar solvent (diethyl ether, pentane, and heptane). ^{1}H NMR, ^{13}C NMR and ^{31}P NMR spectra (only for complex **K10**) were employed to characterize complexes **K10-K12**. The $–CH_3$ and $–CH_2$- groups are again indicative in the ^{1}H NMR spectra showing the expected pattern. The methylene groups are located at 4.28 ppm (**K10**), 3.46 ppm (**K11**) and 3.45 ppm (**K12**). IR spectroscopy of **K10-K12** showed significant resonances for the C=N band at 1615 cm^{-1} (**K10**), 1610 cm^{-1} (**K11**) and 1612 cm^{-1} (**K12**)

indicating similar structures of all three complexes. The molecular structure of complex **K10** was confirmed by single crystal X-ray diffraction analysis. The complexes **K11** and **K12** are assumed to adopt the same structure. The similarity of configuration of **K11** and **K12** is supported by the ^{1}H NMR and NIR/IR data (see Chapter 4) obtained for complexes **K10-K12**.

3.3.4 Molecular structures of complexes of the form [PdX(S-Phoz)L] ,L=donor ligand

Singles crystals of complexes **K6, K9** and **K10** were obtained by slow evaporation of a saturated solution of the corresponding complex in benzene. The molecular structure was determined by X-ray diffraction analysis from these crystals. A molecular view of **K6** and **K10** is given in Figure 14. Selected bond parameters can be found in Table 3.

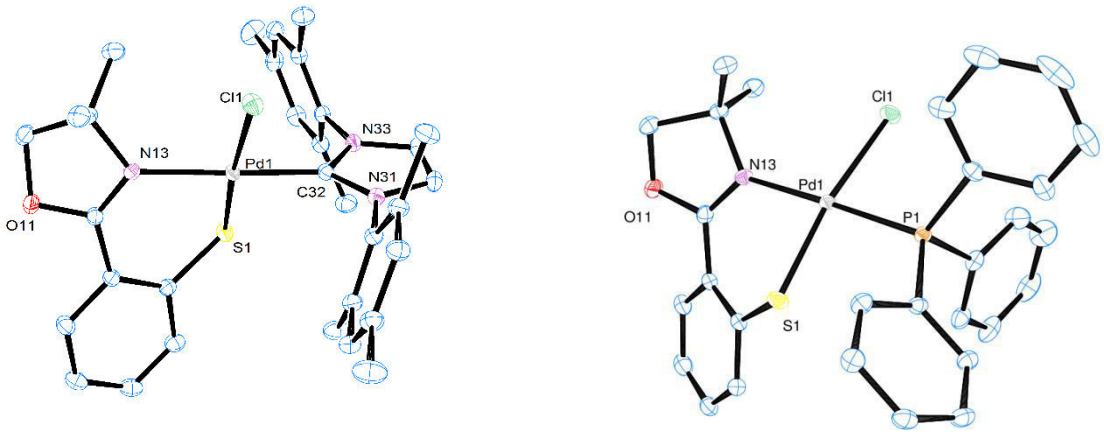

Figure 14: Molecular view of complexes **K6** and **K10**

K6 and **K10** show the typical square-planar coordination geometry of palladium(II) complexes. The S-Pd-Cl bond angle is slightly distorted in both complexes from an ideal 180° angle to 174.739(10)° (**K6**) and 171.306(17)° (**K10**) respectively. The Pd-S bond of both complexes is shortened when compared to complex **K1**. It measures 2.2706(3) Å (**K6**) and 2.2803(4) Å (**K10**) while the Pd1-S1 bond length is at 2.3228(4) in *trans*-**K1.** This is to be expected as the *trans*-effect of sulfur is larger than that of the chloride-ligand. All bond lengths and angles described are within the range of previously published [PdClSN(PPh_3)] and [PdClS(NHC)] type compounds.[10,11,13,35,36,47,78-84]

Complex **K9** consists of a square-planar coordinated palladium center and a linear coordinated silver center. The silver and palladium atom are bridged through the sulfur of the thiophenyl-moiety of the S-Phoz ligand with an angle of 162.89(8)° slightly distorted from the linear coordination. The Pd-S bond (2.2648(5) Å) is slightly shortened when compared to *trans*-**K1** (2.3228(4) Å) and is as expected comparable

to **K6** and **K10**. The $CF_3CO_2^-$ groups are bound in a κ^1-mode to the Ag and Pd center. The Pd1-Ag1 bond distance (3.5145(3) Å) is quite long when compared to X-ray data of another Pd-S-Ag complex of [{Pd(RPPh$_2$)$_2$(SR')}(μ-SR'){Ag(PPh$_3$)}] structure which has a Pd-Ag bond length of 2.950 Å, indicating that the interaction between the Pd and Ag atom is only weak in complex **K9**.[85] Other bond lengths and angles described are within the range of previously published monomeric [Pd-S-Ag] type compounds.[85,86,87]

Table 3: Selected bond lengths [Å] and bond angles [°] of **K6**, **K9** and **K10**

Selected bond length			**Selected bond angles**		
	K6 [Å]	**K9[a] [Å]**		**K6 [°]**	**K9[a] [°]**
Pd1-C32	1.9794(10)	1.9961(7)	**C32-Pd1-N13**	175.95(4)	172.78(9)
Pd1-N13	2.0946(9)	2.1019(7)	**S1-Pd1-Cl/O1**	174.739(10)	176.67(6)
Pd1-S1	2.2706(3)	2.2648(5)	**C32-Pd1-S1**	87.70(3)	87.36(0)
Pd1-Cl/O1	2.3559(3)	2.0754(2)	**N13-Pd1-S1**	89.75(2)	89.76(9)
Pd1-Ag1		3.5145(3)	**C32-Pd1-Cl/O1**	87.08(3)	89.47(0)
Ag1-S1		2.3853(4)	**N13-Pd1-Cl/O1**	95.49(2)	93.26(3)
Ag1-O2		2.1501(5)	**Pd1-S1-Ag1**		98.15(4)
			S1-Ag1-O2		162.89(8)
	K10 [Å]			**K10 [°]**	
Pd1-N13	2.1040(14)		**S1-Pd1-Cl1**	171.306(17)	
Pd1-S1	2.2803(4)		**N13-Pd1-S1**	89.79(4)	
Pd1-P1	2.2467(4)		**N13-Pd1-Cl1**	95.56(4)	
Pd1-Cl1	2.3620(4)		**N13-Pd1-P1**	177.74(4)	
			P1-Pd1-S1	89.094(16)	
			P1-Pd1-Cl1	85.32315	

[a] The values of **K9** are preliminary and therefore subject to minor changes

3.4 Discussion of complex synthesis

The novel palladium complexes, containing the S-Phoz ligand, **K1-K12** were successfully synthesized as described above. **K1** and **K2** showed a high fluxionality in solution, indicated by dynamic equilibria of isomers in solution, as detected by NMR spectroscopy. Therefore it is supposed that the oxazoline moiety of the S-Phoz ligand is only weakly coordinated to the palladium center.

The same precursor that lead to the parent [Pd(S-Phoz)$_2$] (**K1)** also yielded the dimeric product **K3** by changing the reaction conditions (acetonitrile instead of toluene, increasing reaction temperature from RT to reflux conditions). It should be mentioned that from all the synthesized complexes only the bromo substituted complexes **K4** and **K8** displayed an M^+-peak in EI-MS. This could indicate an increased thermal

and overall stability of the Pd-Br bond even under harsh conditions. All three dimeric complexes **K3-K5** could be further split into monomeric complexes by reaction with a sufficient donor ligand. The usage of the N-heterocyclic carbene ligand IMes or triphenylphosphine proved to be sufficient for this task. Starting from the dimeric chloro complex a direct synthesis of the corresponding monomeric IMes complex (**K6**) and triphenylphosphine complex (**K10**) was straightforward. The NHC ligand (IMes) is considered to be a pure σ-donor ligand, with essentially no back-bonding capability. Even though it provides a strong ligand field making this system a good starting point to probe the donor/ligand-field strength of other typical ligands, e.g. halogenides. Therefore the complete series of halide (IMes)-complexes **K6** (X=Cl), **K7** (X=Br^-) and **K8** (X=I^-) were synthesized in order gain further insights. Also an attempt to synthesize the corresponding complex **K9** with X=$CF_3CO_2^-$ was made but did not yield the complex of type [Pd(CF_3CO_2)(S-Phoz)(IMes)]. The X-ray structure determination revealed that complex **K9**, [Pd(CF_3CO_2)(S-Phoz)(IMes)]·Ag(CF_3CO_2), is a heterodinuclear complex with a molecule of $AgCF_3CO_2$ attached to the thiophenol moiety of the S-Phoz ligand. This result was unexpected as the IMes ligand provides large steric bulk, usually preventing further aggregation. The Pd-S(R)-Ag structural motive is rather uncommon in current coordination chemistry. A literature research showed that only five complexes featuring the Pd-S-Ag motive are known (dimers or higher aggregates were omitted).[85,86,87] Bimetallic complexes bearing silver and palladium atoms are highly promising as luminescents.[85] The luminescent properties of these complexes profits from the interaction between the metal centers and the soft sulfur moieties. Therefore large number of metal-metal, metal-ligand or ligand-metal transition becomes possible. Also spin-forbidden transition (singlet-triplet transitions) get more likely in the presence of two 4d metal centers and their quite high spin-orbit coupling constants.[85] The bimetallic complex **K9** synthesized in this work however does not exhibit any luminescence properties. In fact it is the complex with the weakest absorption of all synthesized compounds (vide infra), showing no signs of phosphorescence or fluorescence. This can be rationalized by the fact that the Pd and Ag metal centers are quite far away from each other in contrast to the complexes discussed above and therefore behave like two separate coordinated metal centers without interacting with each other.

4. Suzuki-Miyaura coupling catalyzed by [Pd(S-Phoz)]-type complexes

4.1 Suzuki-Miyaura couplings

To test the catalytic activity of complexes **K1** and **K3-K12** the reaction shown in Scheme 16 was used. The electron-withdrawing acetyl group in para position activates the bromide making it more reactive towards Suzuki-Miyaura couplings.

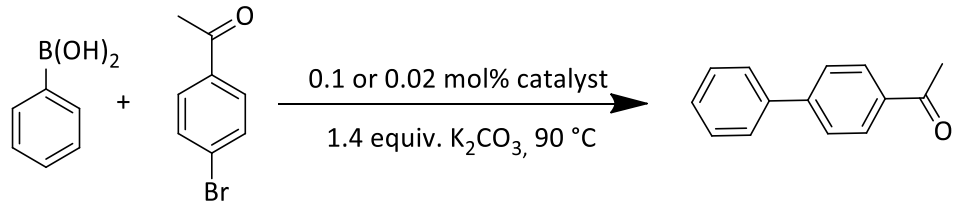

1.4 equiv. 1.0 equiv.

Scheme 16: Test reaction to screen for potential catalysts.

Under standard conditions 1 mmol of 4-bromoacetophenone was reacted with phenylboronic acid (1.4 mmol) in the presence of 0.1 mol% of the respective palladium complex in 5 ml of water at 90 °C. Potassium carbonate (1.4 mmol) was added as base. The results of this screening are given in Table 4.

After 24 h reaction time all tested catalysts with the exception of **K1** showed catalytic activity in water, and most catalysts were able to deliver full conversion with a catalyst loading of 0.1 mol% under the reaction conditions. To further discriminate between catalysts the conditions were changed to a reaction time of 3 h and the catalyst loading was reduced to 0.02 mol%. The other conditions were kept the same. Under these reaction conditions the dimeric complexes **K3** and **K4** display high conversions to product (90 and 97% yield respectively). For these two complexes the reaction time was even further reduced to 1.5 h because of their high observed reactivity. Also complex **K10** (L=PPh_3) reaches a product yield of >98% after 3 h.

The most active catalysts (**K3**, **K4** and **K10**) reach an average turn-over frequency (TOF) of approx. 1600 h^{-1} per palladium atom, which is nearly one turnover every two seconds. The turn-over number of a single catalyst molecule **K10** (TON) is determined to be approx. 5000.[88]

$$TOF = \frac{mol\ substrate}{mol\ catalyst * time\ [h]} \qquad \text{Eq. 1}$$

$$TON = \frac{mol\ substrate}{mol\ catalyst} \qquad \text{Eq. 2}$$

Table 4: Suzuki-Miyaura cross coupling of phenylboronic acid with p-bromoacetophenone

Catalyst	Loading (mol%)[a]	Solvent	Time(h)	Conversion (%)	TOF[b]	TON[b]
K1	0.1	H_2O	24 h	2 %	-	20
K1	0.1	dioxan	24 h	0 %	-	-
K3	0.1	H_2O	24 h	> 98 %	42	1000
K3	0.1	dioxan	24 h	34 %	14	340
K3	0.02	H_2O	3 h	> 98 %	833	2500
K3	0.02	H_2O	1.5 h	90 %	1500	4500
K4	0.1	H_2O	24 h	> 98 %[a]	42	1000
K4	0.1	dioxan	24 h	50 %	21	500
K4	0.02	H_2O	3 h	> 98 %	833	2500
K4	0.02	H_2O	1.5 h	97 %	1667	5000
K5	0.02	H_2O	3 h	35 %	583	1750
K6	0.1	H_2O	24 h	> 98 %	42	1000
K6	0.1	dioxan	24 h	61 %	42	1000
K6	0.02	H_2O	3 h	57 %	950	2850
K7	0.1	H_2O	24 h	> 98 %	42	1000
K7	0.1	dioxan	24 h	48 %	42	1000
K7	0.02	H_2O	3 h	50 %	833	2500
K8	0.02	H_2O	3 h	87 %	1450	4350
K9	0.02	H_2O	3 h	58 %	967	2900
K10	0.1	H_2O	24 h	> 98 %	42	1000
K10	0.1	dioxan	24 h	20 %	42	1000
K10	0.02	H_2O	3 h	> 98 %	1667	5000
K11	0.02	H_2O	3 h	60 %	1000	3000
K12	0.02	H_2O	3 h	20 %	333	1000

a) mol% refer to mol of catalyst, not mol% Pd. [b)] TON and TOF are calculated per Pd center. General procedure: 1.0 mmol p-bromoacetophenone was reacted with 1.4 equiv. of phenylboronic acid and 1.4 equiv. of K_2CO_3 in 5 ml solvent at 90 °C. Reaction yields and times in H_2O and dioxan given. Conversion was determined using standard GC-MS techniques.

4.2 Discussion of catalytic activity of the synthesized Pd(S-Phoz) complexes

In the investigated Suzuki-Miyaura coupling complexes [{PdCl(S-Phoz)}$_2$] (**K3**), [{PdBr(S-Phoz)}$_2$] (**K4**) and complex [PdCl(S-Phoz)(PPh_3)] (**K10)** show the highest efficiency in turn-over frequency per palladium center. All three exhibit turn-over frequencies of up to 1600 h^{-1} per palladium atom. Surprisingly the PPh_3-complex **K10** exhibited better catalytic performance that its NHC counterpart **K6**. PPh_3 is assumed to be a weaker σ-donors but better π-acceptors than N-heterocyclic carbenes like IMes, and often the latter did show higher catalytic activity in many precious-metal catalyzed reactions. Also the influence of the halogenide ions is surprising. Chlorine and bromine complexes behave quite similar while the iodine complex is strikingly different. It can either decrease catalytic activity (**K3/K4 – K5**) or increase it (**K6/K7 – K8**). So the influence of the anion (as it is assumed that the halogenide will be a good leaving group in water during catalysis) can be quite important as stated by Amatore and Jutand (see chapter 1.4).[62,64]

The catalytic activity of group-15 donor ligands [PdCl(S-Phoz)(EPh_3)] (**K10-K12**) decreases in the order PPh_3 > $AsPh_3$ > $SbPh_3$. This can be rationalized by enhanced donor ability of PPh_3 when compared to $AsPh_3$ and $SbPh_3$. Also the *trans*-effect is decreasing in the row PPh_3 >> $AsPh_3$ > $SbPh_3$ therefore maybe taking influence in the rate limiting step during synthesis.[89]

The catalytic performance is comparable to other known anionic sulfur-containing complexes of similar structure reaching TOFs of about 1600 h^{-1} in water. Comparable catalysts show TOFs of a few 100 to 4500 h^{-1} in water. [36,45,46] In other solvents sulfur-bearing palladium catalysts (although sulfur is often neutral and not anionic) can reach TOFs of up to 15.000 h^{-1} for the same coupling reaction as given in Scheme 16. The highest turn-over frequency obtained in water up to date was for the reaction of 4-nitro-1-bromobenzene with phenylboronic acid where [$PdCl_2$(dppf)] reaches a turn-over frequency of about 16000 h^{-1}.[4] The highest obtained TOF values in aqueous solvents were obtained for biarylphosphine ligands giving TOFs of up to 184000 h^{-1} in a 1:1 mixture of acetonitrile:water.[39]

5. UV/VIS/NIR spectroscopy and ab-initio theoretical calculation of complex geometries and electronic excitation spectra

5.1 DFT methods

DFT is a convenient tool nowadays when it comes to transition metal complexes. The "real-life" complexes that are used as catalyst comprise 56 (**K3**) – 75 (**K6**) atoms making them very demanding in terms of calculation power required. Most Hartree-Fock wave-function based methods can therefore not be applied, as their computational scaling is too steep with respect to basis functions/number of atoms (pure HF: N^{3-5}; MP2: N^5, CCSD: N^6). DFT bypasses this problem, as the computational effort scales near-linearly with computational requirements (about 3N, in realty as memory gets low more like $N^{2.5}$).

5.2 Assessment of density functionals

The geometry was assessed by comparison of calculated data with the crystal structures of complexes **K3** and **K6**. For all geometry optimizations the crystal structure was used as starting point and no restraints were put on the structure.

The structures of complexes **K3** and **K6** were optimized with the functionals BLYP, PBE, BP86, PW91, TPSS, B3LYP, PBE0, TPSSh and M06. The main criterion was placed on bonding lengths and bonding angles between atoms. Also the angle between the two intersecting planes of the PdL_4-plane and the plane consisting of the phenyl ring of the S-Phoz ligand was measured for **K3**. For **K6** the angle between the intersecting planes of both Mes-groups und the intersecting angle of the imidazole-plane with the PdL_4-plane was used. Calculations were done with the def2-SVP, def2-TZVP, def2-SVP/D3 and def2-TZVP/D3 basis set scheme. The results with def2-TZVP basis set and D3 dispersion correction are shown in Table 5 and Table 6. For detailed data of calculations with def2-SVP, def2-SVP/D3 and def2-TZVP basis sets see Table 13-Table 18 in appendix B2. The quality of obtained geometries improved slightly by using the larger triple-ζ def2-TZVP basis compared to the double-ζ def2-SVP basis set. This is especially true for the M06 method, which profits most from the step-up in basis set size. PBE0 profits from error cancelation between basis-set incompleteness error and the error of the method. Therefore the PBE0/def2-SVP yields slightly better bonding values than the PBE0/def2-TZVP combination. PBE0, TPSSh and TPSS perform best when it comes to pure bonding distances and bonding angles. When computation time is of concern, the combination of a triple-ζ basis set with TPSS and RI-approximation is the best compromise even for larger complexes like **K3** and **K6**. The pure density functionals BLYP, PBE, BP86 and TPSS compare quite well to the hybrid functionals B3LYP, PBE0, TPSSH and M06. The pure DFT functionals only yield slightly worse

results than the very good PBE0 and TPSSh hybrid functionals and even better values than the popular B3LYP hybrid functional. For bond lengths the more expensive hybrid functionals B3LYP and M06 perform worst with both basis set combinations used (def2-SVP and def2-TZVP). Nevertheless even for those two functionals (M06 and B3LYP) the overall error in bond lengths is acceptable. Changing the basis set size from double-ζ to triple-ζ decreases the relative error in the Pd-S bond length by about 50 %, which is significant. The relative error of the Pd-Cl bond length is also reduced by about 50 %. However the absolute error between measured and calculated bond length is already small (< 1 %) with a double-ζ basis set so the improvement is not that drastic for this bond. Overall bond lengths are described reasonably well by pure density functionals as well as by hybrid functionals. The largest errors in the performed calculations are for dihedral angles. These angles deviates by about 8-18 % (Pd_2S_2/thiophenyl intersecting angle in **K3**, Mes-Mes intersecting angle in **K6**) and for every functional used, except the M06 functional that produces no significant error (< 0.1 % with triple-ζ quality basis set for the Pd_2S_2/thiophenyl intersecting angle in **K3**). A step-up in basis set size only has minor influence on the phenyl-[Pd_2S_2] and Mes-Mes intersecting angles however. The empirical pair-wise dispersion corrections lead to a significant improvement in bonding angles in complex **K3** when compared to the crystal structure. The remaining error of intersecting angles is also reduced for nearly all tested functionals (see Table 5 and Table 14). Bonding lengths nevertheless show a small increase in precision when dispersion correction is included. PBE0 overall outperforms all other functionals, especially when a solid triple-ζ basis set is applied. For PBE0 (and also most other functionals) the trends in errors of bonding lengths become more uniform when the empirical pairwise dispersion correction is applied. The pairwise dispersion correction from Grimme again increases the performance for most tasks significantly without adding substantial cost to calculation time.[90,91]

To conclude from the results in Table 5 and Table 6 the lowest error was obtained for the PBE0 functional in combination with the def2-TZVP basis set and dispersion correction. This method was therefore used to optimize the geometries of complexes **K3-K12**.

Table 5: unsigned errors from the geometry optimization of [Pd(S-Phoz)Cl]$_2$, **K3**, with a given functional and the def2-TZVP / ECP28MWB basis set and pairwise dispersion correction. Deviations are given in % relative to crystal structure.

def2-TZVP/D3	BLYP	PBE	PW91	TPSS	BP86	B3LYP	PBE0	TPSSh	M06
Pd1-S1	2,44%	0,91%	-	1,01%	0,94%	1,66%	0,31%	0,19%	-
Pd1-Cl1	1,62%	0,33%	-	0,15%	0,30%	0,63%	0,58%	0,69%	-
Pd1-N1	1,84%	0,72%	-	0,38%	0,35%	1,19%	0,11%	0,45%	-
S1-C1	0,89%	0,16%	-	0,13%	0,21%	0,01%	0,68%	0,57%	-
S1-Pd1-S2	0,05%	0,76%	-	0,07%	0,40%	0,23%	0,78%	0,92%	-
Pd2S2-C6H5-plane	4,95%	7,27%	-	6,00%	5,12%	4,84%	5,86%	3,66%	-
	BLYP	PBE	PW91	TPSS	BP86	B3LYP	PBE0	TPSSh	M06
MUE	1,97%	0,58%	--	0,35%	0,44%	0,74%	0,49%	0,56%	--

Table 6: unsigned errors from the geometry optimization of [PdCl(S-Phoz)(IMes)], **K6**, with a given functional and the def2-TZVP / ECP28MWB basis set and pairwise dispersion correction. Deviations are given in % relative to crystal structure

def2-TZVP/D3	BLYP	PBE	PW91	TPSS	BP86	B3LYP	PBE0	TPSSh	M06
Pd1-S1	2,42%	0,84%	-	1,04%	0,89%	1,74%	0,43%	0,16%	-
Pd1-Cl1	2,34%	0,86%	-	0,63%	0,78%	1,36%	0,09%	0,20%	-
Pd1-C1	0,72%	0,12%	-	0,13%	0,43%	0,62%	0,33%	0,67%	-
Pd1-N1	2,11%	0,96%	-	0,27%	0,45%	1,13%	0,32%	0,75%	-
S1-C1	0,92%	0,08%	-	0,24%	0,21%	0,52%	0,36%	0,18%	-
N-Pd-Cl angle	0,16%	0,01%	-	0,15%	0,11%	1,80%	0,17%	0,52%	-
Mes-Mes plane	17,94%	10,98%	-	21,14%	24,14%	13,55%	13,19%	27,67%	-
IMes-Pd plane	3,62%	4,04%	-	2,14%	1,10%	9,25%	2,29%	8,25%	-
	BLYP	PBE	PW91	TPSS	BP86	B3LYP	PBE0	TPSSh	M06
MUE	3,78%	2,24%	--	3,22%	3,51%	3,74%	2,15%	4,80%	--

5.3 UV/Vis/NIR spectroscopy

For all complexes bearing one sulfur moiety (**K3-K12**) UV/Vis/NIR spectra were measured in solid state, where absorptions from solvent are avoided. Reflectance spectra were recorded in a range from 250 nm to 2500 nm (40000 cm^{-1} to 4000 cm^{-1} respectively) in reflectance mode. A minimum in reflectance therefore correspond to a maximum in absorption of the corresponding compound. The obtained spectra therefore show an inverse picture of more common used absorption UV/Vis spectra. Other than that reflectance spectra can be treated in the same way as standard absorption spectra.

Due to the broad range these spectra can therefore yield information about IR overtones as well as electronic excitations of the corresponding complexes. Measured spectra of complexes **K3-K12** are shown in Figure 15-15.

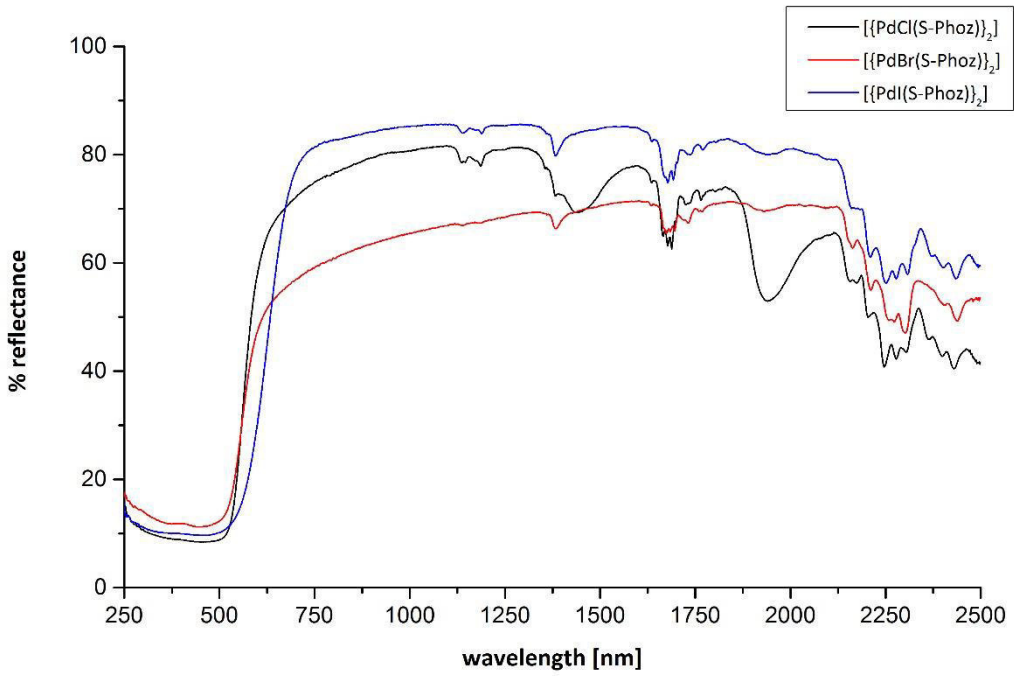

Figure 15: Reflectance spectra of dimeric complexes [{PdX(S-Phoz)}$_2$] (**K3-K5)**

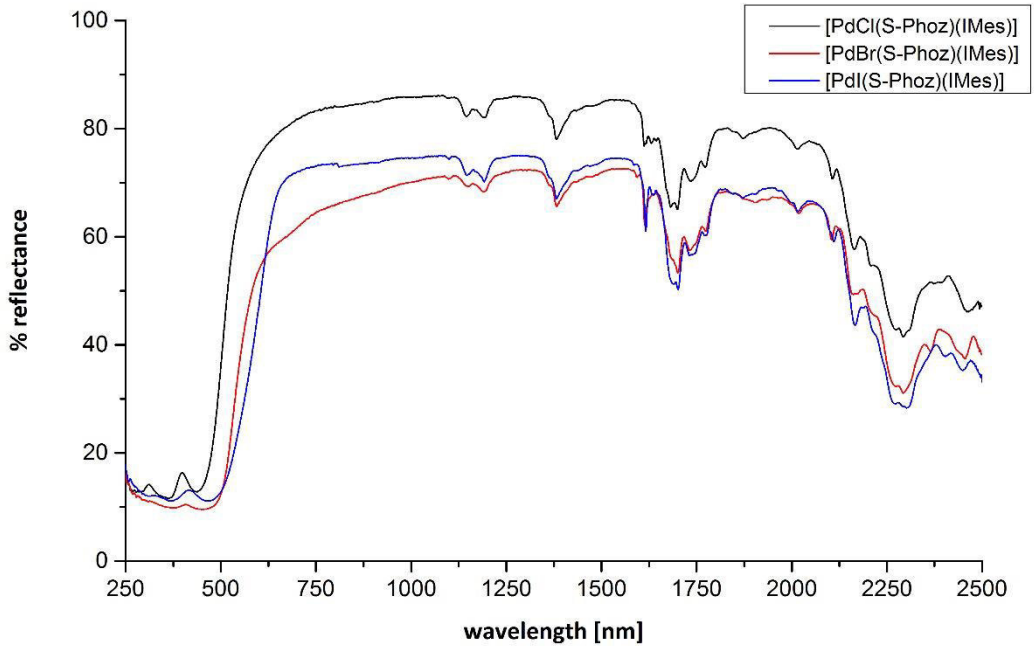

Figure 16: Reflectance spectra of complexes [PdX(S-Phoz)(IMes)] (**K6-K8**)

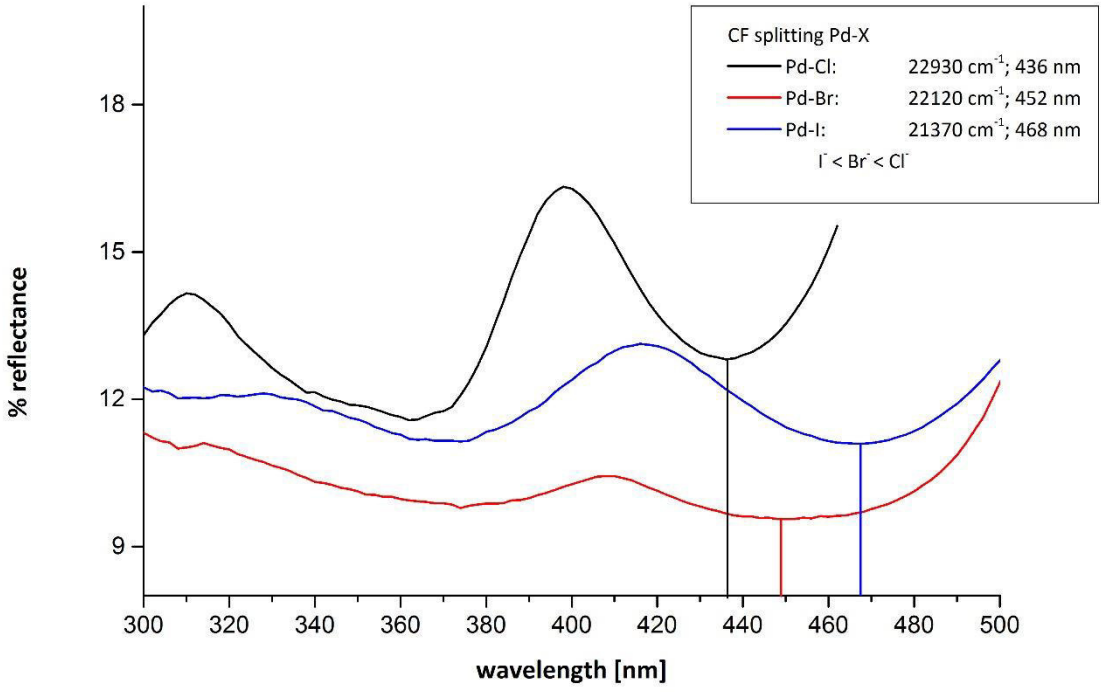

Figure 17: UV/Vis-spectra of complexes [PdX(S-Phoz)(IMes)] (**K6-K8**) in the range of 300 - 500 nm

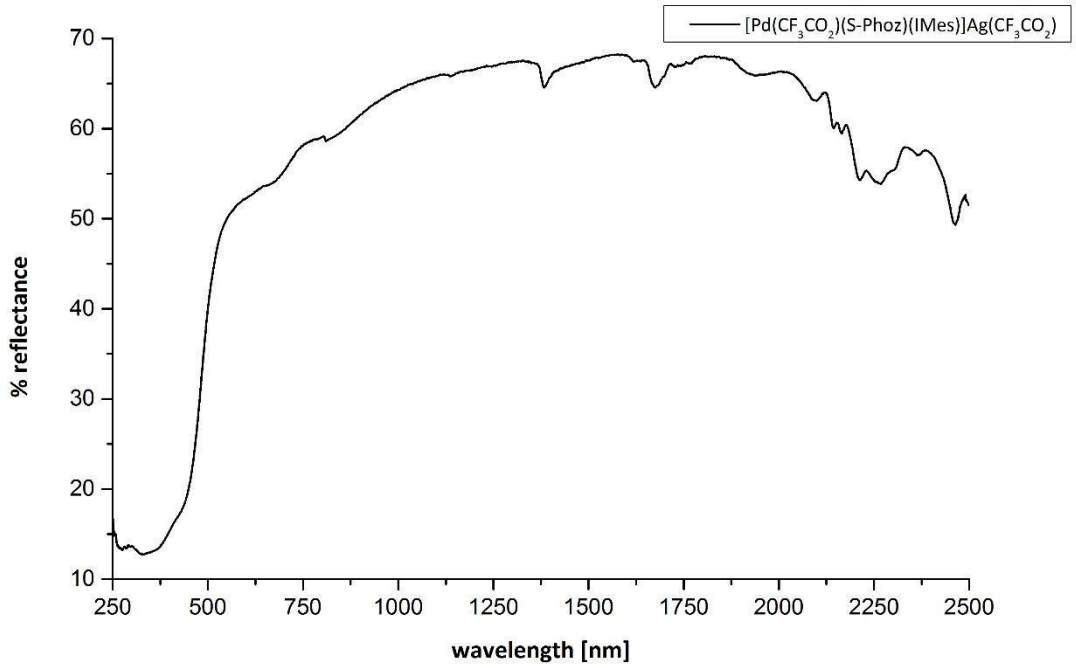

Figure 18: Reflectance spectra of [PdX(S-Phoz)(IMes)] complex **K9**

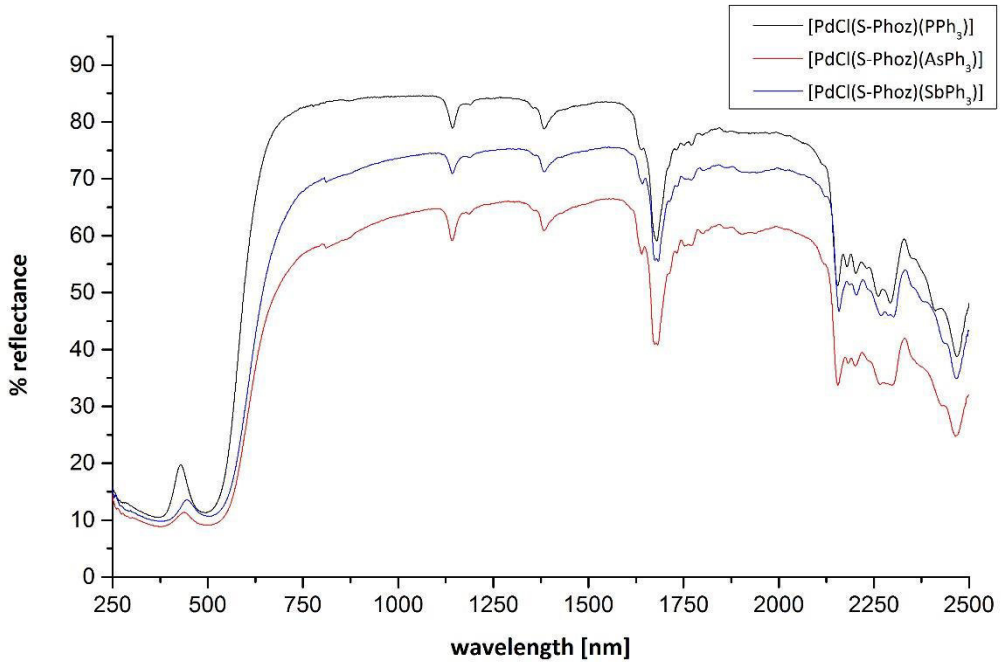

Figure 19: Reflectance spectra of complexes [PdCl(S-Phoz)(EPh_3)] (**K10-K12**)

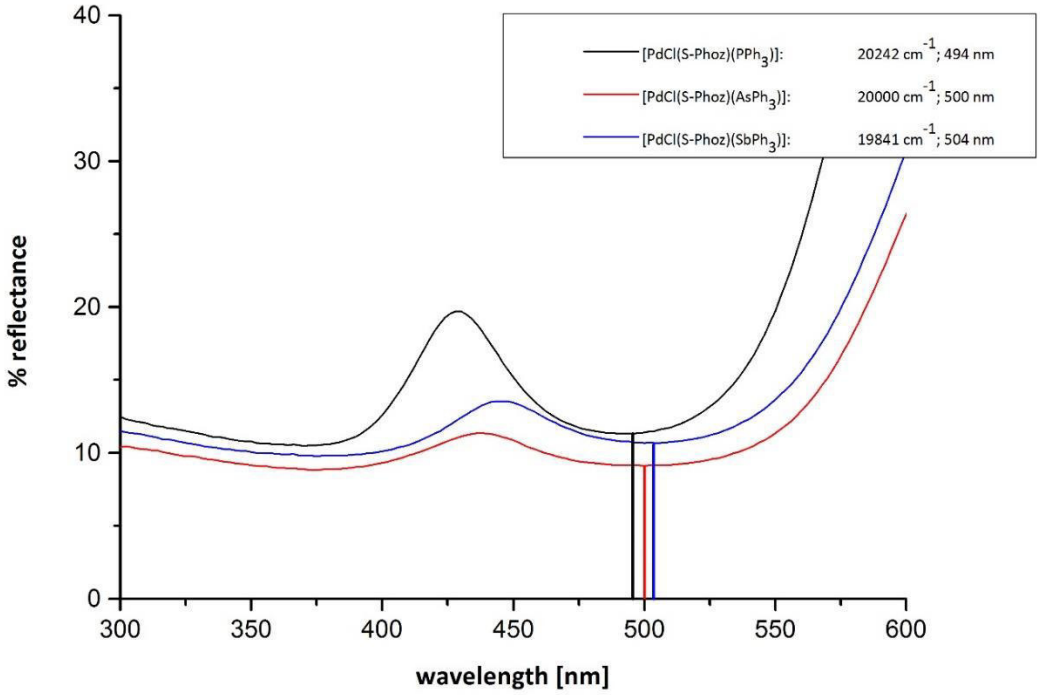

Figure 20: UV/Vis-spectra of complexes K10-K12 in the range of 300 - 600 nm

In Table 7 the lowest electronic excitations in the UV/Vis range for complexes **K3-K12** are listed. For the dimeric complexes **K3** and **K4** the values are in parenthesis since the peak maxima were very diffuse and therefore the exact excitation energies difficult to determine. In contrast for complexes **K6-K12** sharp maxima were observed. The apparent colors of all complexes are also listed in Table 7. The colors of the dimeric complexes intensify strongly along the series Cl (**K3**) ≈ Br (**K4**) < I (**K5**). A similar trend was observed for the IMes complexes **K6-K8** with color intensification from yellow (**K6**) to yellow-orange (**K7**) to orange (**K8**). Complex **K9** only has a very pale apparent color, seeming almost colorless. The group-15 donor complexes **K10-K12** do not show a similar observable trend as they are all red.

Table 7: UV/Vis absorption maxima of solid samples of complexes **K3-K12** in the UV/Vis range from 250-800 nm**.**

K3	**K4**	**K5**	
$[PdCl(S\text{-}Phoz)]_2$	**$[PdBr(S\text{-}Phoz)]_2$**	**$[PdI(S\text{-}Phoz)]_2$**	
orange	orange	red	
(468 nm)	(460 nm)	No single band	
K6	**K7**	**K8**	**K9**
[PdCl(S-Phoz)(IMes)]	**[PdBr(S-Phoz)(IMes)]**	**[PdI(S-Phoz)(IMes)]**	**$[Pd(CF_3COO)(S\text{-}Phoz)(IMes)]$**
yellow	yellow-orange	orange	light yellow
436 nm	452 nm	468 nm	326 nm
K10	**K11**	**K12**	
$[PdCl(S\text{-}Phoz)(PPh_3)]$	**$[PdCl(S\text{-}Phoz)(AsPh_3)]$**	**$[PdCl(S\text{-}Phoz)(SbPh_3)]$**	
orange-red	red	red	
496 nm	500 nm	504 nm	

5.3.1 Analysis of UV/Vis/NIR spectra of complexes K3-K5

The dimeric complexes **K3-K5** lack the presence of distinct peaks in the UV/Vis region. As shown in Figure 15 only a broad band is found below 500 nm in the corresponding reflectance spectra. Only complex **K4** (X=Br, red line in Figure 15) shows (weak) distinct bands starting to separate from each other. For this reason no absorption peaks could be reliably extracted by standard methods (peak search, evaluation of first and second derivative of the spectra) from the UV/Vis region of the spectra from complex **K5** while it was possible to extract a single band from **K3** and **K4** using derivatives of the spectra recorded. Calculations described in chapter 4.4.3 point to the existence of multiple electronic absorptions in these dimeric complexes which heavily overlap and therefore prevent simple extraction of peak maxima from the reflectance spectra. The NIR region of the spectra shown in Figure 15 indicates **K4** and **K5** (X=Br, I) to adopt a similar structure, while the structure may be different for the dimeric complex **K3**. Two bands at 1440 nm and 1940 nm loose intensity when exchanging chloride by bromide or iodide indicating structural changes.

5.3.2 Analysis of UV/Vis/NIR spectra of complexes K6-K9

The UV/Vis/NIR spectra of complexes [PdX(S-Phoz)(IMes)] (**K6-K8)** are shown in Figure 16 and Figure 17. In the range of 250-800 nm (UV/Vis spectral range) two distinct absorptions bands can be identified for all three complexes. The band at lowest energy belongs to an electronic excitation from the occupied sulfur p/palladium d_{xy} molecular orbital to an unoccupied palladium(II) $d_{(x^2-y^2)}$-orbital. The nature of this band basically resembles an S → Pd ligand-metal charge-transfer (LM-CT) band with a d-d transition mixing in. This has been validated by DFT calculations (vide infra). With increasing atomic number of the halogen

atom (Cl < Br < I) the lowest energy absorption band is shifted to lower energies due to the decreasing ligand field strength of the halogen in about 800 cm^{-1} steps (Cl → Br → I) as shown in Figure 17.

NIR spectra (in the range from 800-2500 nm) are similar for all three complexes [PdX(S-Phoz)(IMes)] **K6-K8** (see Figure 16). They show variations smaller than 5 nm, which is not surprising given the similar structure of **K6-K8**. In **K9** the first electronic excitation is shifted to 326 nm, 100 nm below **K6**. This strong shift to higher energy when compared to **K6-K8** can be rationalized by the fact that the first electronic excitation of **K6-K8** is an S → Pd LM-CT band. As the silver atom in **K9** withdraws electron density from the sulfur atom this first electronic excitation is significantly shifted to higher energy.

5.3.3 Analysis of UV/Vis/NIR spectra of complexes K10-K12

The UV/Vis/NIR spectra of complexes [PdCl(S-Phoz)(EPh_3)] (**K10-12)** are shown in Figure 19 are closely related to each other. The lowest energy electronic excitation peak is found at 494 nm (20242 cm^{-1} for E=P), 500 nm (20000 cm^{-1} for E=As) and 504 nm (19841 cm^{-1} for E=Sb) respectively (Figure 20). While there is a significant difference between **K10** and **K11/K12** the latter two have nearly complete identical UV/Vis spectra. The lowest electronic excitation can again be assigned to an S → Pd ligand-metal charge-transfer (LM-CT). An electron from the S p-orbital is promoted to the unoccupied palladium(II) $d_{(x^2-y^2)}$-orbital. Compared to the corresponding IMes complex **K6** this S → Pd LM-CT band is shifted by about 2700 cm^{-1} (0.334 eV) to lower energy (from 22936 cm^{-1} for **K6** to 20242 cm^{-1} for **K10**).

Again NIR spectra (in the range from 800-2500 nm) are similar for all three complexes [PdCl(S-Phoz)(EPh_3)] **K10-K12** (see Figure 19) due to the similar structure of **K10-K12**.

5.4.1 TD-DFT (TDA) electronic excitation spectra of complexes K6-K8

The excitation spectra of complexes **K6-K8** were calculated via time-dependent DFT (TD-DFT) within the Tamm-Dancoff approximation (TDA). For details see the computation section in the experimental part. Complex **K6** was used as prototype to test the functionals. As pure DFT functionals are known to perform worse than their hybrid DFT counterparts for metal complexes in TDA calculations only the hybrid functionals B3LYP, PBE0, TPSSh and M06 were tested.[92] For each functional a TDA calculation with the relativistic contracted Sapporo-DKH3 basis sets were used in conjunction with the Douglas-Kroll-Hess Hamiltonian of second order (DKH2). The calculated excitation spectra of complexes **K6-K8** are listed in Table 8.

Table 8: Excitation energies of complexes **K6-K9**. Values calculated with TPSSh/Sapporo basis set with scalar relativistic DKH2 Hamiltonian.

	K6 (X=Cl)	**f (osc.)**	**K7 (X=Br)**	**f (osc.)**	**K8 (X=I)**	**f (osc.)**
Exp. [nm]	436		452		468	
Exp. [cm^{-1}]	22935		22123		21368	
S0 → S1 [nm]	440.4	0.02549	448.7	0.02254	464.3	0.02068
[cm^{-1}]	22705.5		22287.4		21537.0	
S0 → S2 [nm]	389.5	0.01209	394.6	0.01160	399.3	0.00648
[cm^{-1}]	25674.8		25343.1		25040.7	
S0 → S3 [nm]	349.8	0.00864	358.5	0.00321	391.2	0.00487
[cm^{-1}]	28584.8		27894.8		25560.3	
S0 → S4 [nm]	337.5	0.00189	352.7	0.00991	370.8	0.00429
[cm^{-1}]	29630.4		28349.2		26967.8	
S0 → S5 [nm]	336.1	0.00187	337.0	0.00254	357.6	0.01618
[cm^{-1}]	29749.3		29672.4		27961.0	

The four hybrid functionals PBE0, B3LYP, TPSSh and M06 in combination with the Sapporo-DKH3 basis set were tested to predict the first electronic excitation. Among these four tested functionals TPSSh/Sapporo-DKH3 method showed to give the most reliable results for the first electronic excitation. The details of this small functional evaluation are given in Appendix B3.

The first experimentally measured transition of complex **K6** located at 436 nm is determined to be a mixture of an electronic transition from HOMO → LUMO mixing with the HOMO → LUMO+1 transition. The HOMO and LUMO (and also all valence orbitals) orbitals are not localized but spread over several atoms of complex **K6** (Figure 22). To visualize the electronic UV/Vis transition the difference electron densities of the electronic transitions were calculated with the orca_plot program within the ORCA3.0 program suite. The resulting transition difference densities are mainly localized on the palladium center and the thiophenol-sulfur atom (see Figure 21).

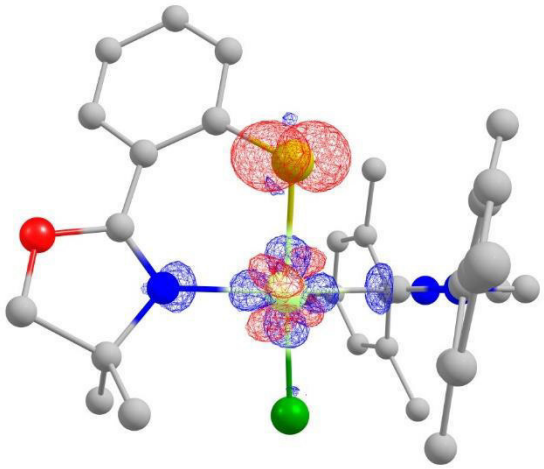

Figure 21: Difference densities of first electronic transition of complex **K6**.

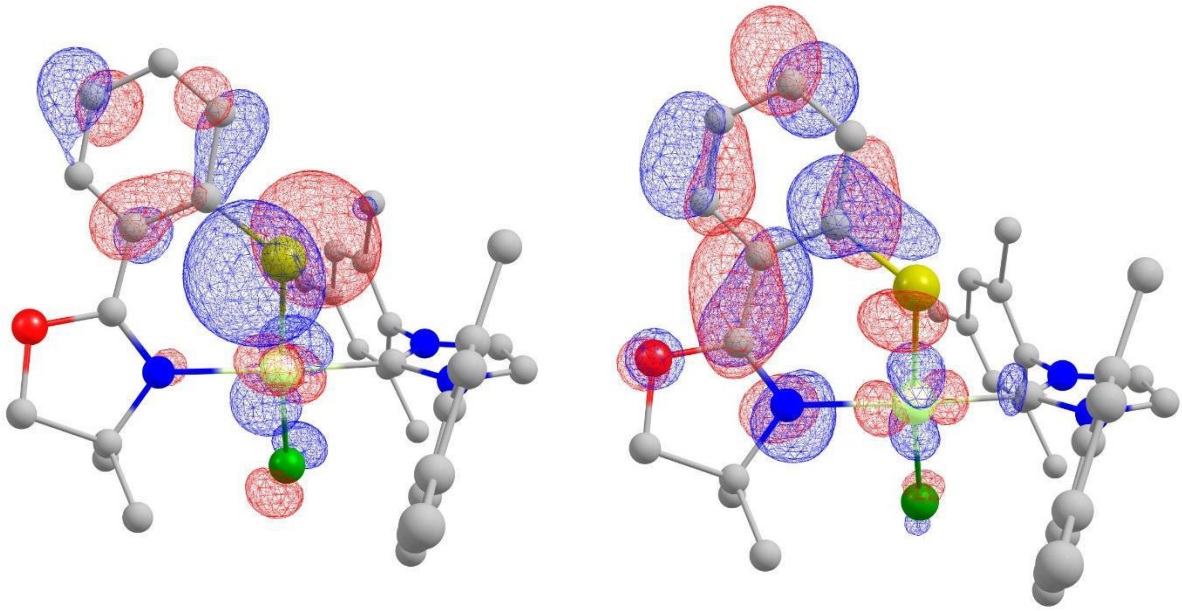

Figure 22: HOMO orbital (left) and LUMO orbital (right) of complex **K6**. The LUMO is clearly identified as an orbital with d(x^2-y^2) character in this plot.

The difference densities for the first excitation shown in Figure 21 helps recovering the one-electron excitation picture from the quite complicated set of excitations that is received from the calculation which include many orbitals. A close look at the HOMO and LUMO orbital reveals the one-electron character of the first excitation. The HOMO molecular orbital is a linear combination of a p-orbital of sulfur and a Pd d_{xy}-orbital while the LUMO has a probability density mainly at the (in the ground-state unpopulated) Pd $d_{(x^2-y^2)}$-orbital. This transition can be classified as a sulfur-palladium ligand-metal charge transfer excitation with a significant amount of a Pd $d_{xy} \rightarrow d_{(x^2-y^2)}$ excitation mixing in.

5.4.2 Excitation spectra of group-15 donor complexes [PdCl(S-Phoz)(EPh_3)] (K10-K12)

The measured reflectance spectra of the complexes [PdCl(S-Phoz)(L)] **K10** (L=PPh_3), **K11** (L=$AsPh_3$) and **K12** (L=$SbPh_3$) are shown in Figure 20. The first absorption peaks for these complexes were found at 496 nm (resp. 20160 cm^{-1}, **K10**, L=PPh_3), 500 nm (resp. 20000 cm^{-1}, **K11**, L=$AsPh_3$) and 504 nm (resp. 19841 cm^{-1}, **K12**, L=$SbPh_3$).

The first absorption peaks of all three complexes are quite similar. The main difference is that **K11** and **K12** possess significantly broader bands than complex **K10**. This leads to a shift towards lower energy for the absorptions peaks measured in the UV/Vis spectra of **K11** and **K12**. Complexes **K11** and **K12** therefore appear in a more intense reddish color. The difference between the latter two complexes is very subtle in both color and spectra.

The first excitations calculated at the TPSSh/Sapporo/DKH2 level of theory for complexes **K10-K12** can be found in Table 9. The first excitation energy calculated for complex **K10** (E=P) deviates by about 10 nm (400 cm^{-1}) from the experimental values.

Table 9: Excitation energies of complexes **K10-K12**. Values calculated with TPSSh/Sapporo basis set with scalar relativistic DKH2 Hamiltonian.

	K10 (L=PPh_3)	**f (osc.)**	**K11 (L=$AsPh_3$)**	**f (osc.)**	**K12 (L=$SbPh_3$)**	**f (osc.)**
Exp. [nm]	494		500		504	
Exp. [cm^{-1}]	20242		20000		19841	
S0 → S1 [nm]	503.9	0.01955	532.1	0.01084	516.3	0.00794
[cm^{-1}]	19846.1		18793.5		19368.1	
S0 → S2 [nm]	432.6	0.01792	443.2	0.01849	433.4	0.01922
[cm^{-1}]	23117.9		22563.9		23075.2	
S0 → S3 [nm]	376.7	0.00337	377.0	0.00934	393.4	0.01977
[cm^{-1}]	26547.7		26524.7		25419.6	
S0 → S4 [nm]	372.8	0.00597	369.6	0.01729	374.4	0.01317
[cm^{-1}]	26822.3		27053.1		26708.0	
S0 → S5 [nm]	366.2	0.03492	362.2	0.01271	360.9	0.00970
[cm^{-1}]	27310.1		27607.0		27709.3	

The calculated first excitation energies of complexes **K11** (E=As) and **K12** (E=Sb) are in good agreement with experimental obtained values. Complex **K10** (E=P) has the highest energy transition. The error for the first electronic excitation of **K10** is about 400 cm^{-1} for the TPSSh functional. The errors of the first excitation energies for **K11** (E=As) and **K12** (E=Sb) are in the range of 500-1100 cm^{-1}. From a theoretical point of view TPSSh predicts the following order in the first electronic transition (from lowest to highest energy): $AsPh_3$ < $SbPh_3$ < PPh_3. For TDA results with the PBE0/Sapporo method see Appendix B.3.

5.4.3 Excitation spectra of dimeric complexes [{PdX(S-Phoz)}$_2$] (K3-K5)

Although synthesized and described first the excitation spectra of the dimeric complexes **K3-K5** are described last as the reader might have noticed. This is due to the fact that dimers **K3-K5** are significantly more complex in their spectroscopic behavior. That presence of two 4d metal centers is quite demanding for current quantum mechanical theories that are able to be applied to systems of the given size. The results of the first ten electronic excitations obtained by the TDA method with the TPSSh functional are given in Table 10.

Table 10: Excitation energies of complexes **K3-K5**. Values calculated with TPSSh/Sapporo basis set with scalar relativistic DKH2 Hamiltonian.

	K3 (X=Cl)	**f (osc.)**	**K4 (X=Br)**	**f (osc.)**	**K5 (X=I)**	**f (osc.)**
Exp. [nm]	468		460		-	
Exp. [cm^{-1}]					-	
S0 → S1 [nm]	471.8	0.06204	448.7	0.02254	533.5	0.02218
[cm^{-1}]	21197.5		22287.4		18745.7	
S0 → S2 [nm]	453.0	0.00000	394.6	0.01160	528.2	0.01225
[cm^{-1}]	22074.7		25343.1		18931.9	
S0 → S3 [nm]	422.5	0.00000	358.5	0.00321	505.9	0.00132
[cm^{-1}]	23670.3		27894.8		19765.5	
S0 → S4 [nm]	413.0	0.01020	352.7	0.00991	505.6	0.00005
[cm^{-1}]	24215.8		28349.2		19776.7	
S0 → S5 [nm]	408.9	0.00000	337.0	0.00255	475.5	0.00021
[cm^{-1}]	24454.3		29672.4		21028.8	

Note that TPSSh predicts that the complex [{PdCl(S-Phoz)}$_2$] (**K3**) has a lower first electronic excitation energy than [PdBr(S-Phoz)]$_2$ (**K4**). Reflectance peaks in the experimentally obtained reflectance spectra of complexes **K3-K5** are broad und therefore poorly resolved. TDA calculation with the TPSSh functionals suggest that the single broad bands of **K3-K5** seen in Figure 15 consists of more than two different excitation peaks with similarly excitation energies. The most interesting property predicted by DFT and verified by the UV/Vis reflectance spectra is that the energy of the first electronic excitation is blue-shifted when exchanging Cl by Br. Therefore the ordering of complexes of type [PdX(S-Phoz)]$_2$ in first electronic excitation energy is I (**K5**) < Cl (**K3**) < Br (**K4**)

5.5 Rationalization of electronic structure and catalytic activity

Although the catalytic activity of complexes **K3-K12** shown in Table 4 does not correlate with a certain structural reason it seems to follow electronic differences in complexes **K3-K12**. Table 11 gives an overview of the first excitation in the UV/Vis spectrum and the catalytic activity in the Suzuki-Miyaura coupling for complexes **K6** to **K12**. The table is arranged in increasing nm number. This shows that there is obviously a range in between where catalytic activity is particularly high, while below and above these nm number catalytic activity is significantly lower. These middle ranged complexes (**K3,K4,K8,K10**) feature a first electronic S → Pd LM-CT excitation between 460 – 495 nm and they appear orange. A good overlap between UV/Vis, DFT first electronic excitation energy and catalytic activity therefore exists. The electronic fine-tuning of complexes with a [Pd(S-Phoz)]-moiety should therefore be aimed at synthesizing complexes within this electronic range.

Table 11: Comparison of first electronic excitation and catalytic activity of complexes K3-K12. The complexes are ordered in descending first electronic excitation energy.

Complex	**K6**	**K7**	**K4**	**K3**	**K8**
First exc.	436 nm	452 nm	460 nm	468 nm	468 nm
catalytic activity	57 %	50 %	> 98 %	> 98 %	87 %
Complex	**K10**	**K11**	**K12**	**K5**[b]	
First exc.	494 nm	500 nm	504 nm	534 nm	
catalytic activity	> 98 %[a]	60 %	20 %	35 %	

b) Due to the lack of reliable experimental values the DFT value was taken for **K5**. The complexes are also marked in their apparent color.

Of course it must be mentioned that this correlation is only true for the [Pd(S-Phoz)]-core in Suzuki-Miyaura couplings in water. It does not necessarily correlate in other reactions with ligands of a different structure as the measured electronic excitation mainly defined by an S → Pd LMCT transition.

5.6 Discussion

The reflectance spectra (UV/Vis/NIR) of complexes **K3-K12** have been measured. Complexes **K6-K8** with the N-heterocyclic carbene ligand IMes show well resolved spectra with clearly distinguishable reflectance peaks. The strong σ-donor character of the IMes ligand effects a strong ligand field. As the IMes ligand itself has no absorption peaks in the visible range it proved ideal to test other weak donor ligand on their influence on the palladium atom. The typical ligand field strengths known as the “spectroscopic row” was nicely reproduced for the three halogenides Cl^-, Br^- and I^-.[93] The first electronic absorption in the

experimental spectra could clearly be identified as an S → Pd LM-CT (HOMO-LUMO) transition in all complexes **K3-K12.** However the HOMO of all complexes calculated has significant Pd d_{xy}-character. This explains the sensitivity of this first transition to the ligand field influence of the ligands. As the halogen atom is located *trans* to the thiophenyl moiety it has significant impact on the bonding length of the Pd-S bond.

The π-back-bonding interaction of triphenylphosphine with the palladium central metal slightly destabilizes the occupied orbitals (mainly the Pd d_{xy}-orbital) and stabilizes the unoccupied orbitals (mainly the Pd $d_{(x^2-y^2)}$-orbital). This leads to the observed shift in the first excitation peak that occurs when IMes is replaced by PPh_3 and the HOMO → LUMO transition is shifted to lower energy by about 2700 cm^{-1}. Pure d-d transitions have not been observed in this study. Although the complexes have overall low symmetry the d-d transitions are still unfavored in square-planar d^8-complexes and genuinely only show low intensity. In the UV/Vis spectra of medium to large complexes with up to hundred atoms like the palladium(II)-complexes in this study the d-d excitations can be located by DFT methods but also DFT states that the oscillator strength of these transitions is very low. Therefore Pd(d^8) d-d transitions are probably "buried" under the LM-CT and π-π* transitions.

The heavier homologues of PPh_3, $AsPh_3$ (**K11**) and $SBPh_3$ (**K12**), behave similar to triphenylphosphine (complex **K10**) in terms of ligand field strength and influence on electronic excitations. DFT calculations indicate that there is only a subtle change in the electronic structure of complexes **K10-K12.** Calculated bond lengths of Pd-Cl, Pd-S and Pd-N are within a range 0.01 Å in all three complexes. Experimental reflectance spectra accordingly show only subtle differences between the two heavier homologues. It can be concluded that $AsPh_3$ and $SbPh_3$ can be used to introduce subtle changes in complexes to alter their behavior and properties. It is however difficult to predict the changes introduced by altering the group-15 donor. DFT predicts the following order of the first electronic singlet excitation (lowest to highest energy): $AsPh_3$ < $SbPh_3$ << PPh_3. This is again in good agreement with the experimentally obtained UV/Vis spectra.

A special case was complex **K9**, were the halogenide was replaced by trifluoroacetate. While the energy gap increases only moderately when going from I^- to Br^- to Cl^- ligand (from 21370 cm^{-1} to 22120 cm^{-1} to 22930 cm^{-1}) there is a significant gap between the halogenides and trifluoroacetate **K9** $AgCF_3CO_2$ adduct of nearly 100 nm (20000 cm^{-1}/ 2.5 eV respectively). This supports the assumption that the first excitation in complexes **K6-K8** is a ligand-metal charge-transfer from the thiophenyl sulfur atom to the palladium(II) center. The silver(I) atom coordinated to the sulfur in complex **K9** in addition to the palladium(II) atom

withdraws electron density from the sulfur atom, lowering the electron density at the sulfur atom. This effect shifts the first electronic excitation, the S → Pd LM-CT, to higher energy.

The dimeric complexes **K3-K5** exhibit a more complex electronic structure. DFT calculations suggest that there are at least 4 absorption bands energetically close enough to overlap to a single broad band. Even with the theoretical data available a deconvolution of the broad absorption peak, extracting all bands, was not possible from the measured UV/Vis-spectra. DFT/time-dependent DFT methods are clearly at the limit for these dimeric palladium compounds and are no longer able to sufficiently predict spectroscopic properties of complexes with two palladium centers.

Last but not least with the help of UV/Vis spectroscopy and DFT techniques it was possible to rationalize the diverging catalytic performance of complexes K3-K12 in Suzuki-Miyaura couplings in water. It was shown that an optimal electronic range for complexes bearing [Pd(S-Phoz)]-cores exists. Complexes within this range show a strong S→Pd (mixed with a d-d) first electronic excitation between 460 – 495 nm. It is assumed that complexes with a first electronic excitation within this range are balanced to stabilize both Pd oxidation staes 0/+2 occuring during the catalytic cycle in Suzuki-Miyaura reactions. Therefore complexes **K3**, **K4**, **K8** and **K10** show the overall best catalytic performance.

6. Conclusion

The chemistry of twelve novel palladium complexes employing the mercaptoaryl-oxazoline ligand (S-Phoz) has been prepared and investigated towards functional cross-coupling catalysts. The newly synthesized complexes can be sorted into three different groups. First the palladium(II) dimers **K3-K5** that are convenient precursors for further synthesis. Complexes of type [PdX(S-Phoz)(IMes)] (X=Cl (**K6**), Br (**K7**) and X=I (**K8**)) were synthesized from their dimeric precursors in good to excellent yields. The palladium complexes with group-15 donors of type [PdCl(S-Phoz)(L)], L=PPh_3 (**K10**), $AsPh_3$ (**K11**) and $SbPh_3$ (**K12**) were synthesized from the dimeric precursor **K3** by addition of the corresponding donor ligand in good to excellent yield. All complexes **K1-K12** incorporate a square-planar coordinated Pd^{II} center as excpected. All found bond lengths, angles and properties are within the range of previously synthesized complexes of similar structures with [PdSN]-cores.[10,11,13,35,36,47,57,74-84]

The spectroscopic properties of all new catalysts **K3-K12** have been determined using reflecto-spectrometry and where compared with current TD-DFT (TDA) methods to reveal the electronic structure of the first excitations of corresponding complexes. The dominant band in the UV/Vis-range of this complexes is a LM-CT band were an electron is formally excited from a linear combination of a sulfur p-orbital and a palladium d_{xy}-orbital to the palladium $d_{(x^2-y^2)}$-orbital. This electronic excitation is therefore sensitive to the ligand field surrounding the palladium atom and the electron density at the sulfur atom. The influence of the halides in complexes **K6-K8** is in good agreement with the spectroscopic row showing that the crystal field splitting is decreasing from Cl^- to Br^- to I^- by about 800 cm^{-1} between each halogenide. If the NHC IMes is replaced by the classic triphenylphosphine the first electronic excitation is shifted by about 2700 cm^{-1} revealing that the electronic structure drastically changes between NHC and phosphine ligands.

The obtained catalysts are active in an aqueous environment with the help of cheap bases like K_2CO_3 for Suzuki-Miyaura type cross-couplings. The activity of the catalysts **K3-K12** was shown to correlate with the first electronic excitation energy of the corresponding complex. The optimal range for this first electronic excitation was discovered to be between 460 – 495 nm. Even slight deviations from this range yield to a strong decrease in catalytic activity. As no complex was obtained that possess a transition exactly in the middle of this range maybe even more potent catalysts could be created by ongoing research on this topic. The highest catalytic activity is shown by complexes **K4** and **K10** yielding TOFs of up to 1600 h^{-1} in water

which is comparable to similar sulfur-containing system which reach up to 4500 cm^{-1} but not en par with the most active catalysts in water which yield TOFs of up to 16000 h^{-1}. [4]

7. Experimental section

All syntheses were performed under ambient conditions if not stated otherwise. Synthesis steps which needed an inert atmosphere (Schlenk technique or glovebox conditions) are described in the respective procedure with either nitrogen or argon as inert gas. Solvents were taken from a Pure Solv Solvent Purification System (acetonitrile, heptane, and toluene). Other used solvents were purified and eventually dried as described below. Palladium chloride was purchased from Degussa and used as is. The *cis*-$[PdCl_2(PPh_3)_2]$, PPh_3, $AsPh_3$ and $SbPh_3$ ligands were obtained from commercial sources and used as is. IR spectra were measured on a Bruker ALPHA-P Diamant ATR-FTIR spectrometer with the spectra recorded at a 2 cm^{-1} step width. All NMR spectra were measured on a Bruker Avance III 300 MHz spectrometer at 25 °C. ^{1}H and ^{13}C NMR spectroscopy chemical shifts are given in ppm and are referenced to residual protons in the solvent. ^{31}P NMR spectra were referenced externally to 85% H_3PO_4. ^{19}F NMR spectra were referenced to $CFCl_3$. Mass spectra were recorded with an Agilent Technologies 5975C inert XL MSD instrument using the direct insertion technique. Elemental analyses were performed by the Microanalytical Laboratory of the University of Vienna using a EuroVector EA3000. UV/Vis/NIR reflectance spectra were measured on a Perkin-Elmer Lambda 150 reflecto-spectrometer. A Labsphere Certified Reflectance Standard was used as baseline correction. Oxazolines / oxazoline ligands and the IMes ligand were synthesized according to literature procedures.[94-100]

Crystallographic Details. X-ray data collection was performed with a Bruker AXS SMART APEX 2 CCD diffractometer by using graphite-monochromated Mo-K_α radiation (0.71073 Å) from a fine-focus sealed tube at 100 K. SHELXS-97 was used as structure solution and structure refinement program.[101] Full-matrix least-squares on F^2 was employed as refinement method. Further details on the solution of the structures can be found in the supporting information. Crystallographic data (excluding structure factors) for the compounds reported in this thesis can be found in Appendix A.

Computational details. All calculations were performed using the ORCA3.0 program suite. All orbital densities, transition densities etc. plotted in this thesis were generated using the Chemcraft 1.7 software.

7.1.1 Geometry optimization

In the current investigation the def2-SVP and def2-TZVP gaussian basis sets developed by Ahlrichs were used in conjunction with different density functionals for geometry optimizations.[102] The generalized-gradient approximated (GGA) density functionals BP86[103,104], PBE[105,106], PW91[107-112] and BLYP[104,113] as well

as the meta-GGA functional TPSS[114] were used in conjunctions with the RI-approximation. The hybrid functionals B3LYP[115], PBE0[111,106,116] , TPSSh[114] and M06[117] incorporating Hartree-Fock-exchange ("exact exchange") were used without any further approximations for evaluating geometries. For the heavy atoms Pd, Ag and I the core electrons (28 core electrons for Pd, Ag, Sb and I) were replaced by an effective core potential (ECP), namely the Stuttgart-Dresden ECP28MWB.[118,102] The corresponding def2-SVP/J and def2-TZVP/J auxiliary basis sets were used when the RI-approximation was applicable.[119] The pairwise dispersion correction by Grimme with Becke-Johnson damping ("D3BJ") was employed for all functionals were parametrization of this empirical dispersion correction exists.[90,91] All methods given above were used as implemented in the ORCA3.0 program package.[120]

7.1.2 Calculation of UV/Vis (electronic) excitation spectra with TD-DFT methods

ECPs have proven to be very successful and moderately time-saving when it comes to optimization tasks at different levels of geometry. However the relativistic effects can no longer be neglected when it comes to property evaluation (like excitation spectra) of compounds incorporating heavy elements (fourth-row and heavier).

Therefore, for evaluating spectral properties of the complexes, ECP basis sets were replaced by the relativistic-contracted Sapporo-DKH3-TZVP basis set for palladium and iodine in conjunction with the Douglass-Kroll-Hess (DKH) approximation to account for scalar-relativistic effects. Spin-orbit splitting of electronic states was expected to be insignificant for a relatively light element like palladium, and therefore only scalar relativistic effects were considered in the model Hamiltonian. All electronic excitation spectra were calculated using the time-dependent DFT (TD-DFT) approach. The Tamm-Dancoff approximation was used within all TD-DFT calculations and will be referred to as "TDA" from now on in this thesis. The hybrid functionals B3LYP, PBE0, TPSSh and M06 were used in conjunction with the chain-of-spheres approximation (RIJCOSX) to speed up the calculations.[121] This approximation showed to have only minor impact on excitations spectra, nearly reproducing the values of the calculation without approximation in a fraction of time.[122,123] For calculation of excitation energies (UV/Vis spectra) the Sapporo-TZP-2012 (C,H,O,N,S) was used for lighter elements.[124] For Cl and S the Sapporo-TZP-2012 with diffuse functions (one set with 1s1p1d1f diffuse functions) was used. The Sapporo-DKH3-TZP-2012 basis set was used for the heavier, more polarizable atoms Pd, Br and I (again with 1s1p1d1f diffuse functions for Br and I).[124] Auxiliary basis sets cc-pVTZ/C (for Sapporo-TZP-2012) by Ahlrichs were used in combination with the RIJCOSX-approximation as described above for the calculation of electronic excitation spectra (UV/Vis excitation energies).[121] In non-relativistic quantum mechanics the nucleus is considered to be a

point nucleus. This approximation however generates a singularity at the nucleus when relativistic calculations are applied. For higher precision in oscillator strength (and therefore calculation of peak heights) the nucleus was considered as a finite nucleus with a charge distribution resembled by a Gaussian function as described by Visscher.[125] All methods given above were used as implemented in the ORCA3.0 program package.[120]

7.2 General Procedure for Catalysis

A 10 ml vial was loaded with 199 mg (1.0 mmol, 1.0 equiv.) bromoacetophenone, 193 mg K_2CO_3 (1.4 mmol) and 171 mg (1.4 mmol, 1.4 equiv.) phenylboronic acid. Then the catalyst and 5 ml of water are added. The reaction is heated to 90 °C for the given time. After the reaction time finished the solution was cooled to room temperature and all organic compounds were extracted with 5 ml ethyl acetate. The ethyl acetate solution was separated and dried over $MgSO_4$. The organic phase was then analyzed via GC-MS and conversion, product yield and selectivity was determined via peak integration of educts, products and possible side products.

7.3 Ligand Synthesis

Lithium-2-(2-thiophenyl)-4,4-dimethyloxazoline (2)

All steps in this Synthesis were carried out under an Ar atomosphere. The product was stored in a glovebox. A 250 ml Schlenk-flask was equipped with a stirring bar and charged with 20 ml (20.5 g, 117 mmol, 1.0 equiv.) 2-phenyl-4,4-dimethyloxazoline and 30 ml dry, air-free pentane are added and the reaction mixture is cooled to -30 °C. Then 50 ml 2.5 M n-BuLi (125 mmol, 1.07 equiv.) solution was added dropwise and the solution stirred for another three hours. The precipitate was filtered off, dried under vacuum and stored under an Ar atmosphere. The lithiated 2-phenyl-4,4-dimethyloxazoline was obtained in 73 % yield (15.5 g, 8.6 mmol) as orange powder. To 15.5 g (8.6 mmol, 1.0 equiv.) lithiated 2-phenyl-4,4-dimethyloxazoline in 250 ml dry, air-free diethyl ether 2.70 g S_8 (1.08 mmol, 1.0 equiv.) were added at once. The suspension was stirred for 20 h under Ar. The precipitate was filtered off, washed with dry, air-free diethyl ether and dried under vacuo. The product was obtained as slightly yellow powder in 72% (11.2 g, 61.8 mmol) yield. NMR and IR spectra according to literature data.[50]

5-fluorosalicylic acid methyl ester

A 50 ml round bottom flask was equipped with a stirring bar and charged with 460 mg (2.94 mmol, 1.0 equiv.) 5-fluorosalicylic acid. The white solid was dissolved in 32 ml of dry Methanol and 6 drops of concentrated H_2SO_4 (98 %) were added. The solution was then refluxed for 24 h. After 24 h the mixture

was allowed to cool to room temperature and solvent removed in vacuo at 40 °C. The residue was dissolved in 50 ml ethyl acetate and washed three times with 50 ml $NaHCO_3$ (sat.), 50 ml brine and 50 ml water subsequently. The organic phase was dried over $MgSO_4$, filtered and solvent removed to yield an off-white solid consisting of 5-fluorosalicylic acid methyl ester in 81% (406 mg, 2.39 mmol) yield. The product was used without further purification for the next step.

2-(4,4-Dimethyl-4,5-dihydrooxazol-2-yl)-4-fluorophenol

A 100 ml round bottom flask was equipped with a stirring bar and charged with 2.20 g (12.9 mmol, 1.0 equiv.) 5-fluorosalicylic acid methyl ester. 1.50 g (16.8 mmol, 1.4 equiv.) 2-methyl-2-aminopropanol were added and the mixture was suspended in 40 ml dry xylol. The flask was equipped with a water separator filled with xylol and the suspension refluxed for 9 days. After 9 days the reaction mixture was cooled to room temperature and 30 ml tBuOMe and 30 ml heptane were added. The organic phase was extracted three times with 30 ml 0.1 M NaH_2PO_4. The organic phase was separated and solvent removed in vacuo at 40 °C. The product was obtained as an off-white oil which solidifies after standing for a few days in 80% yield (2.15 g, 10.3 mmol). No further purification is needed if the product is used directly for the synthesis of **9**.

(2-(4,4-Dimethyl-4,5-dihydrooxazol-2-yl)-4-fluorophenyl) dimethylcarbamothioate (9)

This synthesis was done using a modified literature procedure.[126] A 50 ml Schlenk flask was dried and equipped with a stirring bar and charged with 1.54 g (7.36 mmol, 1.0 equiv.) of dry (2-(4,4-dimethyl-4,5-dihydrooxazol-2-yl)-4-fluorophenol. Then the flask was evacuated for another hour to remove any traces of water. 18 ml of dry DMF were added under N_2 under vigorous stirring. After the starting material has dissolved 324 mg NaH (8.10 mmol, 1.1 equiv.) (60 % w/w in paraffin oil) were added portion wise under an N_2 stream and the mixture was stirred for 15 minutes. Then a solution of 1.18 g (10.9 mmol, 1.5 equiv.) N,N-dimethylcarbamoyl chloride in 6 ml dry DMF was added dropwise over 5 minutes. After addition is completed the reaction mixture was stirred for three hours and 72 ml H_2O were slowly added over 20 min. An oil started to separate during quenching with water. The oil was extracted with three times 30 ml of ethyl acetate. The combined organic phases were dried over $MgSO_4$, filtrated and solvent removed in vacuo at 40 °C. The product was separated by column chromatography using EtOAc:cyclohexane 1:9 as eluent. Fractions 4-8 consisted of starting material (550 mg recovered) and fractions 18-30 yielded 850 mg of the desired product. The product was obtained as colorless oil solidifying after standing for a few days in 39% (850 mg, 2.86 mmol) yield.

^{1}H NMR (300 MHz, $CDCl_3$) δ 7.55 (dd, *J* = 8.9, 3.1 Hz, 1H), 7.19 – 7.10 (m, 1H), 7.05 (dd, *J* = 8.9, 4.8 Hz, 1H), 3.98 (s, 2H), 3.39 (s, 3H), 3.36 (s, 3H), 1.28 (s, 6H). ^{19}F NMR (282 MHz, $CDCl_3$) δ -116.26 (s).

7.4 Palladium complex synthesis

[Pd(S-Phoz)$_2$] (K1)

In a 50 ml round bottom flask 60 mg (0.34 mmol, 1.0 equiv.) of $PdCl_2$ were suspended in dry toluene. Then 152 mg (0.71 mmol, 2.1 equiv.) of LiS-Phoz were added in portions over 10 minutes. After the first addition of LiS-Phoz the suspension immediately turns deep red. The solution is stirred for another 4 h and then filtered through celite. The solvent is removed in vacuo and the remaining dark solid is redissolved in a minimal amount dichloromethane. The solution is again filtered through celite and an equal amount of dry heptane is added to precipitate the product as a dark red powder. Reprecipitation was repeated twice to yield the pure complex **K1** as a dark red powder in 60% (106 mg, 0.20 mmol) yield. Single crystals suitable for X-ray structure analysis were obtained by slow evaporation of a saturated solution of **K1** in benzene.

^{1}H NMR (300 MHz, CD_2Cl_2) S,S-*trans* isomer: δ 7.48 – 7.40 (m, 4H, Ar-*H*), 7.12 – 7.05 (m, 2H, Ar-*H*), 6.95 (td, *J* = 7.7, 1.2 Hz, 2H, Ar-*H*), 4.28 (s, 4H, -CH_2-), 1.69 (s, 12H, -CH_3); S,S-*cis* isomer: δ 7.65 – 7.58 (m, 2H, Ar-*H*), 7.51 – 7.47 (m, 2H, Ar-*H*), 7.20 (td, *J* = 7.7, 1.6 Hz, 2H, Ar-*H*), 7.07 – 7.03 (m, 2H, Ar-*H*), 4.37 (d, *J* = 7.8 Hz, 2H, -CH_2-), 4.10 (d, *J* = 7.5 Hz, 2H, -CH_2-), 1.61 (bs, 6H, -CH_3), 1.42 (bs, 6H, -CH_3). ^{13}C NMR (75 MHz, CD_2Cl_2) S,S-*trans* isomer: δ 163.96 (C-S), 149.51 (Ar-C), 131.72 (Ar-C), 131.11 (Ar-C), 130.02 (Ar-C), 127.32 (Ar-C), 122.68 (Ar-C), 80.28 (-CH_2-), 71.86 (O-**C**-$(CH_3)_2$), 54.00, 28.71 (-CH_3); S,S-*cis* isomer: δ 164.19 (C-S), 149.38 (Ar-C), 132.08 (Ar-C), 131.41 (Ar-C), 129.91 (Ar-C), 127.89 (Ar-C), 123.20 (Ar-C), 80.02 (-CH_2-), 71.12 (O-**C**-$(CH_3)_2$), 31.79 (-CH_3), 26.04 (-CH_3). IR: 1615 (s), 1583 (w), 1550 (w), 1458 (m), 1369 (s), 1330 (m), 1219 (m), 1133 (m), 1056 (s), 961 (m), 768 (s), 741 (m), 728 (s), 689 (m), 654 (m). EI -MS: 518.0 [M^+]. Anal. Calcd. for $C_{22}H_{24}N_2O_2PdS_2$ (518.96): C, 50.91; H, 4,66; N, 5.40; S, 12.36. Found: C, 50.38; H, 4.68; N, 5.26; S, 12.20.

[Pd(S-Phoz)$_2$(PPh$_3$)] (K2)

A 100 ml Schlenk flask was charged with 0.329 g (0.47 mmol, 1.0 equiv.) $PdCl_2(PPh_3)_2$ in a glovebox. The palladium precursor was dissolved in dry, air-free acetonitrile and 0.200 mg (0.94 mml, 2.00 equiv.) LiS-Phoz were added at once. The solution immediately turns deep red when LiS-Phoz is added. After 24 h the solution is filtered through celite and the solvent removed in vacuo. The red solid is redissolved in toluene and filtered to remove LiCl and precursor salts. After removal of solvent in vacuo the obtained product is recrystallized by slow evaporation of acetonitrile to yield **K2** in large, deep red crystals in 74% (0.271 g, 0.37 mmol) yield. The crystals obtained are also suitable for X-ray structure analysis.

^{1}H NMR (300 MHz, CD_2Cl_2) δ 7.81 – 7.65 (m, 7H, Ar-*H*), 7.43 – 7.25 (m, 13H, Ar-*H*), 6.91 – 6.77 (m, 3H, Ar-*H*), 3.99 (bs, 4H, -CH_2-), 1.46 (bs, 12H, -CH_3).[a] ^{13}C NMR (75 MHz, CD_2Cl_2) δ 164.12 (C-S), 164.10 (C-S), 147.91 (Ar-C), 134.38 (Ar-C), 134.24 (Ar-C), 133.84 (Ar-C), 131.39 (Ar-C), 130.70 (Ar-C), 130.67 (Ar-C), 130.64 (Ar-C), 129.79 (Ar-C), 129.20 (Ar-C), 128.58 (Ar-C), 128.43 (Ar-C), 124.07, 122.33, 80.33 (CH_2), 69.70 (O-**C**-$(CH_3)_2$), 28.49 (4 CH_3). ^{31}P NMR (121 MHz, CD_2Cl_2) δ 35.22. IR: 1660 (w), 1633 (s), 1580 (w), 1432 (m), 1368 (m), 1302 (m), 1095 (m), 1053 (m), 1038 (s), 951 (m), 758 (m), 733 (m), 690 (s), 533 (s), 498 (s). EI-MS: 723.4 [M^+- -CH_2-C-$(CH_3)_2$], 573.3 [M^+-S-Phoz]. Anal. Calcd. for $C_{40}H_{39}N_2O_2PPdS_2 \cdot 2\ H2O$ (817.30): C, 58.78; H, 5.30; N, 3.43; S, 7.85. Found: C, 58.84; H, 5.09; N, 3.50; S, 7.86.

[{PdCl(S-Phoz)}$_2$] (K3)

A 100 ml round bottom flask was charged with 400 mg (2.26 mmol, 1.0 equiv.) palladium chloride. Then 25 ml of dry acetonitrile were added and the flask was equipped with a condenser and a calcium chloride charged drying tube. The mixture was heated to reflux for 4 h slowly dissolving the dark red $PdCl_2$. To the still hot solution 506 mg (2.37 mmol, 1.05 equiv.) of LiS-Phoz were added at once and stirred under reflux. In the first few minutes a yellow-orange precipitate started to form. After an hour the solution was allowed to cool to 40-45 °C the solid filtered off. The residue is washed with 20 ml of acetonitrile three times until the washing solution remains colorless. After drying in vacuo for 1 h the product was obtained as a bright orange powder in 80% yield (629 mg, 0.90 mmol). Crystals suitable for X-ray structure analysis were obtained by slow evaporation of a saturated solution of **K3** in CH_2Cl_2.

^{1}H NMR (300 MHz, CD_2Cl_2) δ 8.86 (bs, 2H, Ar-*H*), 7.56 (dd, *J* = 7.5, 1.5 Hz, 2H, Ar-*H*), 7.53 – 7.34 (m, 4H, Ar-*H*), 4.34 (bs, 4H, -CH_2-), 1.73 (bd, *J* = 24.3 Hz, 12H, -CH_3). ^{1}H NMR (300 MHz, $CDCl_3$) δ 8.85 (bs, 2H, Ar-*H*), 7.53-7.36 (bm, 6H, Ar-*H*), 4.32 (s, 4H, -CH_2-), 1.75 (bd, *J* = 15.6 Hz, 12H, -CH_3). ^{13}C NMR (75 MHz, CD_2Cl_2) δ 164.21 (C-S), 134.27 (Ar-C), 133.63 (Ar-C), 130.77 (Ar-C), 127.67 (Ar-C), 82.64 (CH_2), 71.27 (O-**C**-$(CH_3)_2$), 30.24 (-CH_3), 28.46(-CH_3). IR: 1607 (s, C=N), 1433 (m), 1378 (m), 1328 (m), 1222 (m), 1139 (m), 1051 (m), 949 (m), 767 (m), 735 (s), 691 (m), 476 (m). EI-MS: 694.0 [M^+]. Anal. Calcd. for $C_{22}H_{24}Cl_2N_2O_2Pd_2S_2 \cdot 0.85\ CH_2Cl_2$ (696.31): C, 35.71; H, 3.37; N, 3.65; S, 8.34. Found: C, 35.55; H, 3.41; N, 3.86; S, 8.59.

[{PdBr(S-Phoz)}$_2$] (K4)

A 100 ml round bottom flask was equipped with an stirring bar and charged with 290 mg (0.83 mmol, 1.0 equiv.) of [$PdBr_2(acn)_2$]. 40 ml of dry acetonitrile are added and the flask was equipped with a condenser

[a] Strong signal overlap with **4b** and PPh_3 due to the solution equilibrium.

and a calcium chloride charged drying tube. The mixture was heated to reflux. After all $PdBr_2(acn)_2$ had dissolved 186 mg (0.87 mmol, 1.05 equiv.) of LiS-Phoz were added at once at reflux temperature. The mixture was then refluxed for three hours. After cooling to room temperature the precipitated product was filtered of and washed with 3x 15 ml benzene. After drawing in vacuo for 1 h the product was obtained as bright orange powder in 76% yield (250 mg, 0.32 mmol).

^{1}H NMR (300 MHz, $CDCl_3$) δ 8.86 (s, 2H, Ar-*H*), 7.48 (bs, 4H, Ar-*H*), 7.38 (d, *J* = 8.2 Hz, 2H, Ar-*H*), 4.32 (s, 4H, -C*H*$_2$-), 1.79 (s, 6H, -CH_3), 1.71 (s, 6H, -CH_3)., ^{13}C NMR not possible (solubility). IR: 1611 (s, C=N), 1460 (m), 1365 (s), 1322 (m), 1108 (m), 1049 (s), 953 (s), 768 (s), 737 (s), 691 (m). EI-MS: 786.0 [M^+] Anal. Calcd. For $C_{22}H_{24}Br_2N_2O_2Pd_2S_2 \cdot 0.33\ C_6H_6$ (785.21): C, 35.53; H, 3.23; N, 3.45 found: C 35.61, H 3.61, N 3.41

[{PdI(S-Phoz)}$_2$] (K5)

290 mg (0.417 mmol,1.0 equiv.) of [PdCl(S-Phoz)]$_2$, **K3**, and 130 mg potassium iodide (0.783 mmol, 1.9 equiv.) were suspended in acetone. The mixture is stirred at 40 °C for 6 h in a water bath. Cooling to room temperature the red precipitate was filtered off and washed with dry acetone (2x 10 ml) and then dried in vacuo. The product was obtained as a red powder in 99 % yield (365 mg, 0.415 mmol) as a 1:1 mixture of the desired compound and KCl. As KCl does not disturb further reactions and UV/Vis or IR spectra no attempts were made to remove KCl. Washing with water slowly decomposes the product, therefore for all further experiments the 1:1 mixture was used.

^{1}H NMR (300 MHz, $CDCl_3$) δ 8.86 (dd, 2H, Ar-*H*), 6.85 (bd, *J* = 23.6 Hz, 6H, Ar-*H*), 3.96 (d, *J* = 20.5 Hz, 4H, -CH_2-), 1.57 (broad s, 12H, -CH_3). ^{13}C NMR not possible (solubility). IR: 1612 (m, C=N), 1375 (m), 1326 (m), 1050 (m), 766 (m), 735 (s). EI-MS: 518.0 [M^+]. Anal. Calcd. For $C_{22}H_{24}ClI_2KN_2O_2Pd_2S_2$ (879.21): C, 27.70; H, 2.54, N, 2.94, found: C 26.73, H 2.34, N 2.86

General Procedure for complexes K6-K8.

[PdCl(S-Phoz)(IMes)] (K6)

A 25 ml Schlenk-flask was equipped with a stirring bar and charged with 95 mg (0.136 mmol, 0.98 equiv.) [{PdCl(S-Phoz)}$_2$] (**K3**). The Schlenk flask was evacuated and transferred into a glovebox where 85 mg

(0.279, 1.0 equiv.) of free IMes ligand was added and 5 ml of dry, air-free toluene were added. The solution was stirred for 24 h and thereafter filtered over celite. The solvent was removed in vacuo. To remove eventually remaining free IMes ligand the yellow solid was dissolved in dry benzene and IMes crystallizes out within 1 hour. After filtration over the product was crystallized by slow evaporation of benzene. The product was obtained as solvent adduct with 2 benzene molecules per complex in 68% yield (125 mg, 0.192 mmol) as yellow plates. Drying in vacuum did not remove the solvent molecules completely for **K6** (see X-ray structure analysis). Crystals suitable for X-ray analysis were obtained by slow evaporation of a saturated solution of **K6** in benzene.

^{1}H NMR (300 MHz, C_6D_6) δ 7.60 (d, *J* = 8.0 Hz, 1H, Ar-*H*), 7.32 (d, *J* = 9.2 Hz, 1H), 6.90 (ddd, *J* = 8.9, 7.7, 1.6 Hz, 1H, Ar-*H*), 6.78 (d, *J* = 9.4 Hz, 4H, Ar-*H*), 6.74 – 6.67 (m, 1H, Ar-*H*), 6.19 (s, 2H,N-C*H*=C*H*-N) 3.15 (s, 2H, -CH_2-), 2.61 (s, 6H, -CH_3), 2.47 (s, 6H, -CH_3), 2.06 (s, 6H, -CH_3), 1.49 (s, 6H, -CH_3). ^{13}C NMR (300 MHz, C_6D_6) δ 162.83 (N-C-N), 162.50 (C-S), 146.55 (Ar-C), 130.73 (Ar-C), 129.73 (Ar-C), 129.26 (Ar-C), 129.02 (Ar-C), 128.81 (Ar-C), 128.20 (Ar-C), 127.86 (Ar-C), 125.33 (Ar-C), 123.21 (N-CH=CH-N), 121.91, 80.86 (-CH_2-), 70.39 (O-**C**-$(CH_3)_2$), 27.25 (-CH_3), 20.60 (-CH_3), 19.71 (-CH_3), 19.06 (-CH_3). IR: 1610 (m, C=N), 1467 (m), 1376 (m), (1329 (m), 1057 (s), 730 (s). EI-MS: 653.4 [M^+]. Anal. Calcd. For $C_{32}H_{36}ClN_3OPdS \cdot 2C_6H_6$, (652.29) C, 65.34; H, 5.98; N, 5.20, found C 65.97, H 6.13, N 5.21

[PdBr(S-Phoz)(IMes)] (K7)

The same procedure as given for **K6** was used. Instead of [{PdCl(S-Phoz)}$_2$] (**K3**) the corresponding [{PdBr(S-Phoz)}$_2$] (**K4**) (86 mg, 0.110 mmol, 0.99 equiv.) was used as starting material. The appropriate amount of IMes (67 mg, 0.219 mmol, 1.0 equiv.) was used. The product was obtained in 91 % yield (130 mg, 0.199 mmol) as yellow powder. Crystal suitable for X-ray diffraction analysis were obtained evaporation of a saturated solution of **K7** in benzene. Due to the limited timeframe of this master thesis these structures were not included.

^{1}H NMR (300 MHz, C_6D_6) δ 7.55 (d, *J* = 7.9 Hz, 1H, Ar-*H*), 7.26 (d, *J* = 7.8 Hz, 1H, Ar-*H*), 6.89 (s, 1H, Ar-*H*), 6.77 (d, *J* = 4.5 Hz, 4H, Ar-*H*), 6.72 (s, 1H, Ar-*H*), 6.21 (s, 2H, N-C*H*=C*H*-N), 3.18 (s, 2H, -CH_2-), 2.61 (s, 6H, -CH_3), 2.48 (s, 6H, -CH_3), 2.07 (s, 6H, -CH_3), 1.50 (s, 6H, -CH_3). ^{13}C NMR (75 MHz, C_6D_6) δ 163.32, 161.66, 146.62 (Ar-C), 138.28 (Ar-C), 136.56 (Ar-C), 135.88 (Ar-C), 135.45 (Ar-C), 130.62 (Ar-C), 129.72 (Ar-C), 129.39 (Ar-C), 128.91 (Ar-C), 123.44 (-N-CH=CH-N), 122.17, 81.13 (-CH_2), 70.43 (O-**C**-$(CH_3)_2$), 27.60 (-CH_3), 20.65 (-CH_3), 20.52 (-CH_3), 19.36 (-CH_3). IR: 1612 (s,C=N), 1466 (m), 1361 (s), 1327 (m), 1057 (s), 729 (s),

700 (d,s) EI-MS: 697.4 (M^+]. Anal. Calcd. For $C_{32}H_{36}BrN_3OPdS \cdot 0.66\ C_6H_6$ (697.04) C, 57.11; H, 5.34; N, 5.71 found: C 57.26, H 5.65, N 5.83

[PdI(S-Phoz)(IMes)] (K8)

The same procedure as given for **K6** was used. Instead of [{PdCl(S-Phoz)}$_2$] (**K3**) the corresponding [{PdI(S-Phoz)}$_2$] (**K5**) (71 mg, 0.074 mmol, 0.99 equiv.) was used as starting material. The appropriate amount of IMes (45 mg, 0.148 mmol, 1.0 equiv.) was used. The product was obtained in 88 % yield (48 mg, 0.065 mmol) as orange crystals. Crystal suitable for X-ray diffraction analysis were obtained evaporation of a saturated solution of **K8** in benzene. Due to the limited timeframe of this master thesis these structures were not included.

^{1}H NMR (300 MHz, C_6D_6) δ 7.60 (d, *J* = 8.1 Hz, 1H, Ar-*H*), 7.48 (d, *J* = 7.9 Hz, 2H, Ar-*H*), 7.33 (d, *J* = 7.9 Hz, 1H, Ar-*H*), 6.77 (broad m, 4H, Ar-*H*), 6.20 (s, 2H, N-C*H*-C*H*-N), 3.23-3.15 (s, 2H, -CH_2-), 2.59 (s, 6H), 2.49 (s, 6H, -CH_3), 2.08 (s, 6H, -CH_3), 1.49 (s, 6H, -CH_3). ^{13}C NMR (75 MHz, C_6D_6) δ 163.42, 161.13, 146.97 (Ar-C), 138.26 (Ar-C), 136.11 (Ar-C), 135.52 (Ar-C), 130.52 (Ar-C), 130.53 (Ar-C), 130.06 (Ar-C), 129.73 (Ar-C), 129.55 (Ar-C), 129.03 (Ar-C), 123.71 (N-CH=CH-N), 122.26, 80.90 (-CH_2-), 70.42 (O-**C**-$(CH_3)_2$), 28.42 (-CH_3), 22.05 (-CH_3), 20.74 (-CH_3), 19.62 (-CH_3). IR: 1614 (s, C=N), 1362 (s), 1326 (s), 1055 (s), 844 (m), 735 (s), 702 (s), EI-MS: . Anal. Calcd. For $C_{32}H_{36}IN_3OPdS \cdot 0.66\ C_6H_6$, C, 54.31; H, 5.06; N, 5.28 found: C 54.30, H 5.07, N 5.65

[Pd(CF_3CO_2)(S-Phoz)(IMes)]·Ag(CF_3CO_2) (K9)

A 50 ml two-necked flask was equipped with a stirring bar and a reflux condenser on one neck. The whole apparatus was then wrapped in alumina foil to protect the reaction from light during all synthesis steps. Then the flask was charged with 50 mg (0.076 mmol, 1.0 equiv.) [PdCl(S-Phoz)(IMes)], **K6**, and 20 ml of dry acetonitrile were added. To the solution 51 mg (0.231 mmol, 3.0 equiv.) of $AgCF_3COO$ was added under vigorous stirring. After addition of the silver trifluoroacetate the reaction mixture was heated to 70 °C for 18 hours. In this time a white precipitate consisting of AgCl deposited on the wall of the glass flask. After cooling to room temperature the mixture was filtered through celite and the solvent evaporated in vacuo. The light yellow residue was redissolved in about 3.5 ml of dry benzene, filtered through celite and the solvent removed in vacuo. The product was obtained as a light yellow crystals in 86% (62 mg, 0.065 mmol) overall yield.

^{1}H NMR (300 MHz, C_6D_6) δ 7.11 (d, J = 7.8 Hz, 1H, Ar-*H*), 6.82 – 6.63 (m, 2H, Ar-*H*), 6.59 (td, J = 7.6, 1.2 Hz, 5H, Ar-*H*), 5.86 (s, 2H, N-C*H*-C*H*-N), 3.61(s, 2H,-CH_2-) 2.12 (s, 12H, -CH_3), 1.99 (s, 6H, -CH_3), 1.17 (s, 6H, -CH_3). ^{13}C NMR (300 MHz, C_6D_6) δ 163.39, 134.31 (Ar-C), 134.14 (Ar-C), 130.98 (Ar-C), 130.49 (Ar-C), 130.35 (Ar-C), 129.95 (Ar-C), 129.71 (Ar-C), 129.32 (Ar-C), 127.81 (Ar-C), 126.70 (Ar-C), 126.55 (Ar-C), 123.67 (N-CH=CH-N), 81.17 (-CH_2-), 69.66 (O-**C**-(CH_3)$_2$), 27.12 (-CH_3), 20.65 (-CH_3), 18.25 (-CH_3), 17.87 (-CH_3) ^{19}F NMR (300 MHz, C_6D_6) δ 72.94, 72.62 IR: 1693 (s,C=O), 1626 (m, C=N), 1367 (m), 1329 (m), 1188 (s), 1174 (s), 1132 (s), 724 (s). EI-MS: 729.4 [M^+-$AgCO_2CF_3$]

General Procedure for complexes K10-K12

[PdCl(S-Phoz)(PPh_3)] (K10)

A 50 ml round bottom flask was equipped with a stirring bar and charged with 53 mg (0.076 mmol, 1.0 equiv.) of complex **K3**. The complex was suspended in 20 ml of dry benzene and 20 mg triphenylphosphine (0.076 mmol, 1.0 equiv.) are added at once. The solution was then stirred at room temperature for 24 h. After the first hour the solution starts turning red to deep red. After 24 h nearly all solids dissolved into the red solution. The solution was filtered through celite and the solvent evaporated in vacuo. The remaining deep red residue was suspended in 10 ml of pentane and put in an ultra-sonic bath for 10 min. Then the orange-red solid which formed during this was filtered off and thoroughly washed with pentane (3x 15 ml). The product is dried in vacuo for a few hours. The product was obtained in 95% yield (88 mg, 0.144 mmol), as an orange-red powder.

^{1}H NMR (300 MHz, CD_2Cl_2) δ 7.81 – 7.69 (m, 6H, PPh_3), 7.60 (dd, J = 7.5, 1.8 Hz, 1H, Ar-H), 7.54 – 7.38 (m, 9H, PPh_3), 7.26 – 7.18 (m, 1H, Ar-H), 7.17 – 7.03 (m, 2H, Ar-H), 4.28 (s, 2H, -CH_2-), 1.87 (s, 6H, -CH3). ^{13}C NMR (75 MHz, CD2Cl2) δ 164.29 (d, J = 3.5 Hz), 144.73 (d, J = 1.4 Hz), 135.21 (d, J = 10.3 Hz), 131.32 (d, J = 2.0 Hz), 131.20 (d, J = 2.5 Hz), 130.86, 130.11, 129.78, 128.46 (d, J = 11.1 Hz), 128.31, 124.08, 82.40 (d, J = 3.1 Hz, -CH_2-), 71.82 (d, J = 1.7 Hz, (O-**C**-(CH_3)$_2$), 28.81 – 28.55 (m, -CH_3). ^{31}P NMR (121 MHz, CD_2Cl_2) δ 33.35. IR: 1615 (m), 1435 (m), 1055 (m), 966 (m), 775 (m), 737 (m), 690 (s), 532 (s), 516 (m), 502 (s). EI-MS: 611.1 [M+]. Anal. Calcd. for $C_{29}H_{27}ClNOPPdS$ (610.44): C, 57.06; H, 4.46; N, 2.29; S, 5.25. Found: C, 56.78; H, 4.52; N, 2.32; S, 5.11.

[PdCl(S-Phoz)($AsPh_3$)] (K11)

The same procedure as for complex **K10** was used. Instead of triphenylphosphine the homologue triphenylarsine (42 mg, 0.137 mmol 0.95 equiv.) was used. **K11** The product was obtained in 78% (70 mg, 0.107 mmol) yield as a red powder.

^{1}H NMR (300 MHz, C_6D_6) δ 7.85 (s, 6H, $AsPh_3$), 7.65 (s, 1H, Ar-*H*), 7.40 (s, 1H, Ar-*H*), 7.03 (s, 9H, $AsPh_3$), 6.74 (d, *J* = 4.8 Hz, 2H, Ar-*H*), 3.46 (s, 2H,-CH_2-), 1.84 (s, 6H, -CH_3). ^{13}C NMR (300 MHz, C_6D_6) δ 163.22, 134.25 (Ar-C), 133.65 (Ar-C), 131.83 (Ar-C), 130.83 (Ar-C), 130.49 (Ar-C), 129.91 (Ar-C), 128.64 (Ar-C), 128.28 (Ar-C) 127.88 (Ar-C), 122.77 (Ar-C), 81.06 (-CH_2-), 71.56 (O-**C**-$(CH_3)_2$), 27.80 (-CH_3) IR: 1610 (m, C=N), 1434 (m), 1327 (m), 1057 (s), 736 (s), 690 (s). EI-MS: 655.3 [M^+]. Anal. Calcd. for $C_{29}H_{27}AsClNOPdS \cdot 0.5\ C_6H_6$ (654.39) C 55.42, H 4.36, N 2.02, found: 55.05, H 4.28, N 1.84

Complex K12 [PdCl(S-Phoz)($SbPh_3$)] (K12)

The same procedure as for complex **K10** was used. Instead of triphenylphosphine the homologue triphenylstibine (42 mg, 0.119 mmol, 0.80 equiv.) was used. The product was obtained in 84 % (70 mg, 0.100 mmol) yield as a red powder.

^{1}H NMR (300 MHz, C_6D_6) δ 7.66 (s, 6H, $SbPh_3$), 7.50 (dd, *J* = 6.0, 3.2 Hz, 1H, Ar-*H*), 7.04 (s, 2H,Ar-*H*), 6.80 – 6.70 (m, 9H, $SbPh_3$), 3.45 (s, 2H,-CH_2-), 1.81 (s, 1H,-CH_3). ^{13}C NMR (300 MHz, C_6D_6) δ 162.74, 136.46 (Ar-C), 133.44 46 (Ar-C), 131.35 46 (Ar-C), 130.08 46 (Ar-C), 129.32 46 (Ar-C), 128.96 46 (Ar-C), 128.21 46 (Ar-C), 127.86 46 (Ar-C), 127.53 46 (Ar-C), 122.97 46 (Ar-C), 80.81 (-CH_2-), 71.55 (O-**C**-$(CH_3)_2$), 27.87 (-CH_3) IR: 1612 (m, C=N) 1366 (m), 1325 (m), 1056 (s), 997 (m), 739 (s), 690 (s). EI-MS: 700.1 [M^+]. Anal. Calcd. for $C_{29}H_{27}ClNOPdSSb \cdot 0.66\ C_6H_6$ (701.23) C 52.62, H 4.15, N 1.86 found: C 52.60, H 4.09, N 1.52

Appendix

A. Crystal Structures

Crystallographic Data and Structure Refinement Details

Table A1. Crystallographic Data and Structure Refinement for Complexes *trans*-[Pd(S-Phoz)$_2$] (**K1**), [Pd(η^2-S-Phoz)(η^1-S-Phoz)(PPh$_3$)] (**K2**) and [PdCl(S-Phoz)] (**K3**) [57]

	K1	K2	K3
Empirical formula	$C_{22}H_{24}N_2O_2PdS_2$	$C_{40}H_{39}N_2O_2PPdS_2$	$C_{22}H_{24}Cl_2N_2O_2Pd_2S_2$ · 0.590(8)CH_2Cl_2
Formula weight	518.95	781.22	746.45
Crystal description	needle, orange	block, red	plate, orange
Crystal size	0.28 x 0.07 x 0.06mm	0.26 x 0.21 x 0.16mm	0.28 x 0.17 x 0.07mm
Crystal system, space group	monoclinic, P $2_1/n$	monoclinic, P $2_1/n$	orthorhombic, P c c n
Unit cell dimensions	a = 9.6915(5) Å	a = 19.1853(6) Å	a = 15.0475(5) Å
	b = 10.9547(5) Å	b = 8.6988(3) Å	b = 23.4300(7) Å
	c = 20.6209(10) Å	c = 22.8924(8) Å	c = 7.6521(2) Å
	β = 90.443(2)°	β = 111.5480(10)°	
Volume	2189.20(18) Å^3	3553.5(2) Å^3	2697.85(14) Å^3
Z	4	4	4
Calculated density	1.575Mg/m^3	1.460Mg/m^3	1.838Mg/m^3
F(000)	1056	1608	1475.1
Linear absorption coefficient μ	1.059mm^{-1}	0.723mm^{-1}	1.827mm^{-1}
Max. and min. transmission	1.0000 and 0.7760	0.7461 and 0.5794	1.0000 and 0.7685
Θ range for data collection	2.32 to 27.00°	2.38 to 30.00°	2.71 to 30.00°
Index ranges	-12 ≤ h ≤ 11, -13 ≤ k ≤ 13, -20 ≤ l ≤ 26	-26 ≤ h ≤ 26, -9 ≤ k ≤ 12, -16 ≤ l ≤ 32	-21 ≤ h ≤ 21, -32 ≤ k ≤ 32, -10 ≤ l ≤ 10
Reflections collected/ unique	13570/ 4757	25656/ 10368	28367/ 3937
Significant unique reflections	4361 with I > 2σ(I)	8853 with I > 2σ(I)	3219 with I > 2σ(I)
R(int), R(sigma)	0.0352, 0.0401	0.0299, 0.0385	0.0447, 0.0274
Completeness to Θ = 30.0°	99.5%	99.9%	99.8%
Data/ parameters/ restraints	4757/ 303/ 43	10368/ 448/ 0	3937/ 179/ 0
Goodness-of-fit on F^2	1.168	1.035	1.330
Final R indices [I > 2σ(I)]	R1 = 0.0502, wR2 = 0.1070	R1 = 0.0281, wR2 = 0.0721	R1 = 0.0436, wR2 = 0.0957
R indices (all data)	R1 = 0.0562, wR2 = 0.1099	R1 = 0.0354, wR2 = 0.0753	R1 = 0.0606, wR2 = 0.1028
Weighting scheme	w = 1/[σ^2(F_o^2)+(aP)^2+bP] where P = (F_o^2+2F_c^2)/3	w = 1/[σ2(Fo2)+(aP)2+bP] where P = (Fo2+2Fc2)/3	w = 1/[σ_2(F_o^2)+(aP)^2+bP] where P = (F_o^2+2F_c^2)/3
Largest difference peak and hole	1.427 and -1.012e/Å^3	0.927 and -0.916e/Å^3	0.958 and -1.016e/Å^3
CCDC deposition number	1015351	1015356	1015357

Table A2. Crystallographic Data and Structure Refinement for Complexes [PdCl(S-Phoz(IMes)] (**K6**) and [PdCl(S-Phoz)(PPh_3)] (**K10**) [57]

	K6	K10
Empirical formula	$C_{32}H_{36}ClN_3OPdS \cdot 2(C_6H_6)$	$C_{29}H_{27}ClNOPPdS$
Formula weight	808.76	610.40
Crystal description	block, yellow	block, orange
Crystal size	0.24 x 0.21 x 0.20mm	0.19 x 0.17 x 0.12mm
Crystal system, space group	monoclinic, P $2_1/c$	monoclinic, P $2_1/c$
Unit cell dimensions	a = 15.7798(5) Å	a = 14.9793(7) Å
	b = 14.5940(5) Å	b = 10.9549(5) Å
	c = 17.4554(6) Å	c = 17.4456(8) Å
	β = 103.2628(13)°	β = 114.3340(10)°
Volume	3912.6(2) $Å^3$	2608.4(2) $Å^3$
Z	4	4
Calculated density	1.373Mg/m^3	1.554Mg/m^3
F(000)	1680	1240
Linear absorption coefficient μ	0.634mm^{-1}	0.979mm^{-1}
Max. and min. transmission	1.000 and 0.860	0.9922 and 0.8008
Θ range for data collection	2.40 to 35.00°	2.26 to 30.00°
Index ranges	$-25 \leq h \leq 23$, $-23 \leq k \leq 23$, $-28 \leq l \leq 20$	$-21 \leq h \leq 16$, $-9 \leq k \leq 15$, $-21 \leq l \leq 24$
Reflections collected/ unique	65894 / 17222	20782/ 7608
Significant unique reflections	14560 with $I > 2\sigma(I)$	6792 with $I > 2\sigma(I)$
R(int), R(sigma)	0.0308, 0.0273	0.0265, 0.0277
Completeness to Θ = 30.0°	99.9%	99.9%
Data/ parameters/ restraints	17222 / 483 / 0	7608/ 325/ 0
Goodness-of-fit on F^2	1.026	1.043
Final R indices [$I > 2\sigma(I)$]	R1 = 0.0251, wR2 = 0.0616	R1 = 0.0264, wR2 = 0.0683
R indices (all data)	R1 = 0.0345, wR2 = 0.0668	R1 = 0.0311, wR2 = 0.0707
Weighting scheme	$w = 1/[\square^2(F_o^2)+(aP)^2+bP]$ where $P = (F_o^2+2F_c^2)/3$	$w = 1/[\sigma_2(F_o^2)+(aP)^2+bP]$ where $P = (F_o^2+2F_c^2)/3$
Largest difference peak and hole	0.662 and -0.406e/$Å^3$	0.870 and -0.545e/$Å^3$
CCDC deposition number	-	1015358

[a)] Results of **K9** are preliminary and therefore not shown in this thesis.

B. DFT Evaluations

B.1 Structural isomers of K3-K5

Not only the sulfur moiety is able to bridge both palladium centers in complexes **K3-K5** but also the halogenide is capable of doing this. Starting from the crystal structure of **K3** the structures of all 6 possible compounds (**K3, K4, K5** and µ-Cl **K3**, µ-Br **K4** and µ-I **K5**) where determined and their energies compared. Despite the reduction in steric strain the µ-S mode stays the more stable conformer throughout the whole series. The dipole moment is vastly reduced in the µ-I bridged dimer indicating the formation of an inversion center in the molecule.

Table 12: Energy differences between S-bridged and X-bridged mode of K3-K5. Energies and dipole moments were obtained at PBE0/def2-TZVP+D3 level of theory using the ORCA3.0 program.

	K3	**K4**	**K5**
µ-S [Eh]	-3084,2670	-7311,5237	-2759,6014
µ-X [Eh]	-3084,2439	-7311,5051	-2759,5770
	-60,4 kJ/mol	-49,0 kJ/mol	-63,9 KJ/mol
Dipole moment			
µ-S	0,0021 D	0,0022 D	0,0074 D
µ-X	3,8563 D	2,6904 D	0,0025 D

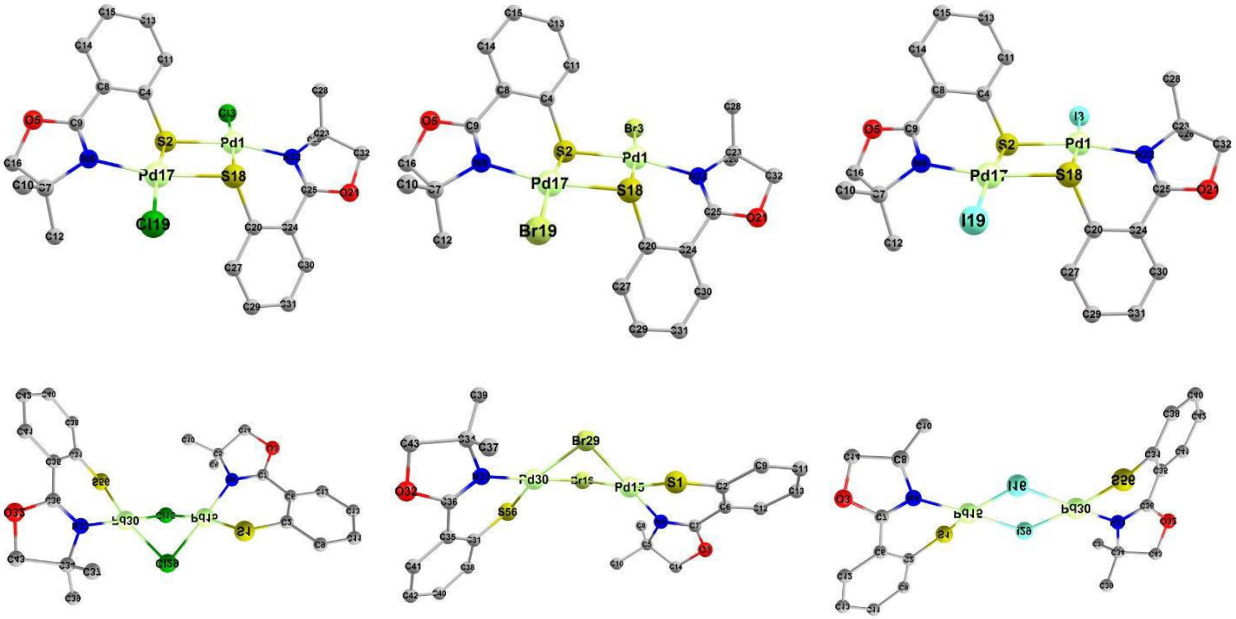

Figure 23: K3-K5 in S-bridged and I-bridged mode. Structures optimized at PBE0/def2-TZVP+D3 level using ORCA3.0. Plots were generated using Chemcraft 1.7. Upper Left: K3, Upper Middle: K4, Upper Right: K5, Lower Left: µ-Cl K3, Lower Middle: µ-Br K4, Lower Right: µ-I K5.

B.2 Results of DFT functional investigation on complexes K3 and K6

Table 13: Unsigned errors from the geometry optimization of $[Pd(S\text{-}Phoz)Cl]_2$, **K3**, with a given functional and the def2-SVP / ECP28MWB basis set. Deviations are given in % relative to crystal structure.

def2-SVP	BLYP	PBE	PW91	TPSS	BP86	B3LYP	PBE0	TPSSh	M06
Pd1-S1	2,62%	2,45%	2,43%	2,59%	2,62%	3,32%	1,79%	2,32%	3,95%
Pd1-Cl1	1,05%	0,96%	0,87%	0,84%	1,05%	1,14%	0,06%	0,49%	0,50%
Pd1-N1	0,78%	0,71%	0,60%	0,59%	0,78%	1,73%	0,14%	0,40%	1,44%
S1-C1	1,05%	0,83%	0,81%	0,89%	1,05%	0,79%	0,07%	0,49%	0,72%
S1-Pd1-S2	0,10%	0,03%	0,00%	0,37%	0,10%	0,07%	0,07%	0,30%	2,96%
Pd2S2-C6H5-plane	9,50%	9,58%	9,80%	10,03%	9,50%	8,21%	8,32%	9,41%	1,88%
	BLYP	PBE	PW91	TPSS	BP86	B3LYP	PBE0	TPSSh	M06
MUE	1,12%	1,00%	0,94%	1,05%	1,12%	1,41%	0,43%	0,80%	1,91%

Table 14: Unsigned errors from the geometry optimization of $[Pd(S\text{-}Phoz)Cl]_2$, **K3**, with a given functional and the def2-SVP / ECP28MWB basis set and pairwise dispersion correction. Deviations are given in % relative to crystal structure.

def2-SVP/D3	BLYP	PBE	PW91	TPSS	BP86	B3LYP	PBE0	TPSSh	M06
Pd1-S1	3,71%	2,25%	-	2,32%	2,25%	2,93%	1,61%	1,07%	-
Pd1-Cl1	1,82%	0,80%	-	0,62%	0,75%	0,87%	0,08%	0,22%	-
Pd1-N1	1,36%	0,23%	-	0,02%	0,08%	0,84%	0,27%	0,80%	-
S1-C1	1,41%	0,68%	-	0,70%	0,78%	0,51%	0,18%	0,01%	-
S1-Pd1-S2	0,75%	0,32%	-	0,88%	0,58%	0,63%	0,25%	1,99%	-
Pd2S2-C6H5-plane	4,95%	4,09%	-	6,58%	5,03%	4,75%	6,00%	4,09%	-
	BLYP	PBE	PW91	TPSS	BP86	B3LYP	PBE0	TPSSh	M06
MUE	1,81%	0,86%	--	0,91%	0,89%	1,16%	0,48%	0,82%	--

Table 15: Unsigned errors from the geometry optimization of [Pd(S-Phoz)Cl]$_2$, **K3**, with a given functional and the def2-TZVP / ECP28MWB basis set. Deviations are given in % relative to crystal structure.

Def2-TZVP	BLYP	PBE	PW91	TPSS	BP86	B3LYP	PBE0	TPSSh	M06
Pd1-S1	1,30%	1,10%	1,12%	1,27%	1,30%	2,04%	0,48%	1,01%	2,44%
Pd1-Cl1	0,62%	0,50%	0,44%	0,38%	0,62%	0,93%	0,43%	0,02%	0,42%
Pd1-N1	1,29%	1,25%	1,12%	1,04%	1,29%	2,17%	0,55%	0,82%	1,97%
S1-C1	0,51%	0,33%	0,29%	0,34%	0,51%	0,31%	0,56%	0,04%	0,04%
S1-Pd1-S2	1,02%	1,07%	1,00%	0,54%	1,02%	0,69%	1,08%	0,61%	1,25%
Pd_2S_2- S-Phoz-plane	9,61%	9,49%	9,58%	9,20%	9,61%	8,20%	8,24%	8,74%	0,00%
	BLYP	PBE	PW91	TPSS	BP86	B3LYP	PBE0	TPSSh	M06
MUE	0,95%	0,85%	0,79%	0,71%	0,95%	1,23%	0,62%	0,50%	1,23%

Table 16: Unsigned errors from the geometry optimization of [PdCl(S-Phoz)(IMes)], **K6**, with a given functional and the def2-SVP / ECP28MWB basis set. Deviations are given in % relative to crystal structure

def2-SVP	BLYP	PBE	PW91	TPSS	BP86	B3LYP	PBE0	TPSSh	M06
Pd1-S1	3,71%	1,96%	1,95%	2,12%	2,06%	2,94%	1,45%	1,91%	3,56%
Pd1-Cl1	3,28%	1,81%	1,74%	1,55%	1,92%	2,14%	0,79%	1,17%	1,47%
Pd1-C1	2,06%	0,51%	0,49%	1,02%	0,70%	1,64%	0,27%	0,88%	1,26%
Pd1-N1	3,74%	1,79%	1,60%	1,32%	1,89%	2,78%	1,07%	1,12%	1,67%
S1-C1	1,44%	0,54%	0,53%	0,67%	0,68%	0,82%	0,07%	0,45%	0,72%
N-Pd-Cl angle	0,31%	0,14%	0,15%	0,45%	0,18%	0,32%	0,03%	0,34%	0,17%
Mes-Mes plane	16,38%	7,83%	6,85%	0,65%	11,41%	12,01%	3,94%	0,00%	32,50%
IMes-Pd plane	16,16%	11,70%	11,61%	5,54%	12,80%	13,31%	8,85%	5,06%	6,52%
	BLYP	PBE	PW91	TPSS	BP86	B3LYP	PBE0	TPSSh	M06
MUE	5,89%	3,28%	3,11%	1,66%	3,95%	4,50%	2,06%	1,37%	5,98%

Table 17: Unsigned errors from the geometry optimization of [PdCl(S-Phoz)(IMes)], **K6**, with a given functional and the def2-SVP / ECP28MWB basis set and pairwise dispersion correction. Deviations are given in % relative to crystal structure

def2-SVP-D3	BLYP	PBE	PW91	TPSS	BP86	B3LYP	PBE0	TPSSh	M06
Pd1-S1	3,43%	1,90%	-	2,07%	1,96%	2,68%	1,40%	1,17%	-
Pd1-Cl1	2,77%	1,54%	-	1,21%	1,43%	1,69%	0,57%	0,37%	-
Pd1-C1	0,61%	0,16%	-	0,11%	0,47%	0,42%	0,35%	0,63%	-
Pd1-N1	2,07%	0,94%	-	0,31%	0,45%	1,37%	0,34%	0,70%	-
S1-C1	1,40%	0,58%	-	0,78%	0,75%	0,82%	0,13%	0,30%	-
N-Pd-Cl angle	0,24%	0,30%	-	0,54%	0,43%	0,01%	0,15%	0,90%	-
Mes-Mes plane	22,20%	13,76%	-	24,48%	26,83%	19,17%	16,12%	30,51%	-
IMes-Pd plane	1,48%	4,38%	-	2,57%	0,68%	2,37%	2,64%	8,76%	-
	BLYP	PBE	PW91	TPSS	BP86	B3LYP	PBE0	TPSSh	M06
MUE	4,27%	2,95%	--	4,01%	4,12%	3,57%	2,71%	5,42%	--

Table 18: Unsigned errors from the geometry optimization of [PdCl(S-Phoz)(IMes)], **K6**, with a given functional and the def2-TZVP / ECP28MWB basis set. Deviations are given in % relative to crystal structure

def2-TZVP	BLYP	PBE	PW91	TPSS	BP86	B3LYP	PBE0	TPSSh	M06
Pd1-S1	2,72%	0,87%	0,88%	1,06%	1,04%	1,96%	0,43%	0,88%	2,09%
Pd1-Cl1	2,88%	1,12%	1,08%	0,95%	0,93%	1,68%	0,11%	0,56%	1,40%
Pd1-C1	2,30%	0,60%	0,59%	1,12%	1,12%	1,81%	0,32%	0,97%	2,07%
Pd1-N1	3,80%	1,78%	1,59%	1,25%	1,29%	2,80%	1,05%	1,05%	1,86%
S1-C1	0,96%	0,01%	0,02%	0,10%	0,09%	0,34%	0,42%	0,08%	0,08%
N-Pd-Cl angle	0,63%	0,08%	0,06%	0,12%	0,18%	0,58%	0,25%	0,00%	0,86%
Mes-Mes plane	19,60%	8,62%	7,85%	2,59%	2,52%	14,10%	2,57%	2,57%	7,40%
IMes-Pd plane	17,14%	10,45%	5,91%	4,13%	4,07%	13,34%	4,25%	4,25%	5,11%
	BLYP	PBE	PW91	TPSS	BP86	B3LYP	PBE0	TPSSh	M06
MUE	6,25%	2,94%	2,25%	1,42%	1,40%	4,58%	1,18%	1,30%	2,61%

B.3 Results of TD-DFT investigation of complexes K3-K12

Table 19: Calculated excitation spectra of complex **K6** with the functionals PBE0, B3LYP, TPSSh and M06 with Sapporo DKH3-TZVP basis set. First excitation measured at 436 nm, second at 362 nm in a solid sample of **K6**. Oscillator strengths of singlet-triplet excitations are zero due to spin symmetry

	PBE0	**f (osc.)**	**B3LYP**	**f (osc.)**	**TPSSh**	**f (osc.)**	**M06**	**f (osc.)**
S0 → S1	420.4	0.02498	476.4	0.01423	458.4	0.02310	471.2	0.01420
S0 → S2	361.1	0.03013	377.5	0.03264	393.4	0.02481	374.6	0.02848
S0 → S3	340.0	0.00718	363.3	0.00072	352.1	0.01279	360.5	0.00068
S0 → S4	325.4	0.00377	355.8	0.02393	345.1	0.00386	353.3	0.02582
S0 → S5	298.2	0.00155	325.2	0.00658	334.0	0.00057	324.1	0.00441
S0 → T0	505.2	-	556.7	-	553.9	-	544.6	-
S0 → T1	424.3	-	545.0	-	457.4	-	465.2	-
S0 → T2	416.5	-	468.3	-	441.4	-	424.1	-
S0 → T3	372.6	-	432.2	-	389.9	-	412.6	-
S0 → T4	351.7	-	423.0	-	382.4	-	391.7	-

Table 20: Excitation energies of complexes **K6-K8**. Values calculated with PBE0/Sapporo basis set with scalar relativistic DKH2 Hamiltonian.

	K6 (X=Cl)	**f (osc.)**	**K7 (X=Br)**	**f (osc.)**	**K8 (X=I)**	**f (osc.)**
Exp. [nm]	436		452		468	
Exp. [cm^{-1}]	22935		22123		21368	
S0 → S1 [nm]	416.5	0.02495	425.7	0.02246	440.6	0.02161
[cm^{-1}]	24009.6		23488.8		22694.5	
S0 → S2 [nm]	358.6	0.02396	360.4	0.02296	369.4	0.00117
[cm^{-1}]	27888.1		27743.9		27072.8	
S0 → S3 [nm]	336.3	0.00893	342.3	0.00960	359.8	0.02445
[cm^{-1}]	29732.6		29214.0		27792.3	
S0 → S4 [nm]	322.6	0.00334	339.2	0.00271	349.9	0.00582
[cm^{-1}]	30995.3		29483.2		28579.3	
S0 → S5 [nm]	296.1	0.00323	308.5	0.00534	339.1	0.00732
[cm^{-1}]	33767.7		32418.1		29494.1	

Table 21: Excitation energies of complexes **K10-K12**. Values calculated with PBE0/Sapporo basis set with scalar relativistic DKH2 Hamiltonian.

	K10 (L=PPh_3)	**f (osc.)**	**K11 (L=$AsPh_3$)**	**f (osc.)**	**K12 (L=$SbPh_3$)**	**f (osc.)**
Exp. [nm]	49		500		504	
Exp. [cm-1]	20242		20000		19841	
S0 → S1 [nm]	478.0	0.01848	506.9	0.01043	494.2	0.00861
[cm^{-1}]	20920.9		19728.7		20232.8	
S0 → S2 [nm]	388.4	0.03176	397.8	0.03052	388.7	0.02310
[cm^{-1}]	25749.4		25138.8		25730.0	
S0 → S3 [nm]	358.6	0.01110	364.9	0.00441	378.7	0.02890
[cm^{-1}]	27886.3		27402.4		26406.8	
S0 → S4 [nm]	354.2	0.02074	362.6	0.02383	369.0	0.00847
[cm^{-1}]	28232.3		27579.5		27098.3	
S0 → S5 [nm]	326.4	0.01894	331.9	0.00564	338.4	0.01801
[cm^{-1}]	30640.0		30125.0		29550.5	

Table 22: Excitation energies of complexes **K3-K5**. Values calculated with PBE0/Sapporo basis set with scalar relativistic DKH2 Hamiltonian.

	K3 (X=Cl)	**f (osc.)**	**K4 (X=Br)**	**f (osc.)**	**K5 (X=I)**	**f (osc.)**
Exp. [nm]						
Exp. [cm^{-1}]						
S0 → S1 [nm]	444.0	0.05414	462.6	0.04483	491.3	0.02793
[cm^{-1}]	22521.5		21616.6		20353.7	
S0 → S2 [nm]	438.1	0.00000	456.7	0.00017	487.0	0.00387
[cm^{-1}]	22828.0		21895.2		20533.5	
S0 → S3 [nm]	399.4	0.00000	422.6	0.00009	464.3	0.00008
[cm^{-1}]	25035.7		23664.6		21537.2	
S0 → S4 [nm]	393.1	0.01133	420.3	0.00661	461.2	0.00538
[cm^{-1}]	25439.0		23793.9		21680.8	
S0 → S5 [nm]	393.1	0.00134	408.6	0.00001	429.0	0.00058
[cm^{-1}]	25440.9		24473.2		23307.5	

References

(1) Miyaura, N.; Yanagi, T.; Suzuki, A. *Synth. Commun.* **1981**, *11*, 513–519.

(2) Mickel, S. J.; Niederer, D.; Daeffler, R.; Osmani, A.; Kuesters, E.; Schmid, E.; Schaer, K.; Gamboni, R.; Chen, W.; Loeser, E.; Kinder, F. R.; Konigsberger, K.; Prasad, K.; Ramsey, T. M.; Repič, O.; Wang, R.-M.; Florence, G.; Lyothier, I.; Paterson, I. *Org. Process Res. Dev.* **2004**, *8*, 122–130.

(3) Martin, R.; Buchwald, S. L. *Acc. Chem. Res.* **2008**, *41*, 1461–1473.

(4) Jiang, N.; Ragauskas, A. J. *Tetrahedron Lett.* **2006**, 197–200.

(5) Proutiere, F.; Aufiero, M.; Schoenebeck, F. *J. Am. Chem. Soc.* **2012**, *134*, 606–612.

(6) Walker, S. D.; Barder, T. E.; Martinelli, J. R.; Buchwald, S. L. *Angew. Chem. Int. Ed. Engl.* **2004**, *43*, 1871–1876.

(7) Barder, T. E.; Walker, S. D.; Martinelli, J. R.; Buchwald, S. L. *J. Am. Chem. Soc.* **2005**, *127*, 4685–4696.

(8) So, C. M.; Lau, C. P.; Kwong, F. Y. *Angew. Chem. Int. Ed. Engl.* **2008**, *47*, 8059–8063.

(9) Kondolff, I.; Doucet, H.; Santelli, M. *Tetrahedron* **2004**, *60*, 3813–3818.

(10) Hayashi, T.; Konishi, M.; Kobori, Y.; Kumada, M.; Higuchi, T. *J. Am. Chem. Soc.* **1984**, 158–163.

(11) Arduengo, A. J. III; Harlow, R. L.; Kline, M. *J. Am. Chem. Soc.* **1991**, 361–363.

(12) Herrmann, W. A.; Elison, M.; Fischer, J.; Kocher, C.; Artus, Georg R. J. *Angew. Chem. Int. Ed. Engl.* **1995**, *34*, 2371–2374.

(13) Fortman, G. C.; Nolan, S. P. *Chem. Soc. Rev.* **2011**, *40*, 5151–5169.

(14) Crabtree, R. H. *J. Organomet. Chem.* **2005**, *690*, 5451–5457.

(15) Díez-González, S.; Nolan, S. P. *Coord. Chem. Rev.* **2007**, *251*, 874–883.

(16) Gstöttmayr, C.; Böhm, V.; Herdtweck, E.; Grosche, M.; Hermann, W. A. *Angew. Chem. Int. Ed. Engl.* **2002**, *41*, 1363–1365.

(17) Fortman, G. C.; Nolan, S. P. *Chem. Soc. Rev.* **2011**, *40*, 5151.

(18) Marion, N.; Navarro, O.; Mei, J.; Stevens, E. D.; Scott, N. M.; Nolan, S. P. *J. Am. Chem. Soc.* **2006**, *128*, 4101–4111.

(19) O'Brien, C. J.; Kantchev, Eric Assen B; Valente, C.; Hadei, N.; Chass, G. A.; Lough, A.; Hopkinson, A. C.; Organ, M. G. *Chem. Eur. J.* **2006**, *12*, 4743–4748.

(20) Hartmann, C. E.; Nolan, S. P.; Cazin, Catherine S. J. *Organometallics* **2009**, *28*, 2915–2919.

(21) Scholl, M.; Ding, S.; Lee, C. W.; Grubbs, R. H. *Org. Lett.* **1999**, *1*, 953–956.

(22) Lebel, H.; Janes, M. K.; Charette, A. B.; Nolan, S. P. *J. Am. Chem. Soc.* **2004**, *126*, 5046–5047.

(23) Grasa, G. A.; Viciu, M. S.; Huang, J.; Zhang, C.; Trudell, M. L.; Nolan, S. P. *Organometallics* **2002**, *21*, 2866–2873.

(24) Beletskaya, I. P.; Cheprakov, A. V. *J. Organomet. Chem.* **2004**, *689*, 4055–4082.

(25) Navarro, O.; Marion, N.; Oonishi, Y.; Kelly, R. A.; Nolan, S. P. *J. Org. Chem.* **2006**, *71*, 685–692.

(26) Navarro, O.; Kelly, R. A.; Nolan, S. P. *J. Am. Chem. Soc.* **2003**, *125*, 16194–16195.

(27) Xiong, Z.; Wang, N.; Dai, M.; Li, A.; Chen, J.; Yang, Z. *Org. Lett.* **2004**, *6*, 3337–3340.

(28) Peris, E.; Loch, J. A.; Mata, J.; Crabtree, R. H. *Chem. Commun.* **2001**, 201–202.

(29) Zim, D.; Nobre, S. M.; Monteiro, A. L. *J. Mol. Cat. A* **2008**, *287*, 16–23.

(30) Rao, G. K.; Kumar, A.; Kumar, S.; Dupare, U. B.; Singh, A. K. *Organometallics* **2013**, *32*, 2452–2458.

(31) Leadbeater, N. E.; Marco, M. *Org. Lett.* **2002**, *4*, 2973–2976.

(32) Leadbeater, N. E.; Marco, M. *J. Org. Chem.* **2003**, *68*, 888–892.

(33) Liu, C.; Zhang, Y.; Liu, N.; Qiu, J. *Green Chem.* **2012**, *14*, 2999.

(34) Hagiwara, H.; Sugawara, Y.; Hoshi, T.; Suzuki, T. *Chem. Commun.* **2005**, 2942–2944.

(35) Yuan, D.; Huynh, H. V. *Inorg. Chem.* **2013**, *52*, 6627–6634.

(36) Yuan, D.; Huynh, H. V. *Organometallics* **2010**, *29*, 6020–6027.

(37) Zhong, R.; Pöthig, A.; Feng, Y.; Riener, K.; Herrmann, W. A.; Kühn, F. E. *Green Chem.* **2014**, *16*, 4955–4962.

(38) Fleckenstein, C.; Roy, S.; Leuthäusser, S.; Plenio, H. *Chem. Commun.* **2007**, 2870–2872.

(39) Huang, R.; Shaughnessy, K. H. *Organometallics* **2006**, *25*, 4105–4112.

(40) Western, E. C.; Daft, J. R.; Johnson, E. M.; Gannett, P. M.; Shaughnessy, K. H. *J. Org. Chem.* **2003**, *68*, 6767–6774.

(41) Godoy, F.; Segarra, C.; Poyatos, M.; Peris, E. *Organometallics* **2011**, *30*, 684–688.

(42) Tsang, M. Y.; Viñas, C.; Teixidor, F.; Planas, J. G.; Conde, N.; SanMartin, R.; Herrero, M. T.; Domínguez, E.; Lledós, A.; Vidossich, P.; Choquesillo-Lazarte, D. *Inorg. Chem.* **2014**, *53*, 9284–9295.

(43) Inés, B.; SanMartin, R.; Churruca, F.; Domínguez, E.; Urtiaga, M. K.; Arriortua, M. I. *Organometallics* **2008**, *27*, 2833–2839.

(44) Dervisi, A.; Koursarou, D.; Ooi, L.-L.; Horton, P. N.; Hursthouse, M. B. *Dalton Trans.* **2006**, 5717–5724.

(45) Wang, H.; Zhong, R.; Guo, X.-Q.; Feng, X.-Y.; Hou, X.-F. *Eur. J. Inorg. Chem.* **2010**, *2010*, 174–178.

(46) Basauri-Molina, M.; Hernández-Ortega, S.; Toscano, R. A.; Valdés-Martínez, J.; Morales-Morales, D. *Inorg. Chim. Acta* **2010**, *363*, 1222–1229.

(47) Yuan, D.; Teng, Q.; Huynh, H. V. *Organometallics* **2014**, *33*, 1794–1800.

(48) Majumdar, A.; Sarkar, S. *Coord. Chem. Rev.* **2011**, *255*, 1039–1054.

(49) Williams, B. R.; Fu, Y.; Yap, Glenn P A; Burgmayer, Sharon J Nieter. *J. Am. Chem. Soc.* **2012**, *134*, 19584–19587.

(50) Peschel, L. M.; Schachner, J. A.; Sala, C. H.; Belaj, F.; Mösch-Zanetti, N. C. *Z. anorg. allg. Chem.* **2013**, *639*, 1559–1567.

(51) Qi-Lin, Z.; Pfaltz, A. *Tetrahedron* **1994**, *50*, 4467–4478.

(52) Mugesh, G.; Singh, H. B.; Butcher, R. J. *Eur. J. Inorg. Chem.* **1999**, 1229–1236.

(53) Guiu, E.; Claver, C.; Castillón, S. *J. Organomet. Chem.* **2004**, *689*, 1911–1918.

(54) Bottini, R.C.R.; Gariani, R.A.; Cavalcanti, C.d.O.; Oliveira, F.; da Rocha, N.L.G.; Back, D.;Lang, E.S.; Hitchcock, P.B.; Evans, D.J.; Nunes, G.G.; Simonelli, F.; de Sá, F.L.; Soares, J.F. *Eur. J. Inorg. Chem* **2010**, 2476–2487.

(55) Wenzel, M.; Meggers, E. *Eur. J. Inorg. Chem.* **2012**, 3168–3175.

(56) Holleman, A. F.; Wiberg, N. *Lehrbuch der Anorganischen Chemie;* de Gruyter, Berlin, **2007**, 1722.

(57) Peschel, L. M.; Holzer, C.; Mihhajlovic-Lalic, L.; Belaj, F.; Mösch-Zanetti, N. C. *Eur. J. Inorg. Chem.* **2015**, accepted, available online DOI: 10.1002/ejic.201403108

(58) Seechurn, J.; Kitching, C.; Matthew O.; Colacot, T. J.; Snieckus, V. *Angew. Chem. Int. Ed. Engl.* **2012**, *51*, 5062–5085.

(59) Stille, J. K. *Angew. Chem. Int. Ed. Engl.* **1986**, *25*, 508–524.

(60) Miyaura, N. Suzuki. A. *Chem. Rev.* **1995**, *95*, 2457–2483.

(61) Beletskaya, I. P.; Cheprakov, A. V. *Chem. Rev.* **2000**, *100*, 3009–3066.

(62) Amatore, C.; Azzabi, M.; Jutand, A. *J. Am. Chem. Soc.* **1991**, *113*, 1670–1677.

(63) Amatore, C.; Jutand, A.; Suarez, A. *J. Am. Chem. Soc.* **1993**, *115*, 9531–9541.

(64) Amatore, C.; Jutand, A. *J. Organomet. Chem.* **1999**, *576*, 254–278.

(65) Jutand, A. *Chem. Rev.* **2008**, *108*, 2300–2347.

(66) Elschenbroich, C. *Organometallchemie,* 6th ed.; B.G. Teubner Verlag, Wiesbaden, **2008**, 600-610.

(67) Holleman, A. F.; Wiberg, N. *Lehrbuch der Anorganischen Chemie;* de Gruyter, Berlin, **2007**, 1725.

(68) Figgis, B. N. *Comprehensive Coordination Chemistry* **1987**, *1*, 243–246.

(69) VanQuickenborne, L. G.; Ceulemans, A. *Inorg. Chem.* **1981**, *20*, 796–800.

(70) Griffith, J. S.; Orgel, L. E. *Q. Rev. Chem. Soc.* **1957**, *11*, 381–393.

(71) Cueva, J. P.; Chemel, B. R.; Juncosa, J. I.; Lill, M. A.; Watts, V. J.; Nichols, D. E. *Eur. J. Med. Chem.* **2012**, *48*, 97–107.

(72) Chambers, R. J.; Koch, K.; Biggers, M. S.; Ramchandani, M. *Bioorg. Med. Chem. Lett.* **1998**, *8*, 1787–1790.

(73) Harvey, J. N.; Jover, J.; Lloyd-Jones, G. C.; Moseley, J. D.; Murray, P.; Renny, J. S. *Angew. Chem. Int. Ed. Engl.* **2009**, *48*, 7612–7615.

(74) Aghatabay, N. M.; Somer, M.; Senel, M.; Dulger, B.; Gucin, F. *Eur. J. Med. Chem.* **2007**, *42*, 1069–1075.

(75) Barrera, H.; Viñas, J. M.; Font-Altaba, M.; Solans, X. *Polyhedron* **1985**, *4*, 2027–2030.

(76) Solans, X.; Font-Altaba, M.; Briansó, J. L.; Sola, J.; Suades, J.; Barrera, H. *Acta Crystallogr., Sect. C: Cryst. Struct. Commun.* **1983**, *39*, 1653–1655.

(77) García-Antón, J.; Pons, J.; Solans, X.; Font-Bardia, M.; Ros, J. *Inorg. Chim. Acta* **2003**, *355*, 87–94.

(78) Viciu, M. S.; Navarro, O.; Germaneau, R. F.; Kelly, R. A.; Sommer, W.; Marion, N.; Stevens, E. D.; Cavallo, L.; Nolan, S. P. *Organometallics* **2004**, *23*, 1629–1635.

(79) Lee, H. M.; Zeng, J. Y.; Hu, C.-H.; Lee, M.-T. *Inorg. Chem.* **2004**, *43*, 6822–6829.

(80) Gupta, M.; Cramer, R. E.; Ho, K.; Pettersen, C.; Mishina, S.; Belli, J.; Jensen, C. M. *Inorg. Chem.* **1995**, *34*, 60–65.

(81) Lobana, T. S.; Bawa, G.; Hundal, G.; Zeller, M. *Z. anorg. allg. Chem.* **2008**, *634*, 931–937.

(82) Nakatsu, Y.; Nakamura, Y.; Matsumoto, K.; Ooi, S. *Inorg. Chim. Acta* **1992**, *196*, 81–88.

(83) Paul, P.; Sengupta, P.; Bhattacharya, S. *J. Organomet. Chem.* **2013**, *724*, 281–288.

(84) Sindhuja, E.; Ramesh, R.; Liu, Y. *Dalton Trans.* **2012**, *41*, 5351.

(85) Crespo, O.; Gimeno, M. C.; Laguna, A.; Lehtonen, O.; Ospino, I.; Pyykkö, P.; Villacampa, M. D. *Chem. Eur. J.* **2014**, *20*, 3120–3127.

(86) Vicente, J.; Chicote, M. T.; Huertas, S.; Bautista, D.; Jones, P. G.; Fischer, A. K. *Inorg. Chem.* **2001**, *40*, 2051–2057.

(87) Fornies, J.; Martin, A.; Navarro, R.; Sicilia, V.; Villarroya, P.; G. Orpen, A. *J. Chem. Soc., Dalton Trans.* **1998**, 3721–3726.

(88) Uhe, A.; Kozuch, S.; Shaik, S. *J. Comp. Chem.* **2011**, *32*, 978–985.

(89) Rezende, J. de; Franco, D. *Transition Metal Chemistry* **1987**, *12*, 267–270.

(90) Grimme, S.; Antony, J.; Ehrlich, S.; Krieg, H. *J. Chem. Phys.* **2010**, *132*, 154104.

(91) Grimme, S.; Ehrlich, S.; Goerigk, L. *J. Comput. Chem.* **2011**, *32*, 1456–1465.

(92) Rudolph, M.; Autschbach, J. *J. Chem. Phys. A* **2011**, *115*, 14677–14686.

(93) Holleman, A. F.; Wiberg, N. *Lehrbuch der Anorganischen Chemie;* de Gruyter, Berlin, **2007**, 1357.

(94) Bernardi, A.; Ouellet, S. G.; Angelaud, R.; O'Shea, P. D. *Tetrahedron Lett.* **2008**, *49*, 6707–6708.

(95) Siegl, W. O. *J. Org. Chem.* **1977**, *42*, 1872–1878.

(96) Newman, M. S.; Kannan, R. *J. Org. Chem.* **1979**, *44*, 3388–3390.

(97) Dombroski, M. A.; Koch, K.; Piscopio, A. D. Benzopyran and benzo-fused compounds, their preparation and their use as leukotriene B4 (LTB4) antagonists. US19970809728 19970409.

(98) Clarke, D. S.; Wood, R. *Synthetic Commun.* **1996**, *26*, 1335–1340.

(99) Black, D. S.; Wade, M. J. *Aust. J. Chem.* **1972**, *25*, 1797–1810.

(100) Arduengo, A. J., III; Dias, R. D.; Harlow, R. L.; Kline, M. *J. Am. Chem. Soc.* **1992**, 5530–5534.

(101) Sheldrick, G. M. *Acta Crystallogr., Sect. A: Found. Crystallogr.* **2008**, *64*, 112–122.

(102) Weigend, F.; Ahlrichs, R. *Phys. Chem. Chem. Phys.* **2005**, *7*, 3297–3305.

(103) Perdew, J. P. *Phys. Rev. B* **1986**, *33*, 8822–8824.

(104) Becke, A. D. *Phys. Rev. A* **1988**, *38*, 3098–3100.

(105) Perdew, J. P.; Burke, K.; Ernzerhof, M. *Phys. Rev. Lett.* **1996**, *77*, 3865–3868.

(106) Perdew, J. P.; Burke, K.; Ernzerhof, M. *Phys. Rev. Lett.* **1997**, *78*, 1396.

(107) Perdew, J. P. *Electronic Structure of Solids* **1991**, 11.

(108) Perdew, J. P.; Chevary, J. A.; Vosko, S. H.; Jackson, K. A.; Pederson, M. R.; Singh, D. J.; Fiolhais, C. *Phys. Rev. B* **1992**, *46*, 6671–6687.

(109) Perdew, J. P.; Wang, Y. *Phys. Rev. B* **1992**, *45*, 13244–13249.

(110) Perdew, J. P.; Chevary, J. A.; Vosko, S. H.; Jackson, K. A.; Pederson, M. R.; Singh, D. J.; Fiolhais, C. *Phys. Rev. B* **1993**, *48*, 4978.

(111) Perdew, J. P.; Burke, K.; Wang, Y. *Phys. Rev. B* **1996**, *54*, 16533–16539.

(112) Dobson, J. F.; Vignale, G.; Das, M.P. Ed. *Electronic Density Functional Theory: Recent Progress and New Directions* **1998**, 261-292.

(113) Lee, C.; Yang, W.; Parr, R. G. *Phys. Rev. B* **1988**, *37*, 785–789.

(114) Tao, J.; Perdew, J. P.; Staroverov, V. N.; Scuseria, G. E. *Phys. Rev. Lett.* **2003**, *91*, 146401.

(115) Becke, A. D. *J. Chem. Phys.* **1993**, *98*, 5648.

(116) Adamo, C.; Barone, V. *J. Chem. Phys.* **1999**, *110*, 6158.

(117) Zhao, Y.; Truhlar, D. G. *J. Phys. Chem. A* **2006**, *110*, 13126–13130.

(118) Andrae, D.; Häußermann, U.; Dolg, M.; Stoll, H.; Preuß, H. *Theor. Chem. Acc.* **1990**, *77*, 123–141.

(119) Weigend, F. *Phys. Chem. Chem. Phys.* **2006**, *8*, 1057–1065.

(120) Neese, F. *WIREs Comput. Mol. Sci.* **2012**, *2*, 73–78.

(121) Petrenko, T.; Kossmann, S.; Neese, F. *J. Chem. Phys.* **2011**, *134*, 054116.

(122) Neese, F.; Wennmohs, F.; Hansen, A.; Becker, U. *Chem. Phys.* **2009**, *356*, 98–109.

(123) Kossmann, S.; Neese, F. *Chem. Phys. Lett.* **2009**, *481*, 240–243.

(124) Noro, T.; Sekiya, M.; Koga, T. *Theor. Chem. Acc.* **2012**, *131*.

(125) Visscher, L.; Dyall, K. G. *At. Data. Nucl. Data Tables* **1997**, *67*, 207–224.

(126) Moseley, J. D.; Sankey, R. F.; Tang, O. N.; Gilday, J. P. *Tetrahedron* **2006**, *62*, 4685–4689.